Multi-scale analysis of wrinkling during consolidation of thermoset composites

by Vu An Le

Thesis submitted in fulfilment of the requirements for the degree of

Doctor of Philosophy

under the supervision of
Dr Sanjay Nimbalkar
Dr Sardar Malekmohammadi
Dr Emre Erkmen
Dr Navid Zobeiry

University of Technology Sydney
Faculty of Engineering and Information Technology

July 2022

Declaration

CERTIFICATE OF ORIGINAL AUTHORSHIP

I, Vu An Le declare that this thesis, is submitted in fulfillment of the requirements for the award of Doctor of Philosophy, in the School of Civil and Environmental Engineering, Faculty of Engineering and Information Technology at the University of Technology Sydney.

This thesis is wholly my own work unless otherwise referenced or acknowledged. In addition, I certify that all information sources and literature used are indicated in the thesis.

This document has not been submitted for qualifications at any other academic institution.

Signature: Production Note: Signature removed prior to publication.   Vu An Le

Date: 15/07/2022

Acknowledgements

This work would not have been possible without the support of my colleagues, friends and family and I owe all of them my most profound thanks.

I am sincerely grateful to all my supervisors, Dr Emre Erkmen, Dr Sardar Malek, Dr Rijun Shrestha, Dr Sanjay Nimbalkar and Dr Navid Zobeiry for their invaluable support, encouragement and guidance throughout my PhD study. I would like to thank Dr Emre Erkmen for accepting me as his PhD student, giving me a chance to work with Dr Sardar Malek when he was about to leave UTS and still providing me with his supervision remotely. Great appreciation for the excellent inspiration and continuous support from Dr Sardar Malek is expressed. His constructive criticisms and encouragement constantly motivated me. Particular gratitude is given to Dr Sanjay Nimbalkar for his kindness and assistance in the final year of my PhD. I would like to acknowledge and thank Dr Navid Zobeiry who was always willing to provide me with important advice for achieving my major milestones during my 4-year study. Without his advice, detailed comments and constructive feedback, my work would not have been possible.

My sincere and deep respect goes to the staff at the Faculty of Engineering and IT, especially Prof Hadi Khabbaz, Dr Nadarajah Gowripalan and Mrs Van Le for their dedicated encouragement, attention and support throughout my PhD candidature. I would like to acknowledge the financial support provided by International Research Scholarship and UTS-VIED scholarship. I also truly value the friendship of several close friends who I met in Sydney. I appreciate their time for listening, sharing and encouraging me during my PhD.

Lastly, I would like to thank my family without whom this work would not have been accomplished. I would like to thank my beloved parents for their endless and unconditional love throughout my life. I would like to thank my dear sisters and brothers for standing at my side and encouraging me to follow my passion. Special thanks go to my parents-in-law for taking care of my lovely son, as this helped me to accomplish my PhD program as planned.

List of publications

Le, A., Zobeiry, N., Erkmen, E. & Malek, S. 2019, 'Buckling analysis of multilayered beams with soft and rigid interfaces', *ICCM22*, Engineers Australia, Melbourne, Vic, pp. 204-12.

Le, V.A., Zobeiry, N., Erkmen, E. & Malek, S. 2021, 'Buckling behaviour of laminated viscoelastic composites under axial loads', *Mechanics of Materials*, 159, 103897.

Le, V.A., Nimbalkar, S., Zobeiry, N. & Malek, S. 2022, ' An efficient multi-scale approach for viscoelastic analysis of woven composites under bending', *Composite Structures*, 292, 115698.

Le, V.A., Nimbalkar, S., Zobeiry, N. & Malek, S. 2022, ' Multi-scale viscoelastic bending analysis of laminated composites with soft interfaces', Full paper submitted to *ECCM20*, Lausanne- Switzerland.

Table of content

List of figures

ix

List of tables

Abstract

Carbon fibre is known for its high strength, light weight and durability. The aerospace and automotive industries have demonstrated a strong interest in utilising carbon fibre when designing their structural parts. However, there are still barriers preventing other industries from realising the full potential of such advanced laminated composites. Among these challenges are the formation of wrinkles and defects throughout the manufacturing process. Currently, manufacturing composite parts with mitigation of defects greatly relies on the designers' experience and the outcomes of trial-and-error procedures. Due to the high cost of experiments and a large number of process parameters involved in composite manufacturing, an improved understanding of wrinkle formation is desirable for industries. Therefore, predictive modelling to aid design engineers in their understanding of the wrinkling phenomenon has become vital over the past two decades.

According to a few recent studies, fibre waviness, misalignment and the complex viscoelastic behaviour of a composite's layered structure during cure are the primary causes of defects, wrinkle formation, and eventual rejection of large composite components. However, the relationship between these factors and the wrinkling of plies caused by micro-buckling has not been investigated quantitatively. Furthermore, these effects are not fully captured in current process models. This research aims to develop an efficient strategy for analysing the multi-scale mechanisms of wrinkling due to buckling of plies during the composite consolidation process. A multi-scale approach that can be incorporated into current process models is proposed for this purpose. Using the suggested approach, the wrinkling response of plies under compressive and bending loads are predicted numerically. Wrinkling wavelengths and critical buckling strength of flat laminates are compared with wrinkling profiles and the strength values reported in the literature. Unlike previous studies, the viscoelastic contribution of resin as well as fibre stiffness and fabric architecture (for woven composites) are taken into account. The effect of these parameters on the buckling behaviour of fibres and the orthotropic nature of plies are also investigated at different scales, quantitatively. Results highlight that the viscoelastic properties of the resin have a considerable effect on the buckling response of woven composites and thus on wrinkle formation during the early stage of cure. Experimental studies are suggested for characterizing the viscoelastic behaviour of resins and its effect on the micro-buckling response of fibres during cure.

Chapter 1. Introduction

1.1. Laminated composites

A composite material is composed of at least two materials or constituents. Often, the resulting material exhibits improved properties over its constituents. The two constituents are often a reinforcement fibre and a bonding matrix. Fibre reinforcements may include glass, aramid, natural fibres (e.g. wood or flax) and carbon, which may be continuous or discontinuous. Three examples of continuous fibre reinforcements are unidirectional (UD), woven fabric and helical winding fibres, as shown in Fig. 1.1a. Examples of discontinuous reinforcements include glass fibres and wood strands (mat) (Fig. 1.1b). The primary role of fibres is to provide strength and stiffness. Fibres carry longitudinal loads while the matrix secures them in place and distributes the loads among the tensioned fibres. The matrix is also the primary load carrier for shear between the layers and in the transverse direction. Although unreinforced fibres are incapable of carrying compressive loads, reinforced composites can do so via this shear transfer mechanism between matrix and fibre. Polymers, metal or ceramics can all be used as matrix materials. Thermoset-based or thermoplastic-based matrices can be used to manufacture polymeric composites. Under elevated temperatures, uncured thermosets have low viscosities such that fibre reinforced thermoset composites can be consolidated and cured under low pressure, forming an intractable solid. In contrast, a thermoplastic forms a high-viscosity polymer melt if heated above its melting temperature during processing and requires higher pressures for consolidation. Unlike thermosets, thermoplastics can be reheated for additional processing and recycling. In this study, only thermoset composites are considered.

Laminated composites are made by stacking composite sheets (i.e. lamina) in different orientations to obtain the desired strength and stiffness properties. Unidirectional (0°) layup as depicted in Fig. 1.2a is extremely strong and stiff in the 0° direction, yet it is a lot more compliant and brittle in the 90° direction because the load must be carried by the much weaker polymeric matrix. For some structural applications, it is necessary to balance the load-carrying ability in a number of different directions, for instance 0°, $+45^o$, -45° and 90°. The quasi-isotropic laminate illustrated in Fig. 1.2b is often preferred in practice since its stiffness is independent of loading direction.

1

Continuous

Unidirectional (UD)

Cloth

Roving

0°

0°/90° (Woven)

±30° Helical
Filament Wound

(a)

Discontinuous

Chopped

Mat

(b)
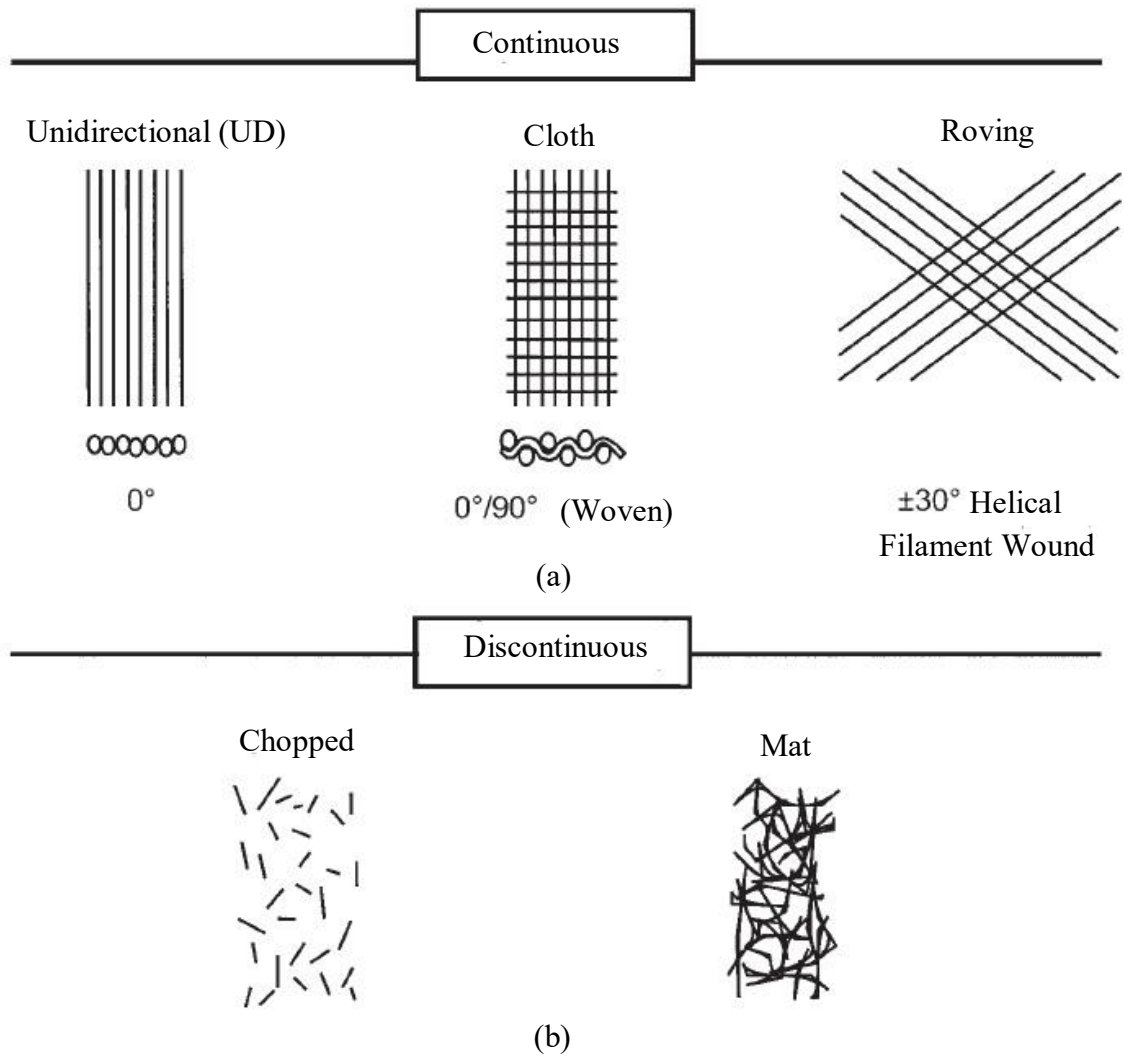
Figure 1.1: Typical reinforcement types
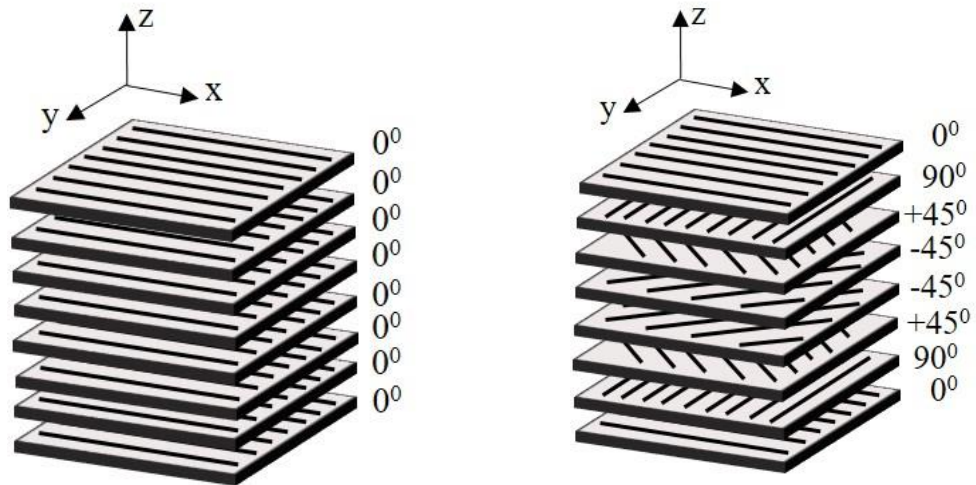
Figure 1.2: Arrangement of plies in (a) a unidirectional (UD) layup (b) a quasi-isotropic layup

1.2. Textile composites

Textile composites provide an attractive alternative to unidirectional composites (UD) because they offer superior forming capabilities to produce complex shapes. Several scales are evident on the internal structure of textile composites. During the manufacturing process of textile composites, four important levels are usually categorised (Dixit & Singh 2013). Firstly, fibres are assembled into yarns. A yarn has a large length and a relatively small cross-section, with and without twist. The fibres are then arranged into a sheet, which is referred to as a fabric. Finally, composite part is consolidated by the infiltration of resin and curing in a mould. Textile composites can be classified into three categories as shown in Fig. 1.3, based on textile techniques used, such as weaving, braiding and knitting (Long 2005).

Textile composite

Weaves — Braids — Multi-Axial warp knit

2D — 3D (under Weaves)

Plain | Satin | Triaxial | Unweaves | Angle interlock | Orthogonal interlock

Layer to layer | Through thickness

2D — 3D (under Braids)

Bias | Triaxial | Tubular | Cartesian

2-Step | 4-Step | Multi-Step
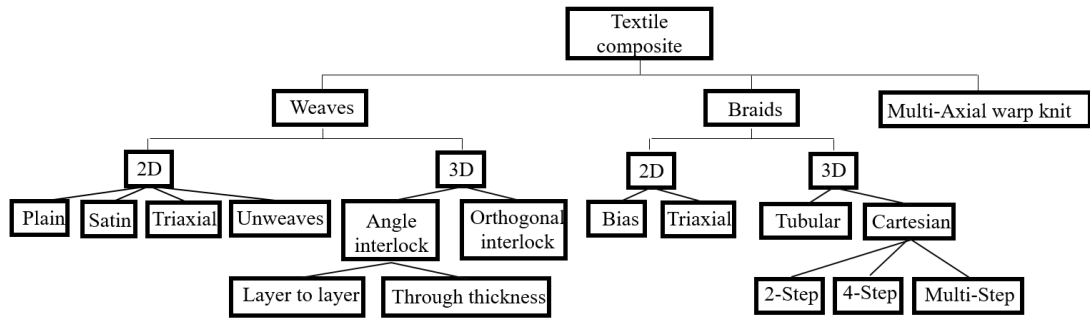
Figure 1.3: Classification of textile composites.
(Dixit & Singh 2013)

Woven fabric textile composites are created by the interlacing of warp fibre tows and weft fibre tows in a regular pattern or weave style. Fig. 1.4 shows the most common weave styles that present how the warp and weft tows are interwoven. Three-dimensional (3D) woven fabrics have additional yarns placed in through-the-thickness direction. Currently, most of the woven fabrics used in textiles are simple 2D fundamental weaves, i.e., plain, twill and satin weaves, which are identified by the repeating patterns of the interlaced regions in warp and weft directions (Alshahrani 2017). Plain weave is the most commonly used basis reinforcement for woven composites. In a plain weaving structure, one warp yarn is repetitively woven over and under weft yarns as shown in Fig. 1.4a. Such frequent undulation of yarn reduces the composite's strength and stiffness. Twill weave has a looser interlacing and the weave is characterised by a diagonal line. Satin weave has a good drapability (Alshahrani 2017) with a smooth surface and minimum thickness. In a satin weave (seen in Fig. 1.4c), one warp yarn is woven over n_g ($n_g > 2$) successive weft yarns, and then under one weft yarn. This weave structure which features disconnected interlaced regions, is referred to as ($n_g + 1$) – harness satin weave. The selected weave style used in Chapter 6 is 5HS satin weave as shown in Fig. 1.4c.

(a) Plain weave   (b) Twill weave   (c) 5-harness satin weave

    █ Warp yarn   █ Weft yarn
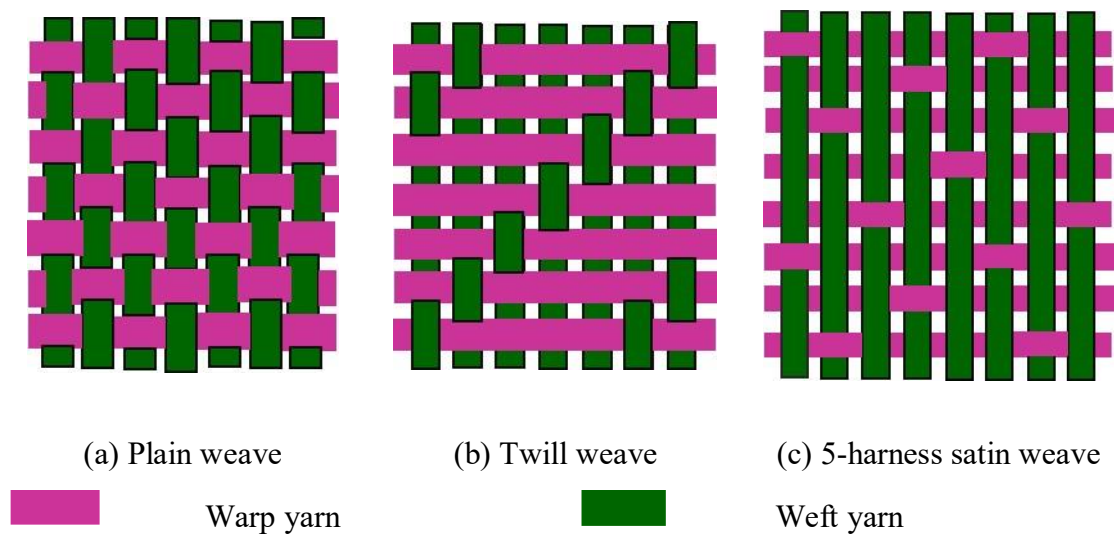
Figure 1.4: Schematic of the common weaves. (a) Plain weave. (b) Twill weave. (c) 5-harness (5HS) satin weave

1.3. Overview of composite manufacturing techniques

Fibre reinforced plastics (FRP) can be manufactured in a variety of ways. While this research is not primarily concerned with this aspect of the subject, it is important to recognise the profound effect that the manufacturing routes and processes have on the final properties of composite materials due to their effect on the microstructure and internal stresses. Autoclave processing is commonly employed for aerospace applications. In this process, composite components are fabricated by laying up multiple layers, usually pre-impregnated fibre sheets with B-stage cured resin (i.e. prepregs), on the mould surfaces in specified orientations until the appropriate thickness is achieved. They are then sealed in a flexible bag and consolidated using a vacuum or pressure bag in an autoclave vessel at the required curing temperature and pressure. The autoclave curing process is demonstrated in Fig. 1.5.
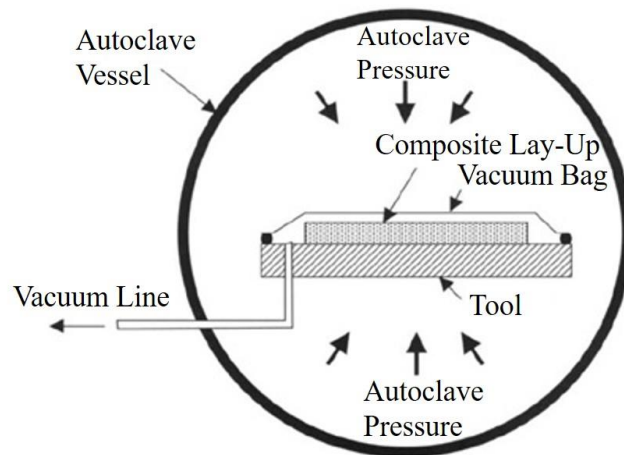
Figure 1.5: Principle of autoclave curing

1.4. Applications and challenges

Carbon fibre-reinforced plastics (CFRPs) have been widely used in engineering applications in recent years due to their excellent characteristics relative to their weight (Friedrich & Almajid 2012). This rapid growth has been achieved mainly by the substitution of traditional materials, primarily metals in structural members. If only strength or stiffness is compared with those of metal alloys, fibre-reinforced composite materials do not provide a clear advantage. However, the strength and stiffness per unit weight of composite materials, also known as specific strength and specific modulus respectively, are factors of great importance in engineering design (Hilburger & Starnes Jr 2002; Leissa 1987). Moreover, composite materials can be tailored to generate different directional properties which potentially can contribute to reducing structural weight. Apart from inheriting high strength and stiffness of the fibres, the composite materials maintain the chemical resistance of the plastic. The cost savings associated with routine maintenance constitute an important factor for the preference of these advanced materials in deep-water applications (Beyle et al. 1997).

In civil infrastructure, application of CFRPs in strengthening structural elements has been explored in recent decades. Compared to conventional reinforcing materials (i.e. steel), the lightweight CFRPs are easy to handle and do not need any heavy lifting and handling equipment. Such advantages make CFRPs more widely accepted for the repair and rehabilitation of steel buildings (Danilov 2016; Täljsten, Hansen & Schmidt 2009). Additionally, due to durability under cyclic loading conditions and corrosion resistance, CFRP plates have been employed extensively for the maintenance or repair of old bridges

6

and infrastructure (Bocciarelli et al. 2009). Furthermore, the use of composites for electrical towers, light poles or the blades of large wind turbines has also increased markedly.

Advanced composites are also replacing steel and aluminium parts in aircraft and road vehicles. In fact, the primary structural elements of the Boeing 787 Dreamliner and the Airbus A350 XMW including the wing and fuselage are built mostly from composite materials. It was reported by Soutis (2005) that in the twenty-first century, CFRPs can and will contribute to more than 50% of the structural mass of an aircraft. More recently, automobile manufacturers like BMW, Mercedes-Benz and Lamborghini have been moving towards increased carbon fibre usage in their vehicles. With automakers putting a priority on fuel economy, it is predicted that CFRPs will soon be the preferred material for the bodies of future cars. Due to the fact that corrosion is a significant issue and expense for the maritime industry, the hulls of boats ranging in size from small fishing boats to huge racing yachts have consistently been constructed using composite materials comprised of glass fibres and polyester or vinyl ester resins. Masts and scuba tanks are other applicants of composites improving the marine industry.

Despite their great benefits, the uncured composite prepreg materials are susceptible to defects in the course of the manufacturing process (Belnoue et al. 2018; Bloom, Wang & Potter 2013; Boisse, Huang & Guzman-Maldonado 2021; Hallander, Sjölander & Åkermo 2015; Johnson et al. 2019; Rashidi et al. 2021). For example, under a predefined heat and pressure cycle in an autoclave, the resin changes from a liquid to a solid. The major transformation in terms of physical and mechanical properties contributes to the change in thickness and subsequent formation of defects (often referred to as wrinkles). When forming quasi-isotropic, multilayer unidirectional (UD) prepreg over a double curved geometry, out-of-plane wrinkling is a general problem (Hallander et al. 2013).

Furthermore, the components commonly used for aerospace applications consist of multiple thin sheets (plies) of unidirectional (UD) carbon or glass fibres. When they are subjected to compressive stresses that usually occur during various curing processes, out-of-plane misalignment of the fibre paths, generally known as wrinkling is a relatively common phenomenon (Alshahrani & Hojjati 2017c; Wang, Long & Clifford 2009; Weber et al. 2019). Based on an experimental study, Wang et al. (2011) developed three

fabrication techniques to generate fibre waviness within flat laminates. These techniques were aimed at creating similar wrinkling patterns to those usually observed in industrial components. However, in other research conducted by Hallander et al. (2013), it is shown that out-of-plane defects also occur in a recess area where a tensile force is applied globally. This is due to the development of local compressive forces in some areas during the forming process.

Wrinkles are more likely to be formed when composite plies have excess length and restrained from slipping over one another due to friction or fixed ends (Dodwell, Butler & Hunt 2014; Weber et al. 2019). As shown in Fig. 1.6, under the applied debulk pressure during the consolidation of the uncured curved laminate, the reduction of the thickness results in a diminished length from l_{before} to l_{after}. Meanwhile, the applied boundary constraints prevent plies from moving with respect to another. Therefore, buckling of the plies is the only way to accommodate that excess length. Lightfoot, Wisnom & Potter (2013) proposed a mechanism for the formation of ply wrinkles due to shear forces between plies. Such forces were the result of mismatches in the coefficient of thermal expansion between composite and tool or ply slippage during consolidation.
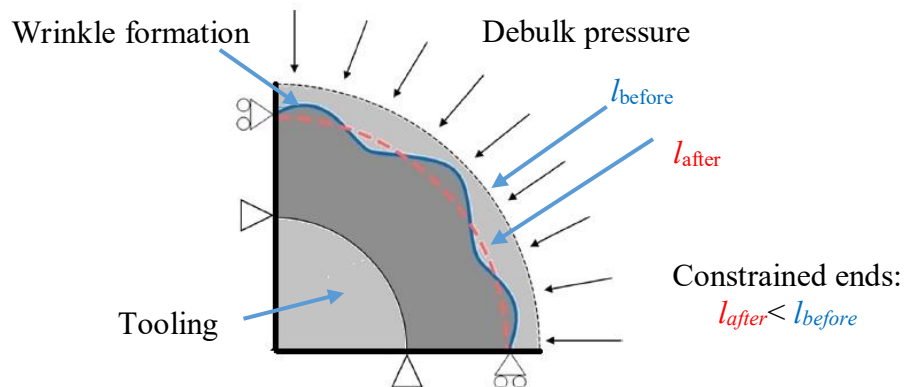
Figure 1.6: Buckling of the plies due to the excess length with fixed ends during consolidation (Adapted from Belnoue et al. (2018))

The presence of wrinkled fibre compromises the service life of the components as it can lead to a very significant reduction in mechanical performance such as compressive strength (Lightfoot, Wisnom & Potter 2013; Varkonyi et al. 2019). In comparison with stresses at initial failure stage of samples without defects, out-of-plane wrinkles with all plies affected and in-plane wrinkles with 50% of plies affected made significant reductions to about 25% and 50% of the corresponding stresses (Potter et al. 2008).

Therefore, the wrinkle formation mechanisms need to be better understood in order to mitigate them in the manufacturing process (Alshahrani & Hojjati 2017c).

Specific material properties of prepregs or their constituents may affect wrinkle formation differently. A mere 5% variation in the thickness of a tapered laminate can result in a dramatic difference in the severity of wrinkles (Belnoue et al. 2018). Forming temperature, consolidation pressure and layup sequence were found to be important contributors to the fibre misalignment in hot drape forming process of a C-shaped part (Farnand et al. 2017). Furthermore, although process simulation has advanced significantly in recent years, currently, mitigating defects during composite manufacturing relies heavily on the designers' experience and trial-and-error methods (Belnoue et al. 2018). Proceeding with trials is very expensive and a large number of process parameters is required. For this reason, predictive modelling and improved understanding of the involved wrinkling phenomena are now of paramount importance to the industrial and scientific community.

Previous results have shown that the forming behaviour of a composite was influenced by the uncured material properties of its plies such as their stiffness as well as their geometrical characteristics (Larberg & Åkermo 2011), resin compound, degree of impregnation and level of consolidation (Hubert & Poursartip 2001; Lukaszewicz & Potter 2011). Moreover, viscous composite materials generally exhibit non-linear bending behaviour. The fibres in a composite are assumed to be rigid and inextensible. Due to the mobility of polymer matrix, these fibres are free to move relative to one another. This imparts some flexibility to the composite and reduces its bending rigidity in comparison to solid composites (Boisse et al. 2018). A computational tool which is able to relate the flexibility of plies to the wrinkle formation is still missing. With this in mind, it is envisioned that a multi-scale model should be developed for analysing the wrinkling response of plies during the consolidation process.

1.5. Knowledge gaps

Some knowledge gaps in predicting the wrinkle formation during consolidation of thermoset composites are identified below:

- There is a lack of validated and efficient FE models capable of predicting wrinkle formation during processing.

- Some existing models (Belnoue et al. 2018; Hallander et al. 2013; Johnson et al. 2019) have been developed for specific curved part geometries and processes such as draping or autoclave. However, the wrinkle formation in flat laminates (i.e. those used in the construction industry) at the early stage of manufacturing has not been investigated in detail.

- The accuracy range of commercial tools such as Abaqus built-in composite element for predicting the response of composites with soft interfaces which is relevant to the early stage of cure has not been assessed.

- Despite some experimental evidence (Alshahrani & Hojjati 2017b; Larberg & Åkermo 2014; Wang, Long & Clifford 2009), the effects of ply anisotropy, fibre bed and viscoelasticity on the buckling behaviour of composites are not well understood.

- Although out-of-plane bending has been well known as one of the deformation mechanisms governing wrinkle formation during composite manufacturing, predictions of the out-of-plane properties of viscoelastic composites with various fibre architecture have not been examined comprehensively.

- Multi-scale modelling that accounts for micro-structural effects on the macro-structural response during cure has not been investigated experimentally and numerically.

- The properties of the uncured composites that should be used to represent bending behaviour in the finite element model for forming simulation are still not well understood.

- Contribution of complex deformation mechanisms such as in-plane shear, out-of-plane bending and inter-ply slippage during forming process of laminated composites has not been investigated comprehensively.

1.6. Research objectives

The objectives of this research can be categorised into two main groups. The first one is to investigate the buckling response as well as load-displacement curves of viscoelastic composite laminates under compression for a better understanding of the ply wrinkling behaviour at the early stage of thermoset composite manufacturing. The second one is to develop a multi-scale model for predicting efficiently the effect of various parameters on wrinkle formation such as fibre stiffness, loading rates, ply anisotropy,

resin properties and yarn's architecture on the bending behaviour of viscoelastic laminates. Specific research tasks are to:

- Examine the ability of commercial FE tools, e.g. Abaqus in simulating the buckling behaviour of laminated composites with many numbers of layers and soft thin interfaces.
- Perform nonlinear FE analysis to investigate the ultimate compressive strength and the post-buckling behaviour of UD thermoset carbon/epoxy prepreg sheets during the manufacturing process.
- Employ various material models (e.g. isotropic elastic, transversely isotropic and orthotropic viscoelastic) to demonstrate the importance of consideration of the rate dependence in describing the behaviour of prepreg materials.
- Incorporate viscoelastic micromechanical models proposed by Malek et al. (2014) in a commercial FE software Abaqus to determine the effective time-dependent response of large composite parts.
- Compare the buckling behaviour as well as load-displacement curves obtained from the present multi-scale analysis with the experimental results available in the literature for validation purposes.
- Conduct a mesh convergence study to determine the efficient mesh size that should be used throughout this study.
- Conduct parametric studies on the effect of viscoelastic parameters of the resin such as assumed unrelaxed/ relaxed moduli, relaxation times and weight factors on the post-buckling response of uncured laminated composites.
- Predict the effective mechanical properties and structural responses such as buckling and bending behaviours depending on constituent property (e.g. fibre stiffness), different fabric architectures and loading conditions.
- Determine the overall stiffness of elastic/viscoelastic woven composites using micromechanical equations developed by Naik (1994) and implement in MATLAB. The analytical procedure is verified/validated wherever experimental data are available.
- Investigate deformation mechanisms that may occur simultaneously during the formation of woven composites such as in-plane shear, out-of-plane bending or inter-ply slippage.

1.7. Thesis structure

Based on these objectives, the thesis is organised as shown in Fig.1.1 and the chapter progression of the thesis is illustrated as follows:

Chapter 1: Introduction

This chapter presents a brief introduction to composite materials such as unidirectional (UD) and woven prepregs so that their buckling and bending behaviours during the forming process are later investigated in Chapter 5 and Chapter 6 respectively. Recent engineering applications in different sectors and challenges relating to wrinkling formation during the manufacturing process are also stated to highlight the significance of this research. Lastly, the knowledge gaps and objectives of the study are identified in detail.

Chapter 2: Literature review

A review of micromechanical models for estimating the elastic properties of unidirectional composites is first carried out. However, a comprehensive study had already been done in the literature (Malek 2014). Therefore, only analytical micromechanics equations selected in the current proposed multi-scale modelling framework are shown for clarification purpose. In addition, for thermoset composites during cure, fibre bed referring to the slight waviness of the fibres in prepregs is believed to play a significant part in carrying the load in the transverse fibre orientation. Hence, how to consider such an effect on the viscoelastic properties of composites during cure using an appropriate analogue representation is also revisited for later application in predicting the effective mechanical properties of composites and presented in this chapter.

Secondly, a review of meso-mechanical models for elastic analysis of textile composites is conducted. Both analytical and numerical models in the literature have been presented for estimating the effective mechanical properties of specific composites in terms of geometry modelling and homogenisation techniques. After considering applicability of the reviewed approaches for the current multi-scale modelling framework, the analytical technique proposed by (Naik 1994) for calculating the homogenised material properties of 5HS satin weave is selected and shown in Chapter 3.

Thirdly, as a first step in providing a better understanding of wrinkle formation, the buckling behaviour of laminated viscoelastic composites under axial loads is

reviewed. Subsequently, the bending behaviour of viscoelastic woven composite is studied because the bending properties of uncured thin laminates have been known to govern the appearance of wrinkles, particularly in determining the shape of wrinkles. Finally, to create a reliable forming simulation, the properties of the uncured material must be known and properly represented in the finite element model. A review in detail of experimental studies on uncured composites and calibrated material properties for the corresponding FE simulations is also undertaken. This is done to better understand the mechanical properties of such composites and their constituents under bending.

Chapter 3: Methodology

The chapter describes in general a multi-scale method that is used throughout this study to analyse wrinkling (i.e. buckling and bending responses) during consolidation of thermoset composites. At smaller contexts such as micro and meso levels, the effective viscoelastic properties of a unidirectional Representative Volume Element (RVE) or Repeating Unit Cell (RUC) of the woven fabric reinforced composites are determined using analytical models. Details of the geometric modelling technique of 5HS satin weave as well as discretisation technique of yarns and calculation of three-dimensional effective stiffnesses are presented in this chapter. A specific MATLAB script is written to facilitate the computation of the effective properties of the fabric at the meso-scale with given quantities. The transformation matrix $[T_{\mathrm{m}}]$ used in expression of effective stiffness matrix is documented in Appendix A.1.

At the macro-scale, both analytical and numerical methods are considered. The analytical approach involves different simple mathematical equations for specific problems such as buckling or bending behaviour of assumed isotropic elastic beams. The particular mathematical equations are presented in a separate chapter according to certain problems of concern. In terms of numerical approach, the finite element method using commercial software, Abaqus is used to predict the structural responses such as buckling or bending of both elastic and viscoelastic composite plates at various loading rates. For viscoelastic analysis, the composite plate is first assumed to behave as an isotropic viscoelastic solid and modelled using the Abaqus built-in viscoelastic constitutive model which is based on the integral form (IF) of viscoelasticity. Since the application of Abaqus viscoelastic model is limited to isotropic materials, a more versatile orthotropic viscoelastic constitutive model (based on a differential form of viscoelasticity – DF) that

has been developed and implemented as a UMAT by researchers (Malek 2014; Zobeiry et al. 2016) is employed to elucidate the effect of ply anisotropy on the structural responses of uncured/ partially cured composite plates. For this purpose, both numerical approaches using Abaqus built-in viscoelastic model (IF) and orthotropic viscoelastic user material model (UMAT) are shown in this chapter. The DF approach and its implementation in Abaqus are briefly described in Appendices A.2 and A.3 respectively.

Chapter 4: Buckling analysis of multilayered elastic beams with soft and rigid interfaces

As the first step for better comprehending wrinkle formation, the behaviour of multilayered elastic beams under bending and buckling is examined using available analytical and numerical strategies. A numerical model simulating the tests in Dodwell (2015) is described in detail at the beginning of this chapter. To investigate the effect of very soft interfaces and ply anisotropy on the overall beam rigidity using two types of models (i.e. composite layup option (CE) and physically modelling layers (PML)), two case studies are introduced later. By observing the obtained results, a new model based on the hypothesis that the resin stiffness dominates the longitudinal compressive strength is created in the next chapter. A version of this chapter has been published in conference proceedings (see Le, A., Zobeiry, N., Erkmen, E. & Malek, S. 2019, 'Buckling analysis of multilayered beams with soft and rigid interfaces', *ICCM22*, Engineers Australia, Melbourne, Vic, pp. 204-12).

Chapter 5: Buckling behaviour of laminated viscoelastic composite under axial loads

Following the studies conducted in the previous chapter, here the viscoelastic properties of the resin are included in a macro-scale model. The effective properties of the composites obtained from viscoelastic micromechanical models instead of assumed elastic inputs for the resin properties as in Chapter 4 are used in the macro-scale FE model. A more versatile orthotropic viscoelastic constitutive model based on differential form (DF) of viscoelasticity implemented as a user material subroutine (UMAT) compared to using Abaqus built-in viscoelastic model (IF) is employed. It helps to elucidate the effect of ply anisotropy on the buckling response of uncured/partially cured unidirectional (UD) laminates.

This chapter begins with a description of analytical equations to approximately estimate the critical buckling load of a linear isotropic laminate. Model verification and validation with the experimental data available in Wang, Long & Clifford (2009) are

introduced in later subsections. Some important aspects such as viscoelastic behaviour, effect of resin properties on the post buckling response are also investigated. A version of this chapter has been published in a peer-reviewed international journal paper (see Le, V.A., Zobeiry, N., Erkmen, E. & Malek, S. 2021, 'Buckling behaviour of laminated viscoelastic composites under axial loads', *Mechanics of Materials*, 159, 103897).

Chapter 6: Bending behaviour of viscoelastic woven composite plates

Given that out-of-plane bending is well known as an important deformation mechanism that governs the wrinkle formation during composite manifacturing (Margossian, Bel & Hinterhoelzl 2015), this chapter investigates the bending behaviour of viscoelastic composites under conditions similar to forming processes. For a multi-scale modelling framework involving analyses at different scales and implemented in a general purpose finite element code, Abaqus is used. Due to the limitation of Abaqus built-in viscoelastic model to isotropic materials, an orthotropic viscoelastic constitutive model implemented as a UMAT in other research (Malek 2014; Zobeiry et al. 2016) is employed to consider the influence of ply anisotropy on bending behaviour.

The multi-scale modelling approach that is used in this study was introduced in general in Chapter 3. The detail of the multi-scale framework for a specific problem (i.e. bending behaviour of uncured woven composites) is described in Section 6.2. The details of the FE model and its verification are provided in 6.2. In Section 6.3, numerical results are compared with the experimental data available in the literature (Alshahrani & Hojjati 2017b) for validation purpose. The capabilities and limitations of the developed model are discussed in Section 6.4. Future works and the conclusion are presented in Section 6.5. A version of this chapter has been published in a peer-reviewed international journal paper (see Le, V.A., Nimbalkar, S., Zobeiry, N. & Malek, S. 2022, 'An efficient multi-scale approach for viscoelastic analysis of woven composites under bending', *Composite Structures*, 292, 115698).

Chapter 7: Bending behaviour of multilayered viscoelastic plates with thin and soft interfaces

As reviewed in the previous chapter, bending properties of uncured thin laminates are known to significantly influence the appearance of wrinkles including the shape, magnitude and intensity of wrinkles. Apart from bending stiffness, shear deformation in the form of inter-ply slippage is deemed to be an important deformation mechanism

during the process of forming composites, particularly for multilayered textile composites. Therefore, the method developed in Chapter 6 has been expected to expand the investigation into the bending behaviour of multilayered textile composite separated by relatively soft interfaces. Consequently, this chapter is concerned primarily with the concurrent deformation mechanisms during bending behaviour of orthotropic elastic multilayered beams with thin and soft interfaces. A version of this chapter is submitted to *ECCM20* Switzerland, 26-30 June 2022: Le, V.A., Nimbalkar, S., Zobeiry, N. & Malek, S. 2022, 'Multi-scale viscoelastic bending analysis of laminated composites with soft interfaces'.

Chapter 8: Conclusions and recommendations

This chapter summarises the major outcomes of the research. A discussion of the possible issues that may be attributed to the disparity between the predictions using the proposed numerical model and available experimental results is also included. Recommendations for future research are provided at the end.

Chapter 1.
• Introduction

Chapter 2.
• Literature review

Chapter 3.
• Research methodology

Chapter 4.
• Buckling analysis of multilayered elastic beams with soft and rigid interfaces

Chapter 5.
• Buckling behaviour of laminated viscoelastic composites under axial loads

Chapter 6.
• Bending behaviour of viscoelastic woven composite plates

Chapter 7.
• Bending behaviour of multilayered viscoelastic plates with thin and soft interfaces

Chapter 8.
• Conclusions and recommendations

Figure 1.7: Thesis structure

Chapter 2. Literature review

2.1. Micro-mechanical modelling of circular fibre composites

Numerous studies on micromechanical models for the elastic study of composite materials have been published. While numerical models can take into account the microstructure's complexity, they frequently consume an increasing amount of computational time than simple closed-form equations. In the current study, the analytical micromechanical approach is adopted because it provides accurate and efficient ways to predict the effective mechanical properties of viscoelastic composites with circular fibre that can later be used within a multi-scale modelling framework like process simulation of composite structures. Well-known micromechanical models have been reviewed in detail in Malek (2014). Only chosen models for calculating specific moduli and modification approach for viscoelastic properties of composite materials during cure used in this study are reviewed in the sections below for completeness.

2.1.1. Analytical micromechanics equations for predicting properties of solid unidirectional composites

The Composite Cylinder Assemblage (CCA) model proposed by Hashin & Rosen (1964) was used to estimate the effective viscoelastic characteristics of unidirectional (UD) cylindrical fibre composites. The approach based on the assumption that the volume of composite material can be occupied by a gathering of cylindrical fibres in a surrounding resin as demonstrated in Fig. 2.1. The volume fraction of fibre, V_f, defined as the ratio of the fibre diameter (b) to the matrix diameter (a), is considered to be the same in the whole system.

$$V_f = \frac{A_f}{A_c} = \left(\frac{b}{a}\right)^2, \qquad (2.1)$$

17
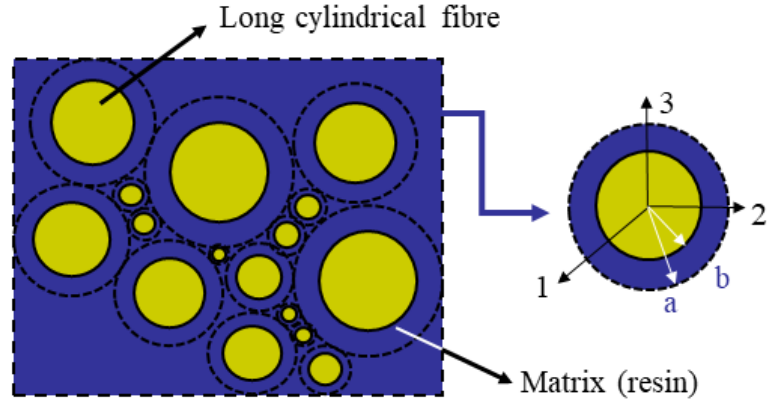
Figure 2.1: Composite Cylindrical Assemblage (Malek 2014)

The longitudinal Young's modulus (E_{1c}) and Poisson's ratio of the UD composite (v_{12c}) are determined from (Hashin & Rosen 1964):

$$E_{1c}=E_{1f}V_f+E_r(1-V_f)+\left[\frac{4\left(v_{12f}-v_r\right)^2V_f(1-V_f)}{\dfrac{(1-V_f)}{K_{23f}}+\dfrac{V_f}{K_{23r}}+\dfrac{1}{G_r}}\right], \tag{2.2}$$

$$v_{12c}=v_{13c}=v_{12f}V_f+v_r(1-V_f)$$
$$+\left[\frac{(v_{12f}-v_r)\left(\dfrac{1}{K_{23r}}-\dfrac{1}{K_{23f}}\right)V_f(1-V_f)}{\dfrac{(1-V_f)}{K_{23f}}+\dfrac{V_f}{K_{23r}}+\dfrac{1}{G_r}}\right], \tag{2.3}$$

Note that subscripts f and r refer to fibre and resin. The effective bulk modulus of the composite in plane strain (K_{23c}) is given by (Hashin 1972):

$$K_{23c}=K_{23r}+\frac{V_f}{\dfrac{1}{K_{23f}-K_{23r}}+\dfrac{(1-V_f)}{K_{23r}+G_r}}, \tag{2.4}$$

where the fibre and the resin plane strain bulk modulus, K_{23f} and K_{23r}, can be determined as follows:

$$K_{23f}=\frac{1}{(1/G_{23f})-(4v_{23f}/E_{3f})-(4v_{12f}^2/E_{1f})}, \tag{2.5}$$

$$K_{23r}=\frac{1}{2(1-v_r-2v_r^2)}, \tag{2.6}$$

18

where v_r and v_f are the resin and the fibre Poison's ratios.

Similarly, the longitudinal shear modulus is given by:

$$G_{12c}=G_{13c} = G_r \left[\frac{G_r(1 - V_f) + G_{12f}(1 + V_f)}{G_r(1 + V_f) + G_{12f}(1 - V_f)}\right], \tag{2.7}$$

$$E_{2c(\pm)}=\frac{4K_{23c}G_{23c(\pm)}}{K_{23c} + mG_{23c(\pm)}}, \tag{2.8}$$

$$v_{23c(\pm)}=\frac{K_{23c} - mG_{23c(\mp)}}{K_{23c} + mG_{23c(\mp)}}, \tag{2.9}$$

where m is defined as:

$$m = 1 + \frac{4K_{23c}v_{12c}^2}{E_{1c}}, \tag{2.10}$$

Using GSC model, Christensen & Lo (1979) proposed the effective transverse shear modulus of UD composites with long fibre by solving the following quadratic equation:

$$A\left(\frac{G_{23c}}{G_r}\right)^2 + B\left(\frac{G_{23c}}{G_r}\right) + C = 0, \tag{2.11}$$

where A, B and C are math functions provided below:

$$
\begin{aligned}
A = 3V_f\left(1 - V_f\right)^2 &\left(\frac{G_{23f}}{G_r} - 1\right)\left(\frac{G_{23f}}{G_r} + n_f\right) \\
&+ \left[\left(\frac{G_{23f}}{G_r}\right)n_r + n_r n_f\right. \\
&\left. - \left(\left(\frac{G_{23f}}{G_r}\right)n_r - n_f\right)V_f^3\right]\left[\left(\frac{G_{23f}}{G_r} - 1\right)n_r V_f\right. \\
&\left. - \left(\left(\frac{G_{23f}}{G_r}\right)n_r + 1\right)\right],
\end{aligned} \tag{2.12}
$$

19

$$B = -6V_f(1 - V_f)^2 \left(\frac{G_{23f}}{G_r} - 1\right)\left(\frac{G_{23f}}{G_r} + n_f\right)$$

$$+ \left[\left(\frac{G_{23f}}{G_r}\right)n_r + \left(\frac{G_{23f}}{G_r} - 1\right)V_f + 1\right]\left[(n_r - 1)\left(\frac{G_{23f}}{G_r} + n_f\right)\right.$$

$$\left. - 2V_f^3\left(\left(\frac{G_{23f}}{G_r}\right)n_r - n_f\right)\right] \tag{2.13}$$

$$+ (n_r + 1)V_f\left(\frac{G_{23f}}{G_r} - 1\right)\left[\frac{G_{23f}}{G_r} + n_f\right.$$

$$\left. + \left(\left(\frac{G_{23f}}{G_r}\right)n_r - n_f\right)V_f^3\right],$$

$$C = 3V_f(1 - V_f)^2 \left(\frac{G_{23f}}{G_r} - 1\right)\left(\frac{G_{23f}}{G_r} + n_f\right)$$

$$+ \left[\left(\frac{G_{23f}}{G_r}\right)n_r + \left(\frac{G_{23f}}{G_r} - 1\right)V_f + 1\right]\left[\frac{G_{23f}}{G_r} + n_f\right.$$

$$\left. + \left(\left(\frac{G_{23f}}{G_r}\right)n_r - n_f\right)V_f^3\right], \tag{2.14}$$

where

$$n_f = 3 - 4v_{23f},$$

$$n_r = 3 - 4v_r, \tag{2.15}$$

2.1.2. Predicting the viscoelastic properties of composites during cure

The accuracy of the above chosen closed-form analytical equations in determining the effective viscoelastic characteristics of UD composites had been verified with numerical reference solutions (Malek 2014) over a variety of fibre volume fractions. However, for thermoset composites during cure, the resin develops from a lowly viscous fluid to a highly cross-linked viscoelastic solid. Therefore, these equations were adjusted by incorporating the fibre bed effect.

In practice, fibres in long-fibre reinforced composites are not ideally straight. We refer the slight waviness of the fibres in prepregs as shown in Fig. 2.2 as fibre bed. As fibre volume fraction is high ($V_f > 0.5$), the fibre bed plays a significant part in carrying

the load in the transverse fibre orientation (Gutowski et al. 1987). Fig. 2.2ab illustrates the deformation behaviour of a fibre bed impregnated with resin under shear loading (Malek, Thorpe & Poursartip 2011). It is believed that in vertical section (see in Fig. 2.2a) the fibre bed and the resin deform equally (isostrain condition) and in the horizontal section (see in Fig. 2.2b), the resin carries the same stress as the fibre does (isostress).
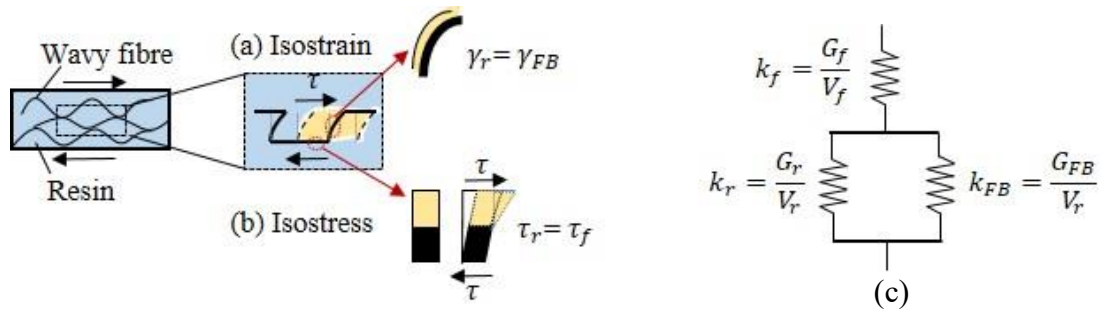
Figure 2.2: Fibre bed deforms under shear stress. (a) Fibre bed deforms together with resin. (b) Fibre deforms under the overall shear stress. (c) Analog representation (Malek, Thorpe & Poursartip 2011).

The mechanism of load transfer then can be represented using a simple analog model indicated in Fig. 2.2c. The impact of each element to the overall stiffness of the composite is expressed by k.

According to this representation, the fibre bed stiffness is parallel to the resin stiffness and therefore the wavy fibre bed perturbs the resin shear modulus G_r by G_{FB}. Then the function of any solid micromechanical model MM (G_r, G_f, V_f, …), for example, the prepreg shear modulus could be represented by:

$$G_{Prep} = MM\ (G_r + G_{FB},\ G_f,\ V_f,\ …),$$

(2.16)

2.2. Meso-mechanical modelling of textile composites

The prediction of elastic properties of textile composites has attracted much research attention in the past two decades because the mechanical characteristics of such composites are highly complex due to many parameters as fibre architecture, matrix properties and fibre properties involved (Balokas, Czichon & Rolfes 2018; Qi, Liu & Chen 2019). Various predictive models have been published and categorised into analytical models and numerical models (Dixit & Singh 2013).

Numerical models are more flexibly applied for different geometries and consider more complex mechanical interaction of yarns and matrix since it relies on available computational solvers (Nguyen et al. 2021; Qi, Liu & Chen 2019). Using FE-based numerical models (Qi, Liu & Chen 2019; Tan, Tong & Steven 1997), the general procedure to predict the mechanical properties of a textile composite includes determining properties of a RVE. The selected RVE is sufficient to represent the fabric architecture for a later calculation of entire textile structure's mechanical properties (Dixit, Mali & Misra 2013; Sun & Vaidya 1996; Udhayaraman & Mulay 2017). With rapid advances being made in computers, the mechanical properties of composites with complex structures have been widely computed using the FE method. Sun et al. (2003) proposed a new method for modelling the effective mechanical properties of three-dimensionally braided composites material via homogenisation theory and incompatible multivariable FEM. Li et al. (2012) described the actual microstructure of 3D five-directional braided composites by using the unit cell model with the FEA method. Tensile behaviour in 0° and 90° directions at the RVE scale of 3D orthogonal woven composites was investigated numerically by Yang, Gao & Ma (2018). The effects of crack damage, yarn/matrix interface and geometric model size of component material (i.e. matrix, warp, weft and z-yarn) were analysed (Yang, Gao & Ma 2018). Based on cross-scale simulation and the homogenisation theory, the mechanical properties of different types of CFRP with the change of angle and different stacking sequences of UD-CFRP were obtained by Qi, Liu & Chen (2019). However, many challenges such as the choice of an appropriate unit cell (Cao et al. 2020) with correct boundary conditions and FE mesh size were involved in modelling a periodic representation of a specific textile composite (Camanho & Hallett 2015).

The need for accurate and less complicated analytical models compared to numerical models in terms of computational effort in predicting mechanical properties of textile composites is increasing (Hallal, Younes & Fardoun 2013). Moreover, there are many parameters involved in calculating the fabric structure such as fabric architecture, the density of yarns in the fabric, properties of warp and weft yarns, characteristics of fibre and matrix etc. Therefore, analytical models are necessary to evaluate the effects of various parameters on the mechanical properties of textile composites. Concerning two major factors such as the geometrical modelling and the homogenisation technique based

on isostrain assumptions, isostress assumptions, mixed isostrain/isostress assumptions etc, many different approaches were proposed by researchers.

Ishikawa & Chou (1982) conducted the first studies that investigated the stiffness and strength of 2D woven fabric composites. Three analytical models were proposed and developed for approximating the elastic behaviour of woven fabric composites. The first model is referred to as "mosaic model" which is idealised as an assemblage of two one-dimensional models for a formation of a two-dimensional cross-ply laminate as a consequence of neglecting the continuity of fibres in the thread direction (see Fig. 2.3a). The upper and lower bounds for stiffness in the tow direction are obtained according to constant strain (isostrain) and constant stress (isostress) assumed.

Considering the fibre undulation and continuity, the second model introduced as "fibre undulation model" or "crimp model" (see Fig. 2.3b) was found to be effective for modelling the mechanical properties of 2D plain weave fabric composites (Ishikawa & Chou 1982). The length of a tow in the fabric repeating unit is divided into small portions (see Fig. 2.3b). For the undulating section, only considered in yarns along loading direction, a sinusoidal expression defines the undulation of the yarns. Then, they are assembled under isostress assumption using the Classical Laminate Theory (CLT).

The "bridging model" was later developed for the analysis of mechanical properties of satin composites. In this model shown in Fig. 2.3c, an interlaced region (labelled as III) is separated from surrounding straight regions (I, II, IV and V) as the local in-plane stiffness in this place was found to be much lower than that of the straight areas. The four regions of straight fill threads (I, II, IV and V) can be regarded as pieces of $0^{\circ}/90^{\circ}$ cross-ply laminates while the undulating tow in region III is modelled using the crimp model. Assuming that a load, N (see Fig. 2.3c) is applied along the weft threads, regions such as II, III and IV are considered to be parallel models and the remaining cross-ply laminates I and V are in series. Therefore, stiffnesses of regions II, III and IV are averaged using an isostrain assumption and stiffnesses of I and V are averaged based on isostress assumption. Employing laminated models to describe the geometry of the woven fabric composites, Ishikawa & Chou (1982)'s studies are based on classical laminate theory (CLT) and demonstrated the validity of the theory for every infinitesimal piece of the repeating unit of a woven lamina. However, these models only considered loading in the x-direction while the undulation and continuity in the warp threads were ignored.

| (a) | (b) | (c) |
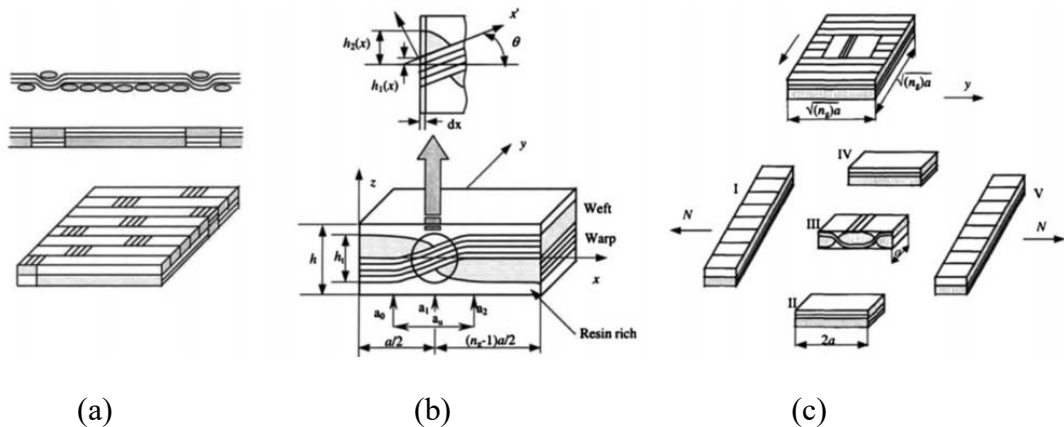
Figure 2.3: Schematic of (a) mosaic model; (b) undulation model and (c) bridging model proposed by Ishikawa & Chou (1982)

Naik & Shembekar (1992) extended the existing 1D models of Ishikawa & Chou (1982) and improved a 2D model for plain weave composites. The model accounts for undulation in both along and across the yarns (i.e, warp and weft) (see Fig. 2.4). The presence of a gap between two adjacent yarns, yarn cross-sectional area and lamina thickness was also investigated and demonstrated to have significant effects on the elastic analysis of woven fabric composites. Two methods used to assemble discrete sections are PS (Parallel-Series) scheme and SP (Series-Parallel) scheme. In the SP model, yarn slices along the loading direction are assembled in series using isostress assumptions and yarn portions across the loading direction are assembled in parallel using isostrain conditions. The PS model is opposite to the SP one and been validated as generating better predictions of in-plane elastic properties.

In later work, Naik (1994) developed an analytical technique for determining overall stiffness of woven composites along with braided textile composites (i.e. 2D braided and 2D triaxial braided composites). Having described the RUC geometry for a specific textile composite, the three-dimensional (3D) effective stiffness for the composite was calculated following two steps. Firstly, each yarn in the RUC was discretised into yarn slices. Secondly, based on an isostrain assumption within the RUC, the 3D effective properties of the composite were obtained by utilising the material characteristics, spatial direction and volume fraction of each yarn slice. The predicted mechanical properties agreed well with numerical solutions and experimental data for both the satin weave and braided composites. Subsequent research by Naik considered the effect of twisted yarns on the strength of plain weave fabric (Naik & Kuchibhotla

2002), leading to an analytical method for determining through-thickness moduli of 3D orthogonal interlock woven composites (Naik et al. 2001; Naik & Sridevi 2002).

a_w: Width of the warp yarn

g_w: Gap between two adjacent warp yarns

a_f: Width of the fill yarn

g_f: Gap between two adjacent fill yarns
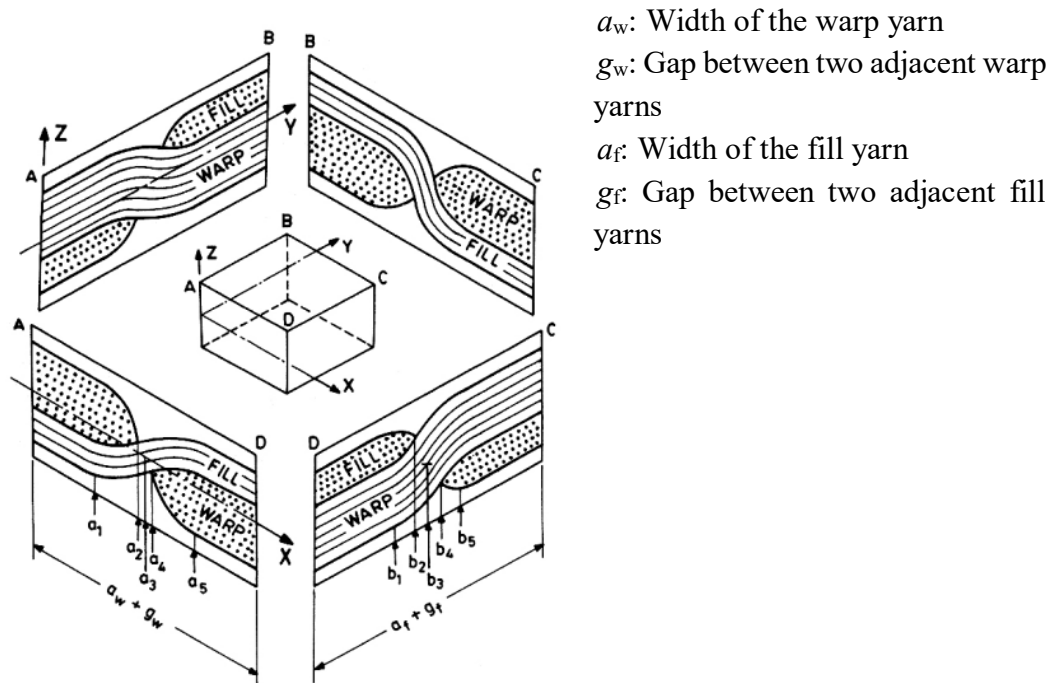
Figure 2.4: Unit cell of plain weave composite improved by Naik & Shembekar (1992)

Sankar & Marrey (1997) proposed an analytical procedure known as the selective averaging method (SAM) for the estimating the thermoelastic properties of textile composite materials. The unit cell is divided into slices of a thickness (meso-scale) which are further subdivided into elements (mico-scale). Both stiffness and compliance coefficients can be averaged selectively based on either isostress or isostrain assumptions. (Tan, Tong & Steven 1999, 2000; Tan et al. 2000) also devised two analytical models to determine the mechanical properties and the thermal expansion coefficients of 3D orthogonal and through-the-thickness angle interlock woven composites. Having discretised the RVE into micro-blocks, they are further assembled for simple strips using the "X model", "Y model" or "Z model" as shown in Fig. 2.5. The micro-blocks can be warp/weft impregnated with resin or tow blocks whose mechanical properties and coefficients of thermal expansions are known. Depending on loading directions and the relative position of assembled blocks, isostrain and isostress assumptions are applied.

(a)	(b)	(c)
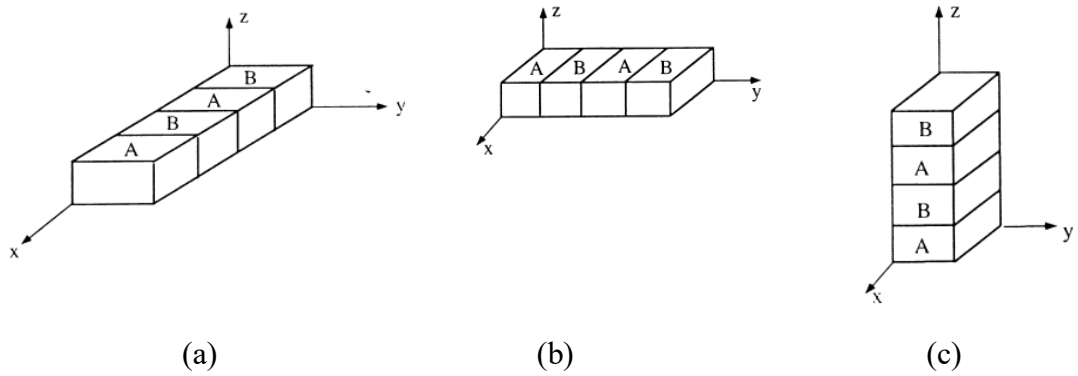
Figure 2.5: Schematic of (a) "X model"; (b) "Y model" and (c) "Z model" developed by Tan, Tong & Steven (1999)

Wu, Brown & Davies (2002) and Wu (2009) introduced an analytical model for determining the stiffnesses of 3D orthotropic laminated fabric composites. The proposed technique includes discretising the representative unit cell into slices (layers) which are later decomposed into stripes (elements) (see Fig. 2.6). In the scenario of either isostress or isostrain following the applying stress, the components of the stiffness matrix of the slices are obtained based on those of the elements. The stiffness of the RUC is subsequently formulated by combining these slices. Although the approach has been shown to be simple and computationally efficient, it overestimates all Young's moduli compared to the experimental values.

Hallal et al. (2012) developed an analytical model labelled as 3SHM for calculating the effective elastic properties of 2.5D interlock woven fabrics composite. The 3SHM is the abbreviation for 3 Stage Homogenisation Method at mico-, meso- and macro-scales. At micro-scale, each yarn is decomposed into sub-volumes with known volumes and these stiffness matrices are calculated using a micromechanics model in the literature. At meso-homogenisation stage, the stiffness matrices of yarns are later determined by assembling sub-volumes using mixed isostrain and isostress assumptions (see Fig. 2.7). Finally, at the macro-scale, the stiffness of the REV is obtained by combining homogenised yarns and matrix stiffness matrices under isostrain conditions (see Fig. 2.7). It is noted that the proposed method accounts for the real geometry of undulated yarns, resulting in flexibility in modelling textile composites with different geometries.

Recently, Zhou et al. (2022) proposed an analytical model based on the energy principles for calculating the uniaxial tensile modulus of plain woven fabric (PWF) composites. By observing computed tomography, the lenticular shape was selected to

describe the cross-section of the plain woven composites' fibre tows and the undulation path was assumed to be composed of equal radius arcs for both the warp and weft yarns. The yarn segments are subjected to uniaxial tension load along with the simplified interaction force between yarns. The analytical equations for the uniaxial tensile modulus of the plain woven fabric are subsequently withdrawn. Such a model results in a small deviation compared to experimental data and high calculation efficiency. However, Zhou's model relies heavily on the input parameters from costly experiments and the cross-section of fibre tows and the interaction between the warp and weft tows are simplified for a specific woven fabric. Therefore, the application of the proposed analytical model for another type of textile composite with different geometric and mechanical properties (i.e. fibre and matrix) should be further investigated.

(a)   (c)
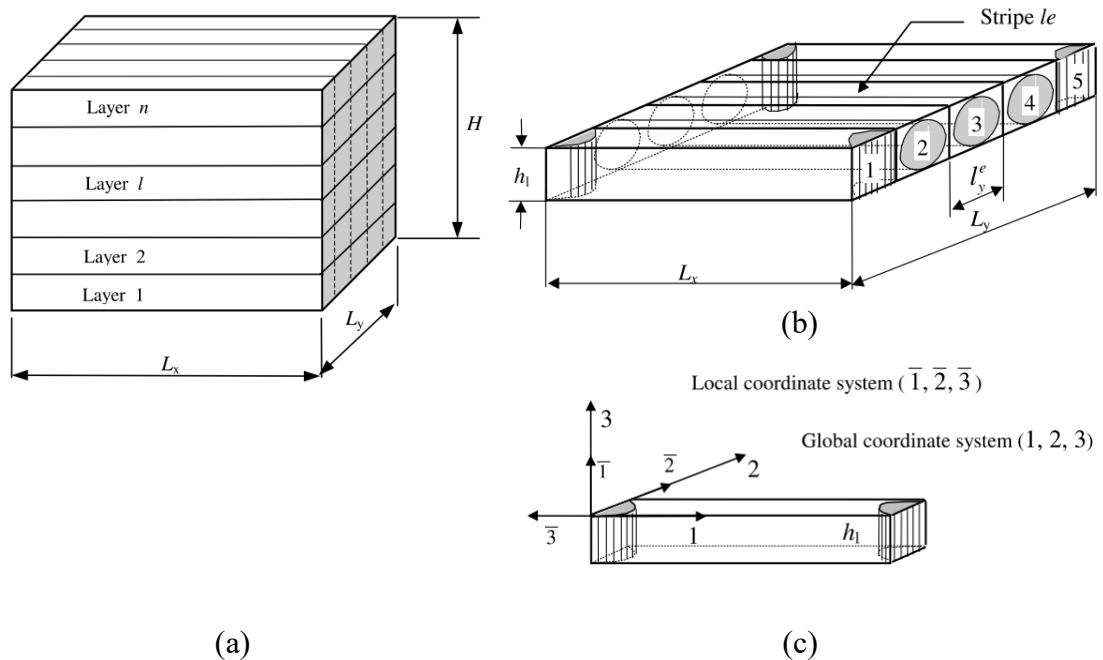
Figure 2.6: Schematic of (a) the representative unit cell in a 3D orthotropic laminated composite; (b) the discretised stripes of layer l; (c) global and local coordinate systems for stripe 1 (Wu, Brown & Davies 2002).
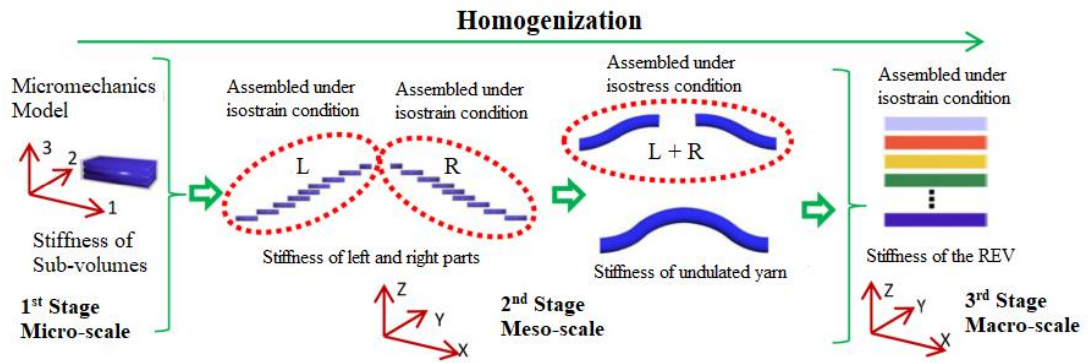
Figure 2.7: Schematic of 3 Stage Homogenisation Method (3SHM) developed by Hallal et al. (2012)

In the literature, the bulk of fairly recent research (Doitrand et al. 2015; Naouar et al. 2014; Wehrkamp-Richter, De Carvalho & Pinho 2018) focuses on FE simulation for accurately predicting the meso-scale mechanical properties of textile composites. However, the current research aims to develop an efficient strategy for multi-scale analysis of wrinkling during the composite consolidation process. Then, an analytical model for determining the effective mechanical properties of woven composite at the meso-scale would be preferred. It has been demonstrated that the analytical model developed by (Naik 1994) for overall stiffness of 5-harness satin weave composite gave good correlation with experimental results, while maintaining flexibility and being easy to apply with less time consumption in comparison with corresponding numerical FE models. Therefore, analytical technique of Naik (1994) would be applied for predicting the mechanical properties of a fabric unit cell via the homogenisation technique as input constants of the structural analysis.

2.3. Buckling behaviour of laminated viscoelastic composites

The composite structures employed in the aerospace industry are commonly composed of multiple thin layers (plies) (Hallander, Sjölander & Åkermo 2015). Buckling of composite elements is one of the characteristic failure modes in such structures (Boisse et al. 2018; Hallander, Sjölander & Åkermo 2015; Leissa 1987). Buckling or ply wrinkling is more likely to lead to a sudden and dramatic failure of a component or the whole structure in service (Hallander, Sjölander & Åkermo 2015). As a result, special attention must be given to the design of laminated composite parts so that they can safely support their intended loadings without buckling.

In the literature, much attention has been paid on mechanisms behind wrinkle formation during consolidation onto curved tools. Lightfoot, Wisnom & Potter (2013) proposed a mechanism for the formation of wrinkles due to frictional shear stresses. At very early stages in the cure cycle when the resin is soft, plies can move relative to other plies and the tool surface. The mismatch between the coefficients of thermal expansion (CTE) of the tool surface and the curing composite, combined with a small amount of ply slippage results in shear forces. These shear forces are known to be the primary cause of wrinkle formation. Following a development of a one-dimensional analytical model comprising of uniformly thick layers laid over an external corner radius under the consolidation onto a tighter geometry, Dodwell, Butler & Hunt (2014) assumed that those layers may form wrinkles if they are prevented from slipping over one another. Wrinkling of a ply or buckling occurs when the ply is subjected to compressive stresses in the direction of its fibres generally (Hallander et al. 2013). According to Hallander et al. (2013), although a tensile force may be applied globally, local compressive forces could still be developed in some recess areas, leading to out-of-plane defects during the forming process of quasi-isotropic, multilayer unidirectional (UD) prepreg over a double-curved geometry. Sjölander, Hallander & Åkermo (2016) simulated two different causes for wrinkle development during forming of multi-layer UD prepregs onto a 3D beam geometry to clarify the experimental findings in Hallander, Sjölander & Åkermo (2015). They are global buckling of the entire tack of material due to excessive material and local compression of single layers.

While wrinkles are commonly found in curved composite parts as the localised band of wavy fibres, buckling behaviour of flat laminated composites at the early stage of forming has also attracted the interest of researchers. Wang, Long & Clifford (2009) investigated the out-of-plane bending behaviour of a 3-ply flat UD laminate using large-displacement buckling tests. A bending model combining classical elastic laminate beam theory and uniaxial continuum theory was also developed for further understanding. Although the shape of buckling curves captured from the experimental data and the prediction models agreed reasonably well, there is a mismatch at the transition region from pure elastic to pure plastic (Wang, Long & Clifford 2009). This inconsistency makes simulating the buckling behaviour challenging using a unified model. The predictive model of elastic buckling is actually set to fit experimental data while the practical bending rigidity of the prepreg is still unknown. Dodwell (2015) applied successfully a

general 2D Cosserat model in modelling defect formation of thickly layered beams consisting of stiff layers separated by weak interfaces. This Cosserat continuum model showed the potential of capturing the internal buckling instabilities of laminated composites at the beginning of cure when the resin is very soft. However, the study focused only on the elasto-plastic behaviour instead of the true viscoelastic nature of polymer composites. In short, the predictive models of wrinkle formation during the composite manufacturing while considering the true viscoelastic nature of composites are still in high demand and of interest to composite manufacturers

Currently, manufacturing composite parts with mitigation of defects relies heavily on the designers' experience and trial-and-error practices (Belnoue et al. 2018; Hallander et al. 2013; Weber et al. 2019). Experiments (Belnoue et al. 2018) are costly because a large number of process, material and geometric parameters are involved in composite manufacturing. For example, when studying the micro-level mechanisms for wrinkle formation during hot drape forming of a C-shaped part, Farnand et al. (2017) showed that forming temperature, consolidation pressure and forming rate were important contributors to the fibre misalignment, leading to out-of-plane wrinkling. Moreover, the wrinkling behaviour has been reported to be influenced by the friction between the two sliding prepreg surfaces of noncured composite prepreg materials from a meso-level perspective. Therefore, many efforts have been made at different resolution levels to characterize inter-ply friction as a function of various parameters including volume fracture of fibres, fibre stiffness and the type of toughener (Larberg & Åkermo 2011). In a later experimental study, Larberg & Åkermo (2014) showed that stacking sequences could influence the deformation behaviour of multi-layered unidirectional thermoset prepreg during the sheet forming process significantly. Similarly, Johnson et al. (2019) also agreed that stacking sequence could potentially be the cause of defect generation and then suggested the most compatible stack arrangement together with application rates and favourable temperatures to minimise defect forming during automated production processes.

In previous works related to the wrinkling of viscoelastic composites, less attention has been given to the viscoelastic nature of the plies and the relaxation of the generated residual stresses during composites curing. Due to many parameters required for specific testing processes, predictive modelling to improve the understanding of

design engineers about the wrinkling phenomena has become of paramount importance in the past two decades (Boisse, Hamila & Madeo 2016). Various process models have been developed by researchers to accelerate the insertion of different composites by simulating the behaviour of composite parts during their manufacturing process (Amini Niaki et al. 2019; Niaki et al. 2018). However, only a few of these models are able to capture the development of wrinkles accurately. The simplified model of Dodwell, Butler & Hunt (2014) was employed to determine parametric influences such as bending stiffness of single uncured ply, part thickness and tool radius on wrinkle wavelength and critical limb length during the forming process. Only the elastic buckling mechanisms coupled with geometric consolidation were considered and therefore the viscoelastic nature of the polymer composite and its effect, especially at the early stage of cure, were not well-investigated. Only recently, Alshahrani & Hojjati (2017c) proposed a theoretical model for predicting the bending behaviour of woven fabric under conditions relevant to forming process. Besides, a new bending test that provides sufficient control of loading rates and processing temperatures, as well as viscoelastic considerations, was also established for prediction of the parameters and validation of the proposed model (Alshahrani & Hojjati 2017b). However, their predictive model which is based on the principle of time-temperature superposition still overestimated the measured bending moment. Also, the test method was almost impossible in high temperature conditions (over 120°C) due to dependence on a non-contact heater facility.

To reduce the number of manufacturing trials, predictive finite element (FE) models for simulating wrinkle formation and its effect have been developed by several researchers. Linear buckling analysis of laminated plates under combined biaxial and shear loading was conducted numerically by Nali, Carrera & Lecca (2011). Two-dimensional plate modelling was considered and materials were assumed isotropic, orthotropic and anisotropic, alternately. Various plate finite element models were analysed to identify the most appropriate model for each class of buckling problem. However, the study focused on only cured (solid) laminates. On the contrary, the predictive numerical models of Belnoue et al. (2018) have proven the potential to capture effectively the wrinkle formation during consolidation. Nevertheless, specific attention is given to thick L- and C-sections and influences of different boundary conditions. Some other numerical studies on the influence of wrinkles on compressive strength were performed by simulating embedded fibre wrinkle defects before proceeding numerical

31

analyses of structural performance (Lemanski & Sutcliffe 2012; Mukhopadhyay, Jones & Hallett 2015; Xie et al. 2018). At present, FE models that can predict wrinkle formation effectively during the composite manufacturing while considering the true viscoelastic nature of composites are still in high demand and of interest to composite manufacturers.

2.4. Bending behaviour of woven composites during forming processes

Advanced composite materials have increasing use in structural applications for aerospace, automotive, and marine industries thanks to their exceptional properties like higher specific stiffness and strength, as well as ability for net shape manufacturing (Farnand et al. 2017). Woven-reinforced composites are preferred due to their improved ability to produce complex shapes (Naik 1994). However, formation of process-induced defects such as wrinkles poses obstacles to fully exploiting the potential of advanced composites (Hallander, Sjölander & Åkermo 2015). Typically, aerospace industry process specifications limit the degree of defects for certification purposes. For instance, when it comes to wrinkles, the length and out-of-plane height of the wrinkles are kept within well-defined limits to minimise their influence on the mechanical performance of the end-part. Wrinkle development is facilitated during the forming process of complex composite components such as stringers by out-of-plane bending as well as in-plane shear deformations (Long 2005; Margossian, Bel & Hinterhoelzl 2015). As such, accurate prediction of in-plane and out-of-plane characteristics of an uncured laminate, as well as inter-ply slippage (Alshahrani & Hojjati 2017a) during the composite forming is highly desirable to optimize the forming process of composites and mitigate wrinkle formation. Although several studies on the bending properties of cured prepreg materials have been published, efficient numerical modelling of large viscoelastic composites remains a significant challenge in the composite manufacturing industry. Given that the high-fidelity simulation of viscoelastic behaviour of large composite parts during forming process takes significant set-up and computational time, industry often relies on trial-and-error experimental methods instead of simulation. This highlights the need for developing efficient simulation methods. This study focuses on predicting the bending behaviour of woven composites using an efficient multi-scale modelling approach as a first step towards developing a fast and comprehensive multi-scale framework for viscoelastic analysis of woven composites during cure.

2.4.1. Bending properties of uncured thin laminates

Bending properties of uncured thin laminates are known to significantly affect the occurrence of wrinkles, particularly in determining the shape of wrinkles (Alshahrani & Hojjati 2017a; Belnoue et al. 2018; Boisse et al. 2018; Huang et al. 2020; Liang et al. 2014). For example, increasing the bending rigidity of the laminate leads to an increase in the size of the wrinkles (Boisse et al. 2011). Numerous experimental studies (Alshahrani & Hojjati 2017b; Bilbao et al. 2009; Liang et al. 2014; Martin, Bhattacharyya & Collins 1995; Wang, Long & Clifford 2009) have been conducted in the recent decade to characterise the out-of-plane bending behaviour of prepregs. To eliminate time-consuming and costly measurement trials, various researchers have developed numerical models for the composite forming process. Forming simulations for composite fabrics were carried out under the membrane hypothesis (Larberg & Åkermo 2014; Skordos, Monroy Aceves & Sutcliffe 2007), i.e., neglecting the bending stiffness. For example, Larberg & Åkermo (2014) developed a methodology for modelling the in-plane deformations of unidirectional (UD) prepregs. Both in-plane shear and inter-ply friction were considered in the forming model of stacked thermoset UD prepregs in Larberg & Åkermo (2014). Subsequently, it was shown that bending stiffness has a substantial influence in determining the magnitude and intensity of wrinkles (Boisse et al. 2018). Other studies (Alshahrani & Hojjati 2017a, 2017c; Haanappel & Akkerman 2014) suggested that the final desired shapes after forming of composite prepregs are determined by the complex interaction of intra-ply shear (including longitudinal and transverse intra-ply shearing), inter-ply slippage and out-of-plane bending. Numerous efforts have been made to incorporate such diverse deformation mechanisms into the composite forming model to accurately predict wrinkle evolution during the forming process. To capture such complex mechanisms, some researchers (Alshahrani 2020; Alshahrani & Hojjati 2017a; Hallander et al. 2013) have employed Aniform Finite Element (FE) software with shell elements to model the viscoelastic bending behaviour of composite plies under conditions relevant to the forming process. It is worth noting that the Aniform shell is a combination of a membrane element (LTR3D) and a Discrete Kirchhoff Triangle (DKT) element, which potentially can capture both in- and out-of-plane properties. However, time-consuming characterisation tests are required to determine the material parameters for a suitable constitutive model. For instance, the bias extension test was conducted and simulated in Aniform in order to obtain the fitted

parameters for the membrane elements (Alshahrani & Hojjati 2017a; Farnand et al. 2017). Furthermore, despite the fact that a plate or shell theory can provide kinematics for points in the thickness, kinematics in the thickness of textile reinforcements is very specific, especially for thick textile reinforcements, due to relative slippage (Boisse et al. 2018).

Accuracy of 3D predictive tools highly depends on the input properties. For a reliable forming simulation, the properties of the uncured material must be accurately represented in the finite element models. As a result, significant research has concentrated on characterizing three types of rigidity that can be used as inputs to wrinkling simulations: tensile, in-plane shear, and bending (Alshahrani 2020; Boisse et al. 2011; Haanappel et al. 2014; Long 2005). For this purpose, mechanical tests such as biaxial tests for tensile stiffness, picture-frame and bias-extension tests for in-plane shear stiffness and bending tests have been performed. The bias-extension test, which is a substitute for the picture-frame test, is intended to introduce pure shear into the material. As the in-plane shear behaviour is considered to be the most dominant deformation mechanism during forming process, finite element models have been developed using material models calibrated with bias-extension tests for in-plane shear stiffness (Alshahrani 2020; Alshahrani & Hojjati 2017a; Haanappel et al. 2014; Larberg & Åkermo 2014; Sjölander, Hallander & Åkermo 2016). Thereafter, the calibrated fibre stiffness values of uncured composites are retrieved from the measured shear data and used as inputs to the corresponding FE simulations of the bias extension tests. These fitted values for bias-extension simulations on specific composite prepregs available in the literature are summarized in Table 2.1. While Larberg & Åkermo (2014) conducted bias-extension tests on cross-plied UD thermoset prepregs (T700/M21 and HTS/977-2), Haanappel et al. (2014) applied bias-extension experiments for a woven glass fibre reinforcement (8HS/PPS). Bias-extension testing on multi-layer stack UD prepreg materials containing either HT (High Tenacity) fibre or IM (Intermediate Modulus) fibre and same matrix was considered by Sjölander, Hallander & Åkermo (2016). In recent studies conducted by (Alshahrani 2020; Alshahrani & Hojjati 2017a), using such a bias-extension test, the in-plane shear properties of 5HS satin weave impregnated with Cycom 5320 at forming conditions were characterized over a range of processing temperatures. The bias-extension response and simulation fit lead to a prediction of fibre stiffness as shown in Table 2.1. However, it should be noted that the value of the fibre stiffness was reduced compared to the real value reported in the data sheets to obtain a more stable simulation

without a comprehensive investigation (Alshahrani 2020; Larberg & Åkermo 2014; Sjölander, Hallander & Åkermo 2016).

Bending tests have been widely used in the literature to assess ply bending stiffness for out-of-plane behaviour. Unlike cured composites, uncured prepregs may simultaneously promote mechanisms such as intra-ply slippages between fibres and local micro-buckling of fibres during bending since the resin is not stiff enough to prevent their occurrence (Belnoue et al. 2018; Boisse et al. 2018). The combined deformations result in the composite prepregs having an apparent lower bending rigidity than conventional solid materials. Therefore, the bending properties have been investigated experimentally and characterized separately from the in-plane properties (tensile and compressive moduli) by (Alshahrani & Hojjati 2017a; Sjölander, Hallander & Åkermo 2016). (Alshahrani & Hojjati 2017a; Sjölander, Hallander & Åkermo 2016) carried out cantilever bending tests and later calibrated the bending properties of a single ply using replication of the bending simulations. While Sjölander, Hallander & Åkermo (2016) used an orthotropic elastic model to simulate the bending stiffness in the fibre direction and transverse to the fibre direction, Alshahrani & Hojjati (2017a) employed an isotropic viscoelastic material model for the out-of-plane bending elements. Table 2.1 lists the input parameters for the out-of-plane material properties based on the cantilever bending experiments. Similarly, Belnoue et al. (2018) adapted the cantilever test proposed by Liang et al. (2014) for capturing bending behaviour of a thermoplastic based prepreg at different temperatures. By measuring the bending stiffness in the fibre direction of an uncured prepreg ply (IMA-M21), material characteristic (i.e. Young's modulus along the fibre direction) was derived from the beam theory (see Table 2.1) and used as an input for the FE consolidation model. Dörr et al. (2017), on the other hand, used a dynamic rheometer within a thermal chamber, rather than the more typically used static cantilever, to characterize the bending properties of a single ply of unidirectional (UD) reinforced PA6-CF tape. A constant parameter was used for the spring element in the viscoelastic material model to fit the bending characterization curve.

As discussed previously, the bending properties of an uncured prepreg were modelled separately from its in-plane properties using specific material models for the fibre and matrix (Alshahrani 2017; Sjölander, Hallander & Åkermo 2016). However, other researchers (Dangora, Mitchell & Sherwood 2015; Yu et al. 2005) have attempted

to relate bending stiffness to axial moduli (i.e. compressive and tensile modulus) using a hybrid model. Contrary to traditional isotropic materials, it is hypothesised that fibrous materials can exhibit significantly varied responses in tension and compression (Dangora, Mitchell & Sherwood 2015). While fibre is extremely strong and stiff under tension, it will buckle with extremely modest compressive stresses. As a result, the bending stiffness of fibrous materials cannot be obtained directly from the tensile modulus; it must be measured through experiments (Dangora et al. 2016). For instance, the vertical cantilever method was used to analyse the bending behaviour of a cross-ply thermoplastic lamina, Dyneema HB80 (Ultra-High Molecular Weight Polyethylene fibres embedded in a polyurethane matrix (DSM 2014), at elevated temperature (up to 120°C). A tensile test was also conducted to measure the apparent elastic modulus of such thermoplastic composites as a function of temperature. Subsequently, the obtained tensile modulus and bending stiffness were used to calculate an effective compressive modulus following an equation proposed by Dangora, Mitchell & Sherwood (2015) for implementation into the finite element model. Similarly, Yu et al. (2005) introduced an asymmetric axial modulus to calculate bending rigidity from the in-plane stiffness (i.e. tensile and compressive rigidities). The asymmetric axial modulus, defined as the ratio of compressive modulus to tensile modulus, was determined by conducting a cantilever deflection test in the warp and weft directions and then implemented into the FE software through a user material subroutine (Abaqus UMAT) for simulation of three-dimensional bending deformation. Alshahrani & Hojjati (2017c) derived an expression for the equivalent bending stiffness as a function of compressive, tensile and relaxation modulus. The compressive modulus of prepreg was calculated by the slope of the stress-strain curve of an elastic region in a buckling test, while the tensile modulus was provided by the supplier. A generalised Maxwell model was applied to fit the stress-relaxation response measured from the cantilever bending test, and parameters for the relaxation modulus were consequently obtained. The computed in-plane properties of the prepreg samples used as input parameters for FE bending models are listed in Table 2.1.

Considering experimental studies on uncured composites, it is apparent that accurate prediction of the mechanical properties of composites under bending is quite challenging. According to the extensive literature review conducted in this chapter, it was found that regardless of the fibre type (i.e. carbon or glass fibre), fabric architecture (i.e. UD or woven fabrics) or impregnated resin, a low value of around 1 GPa, downscaled

from a real value for the fibre stiffness (e.g., 200 GPa for carbon fibre), is commonly used in most numerical models (Alshahrani 2020; Alshahrani & Hojjati 2017a; Haanappel et al. 2014; Larberg & Åkermo 2014). However, this low value has not been justified clearly in the literature (Sjölander, Hallander & Åkermo 2016). Moreover, bending properties at elevated temperatures were estimated based on an educated guess (Haanappel et al. 2014). Hence, a better understanding of the mechanical properties of uncured composites under bending is crucial for successful forming simulations. This is accomplished using a multi-scale modelling framework that incorporates analyses at different scales and is accomplished in a general-purpose finite element code, Abaqus. Due to the limitation of Abaqus built-in viscoelastic model to isotropic materials, an orthotropic viscoelastic constitutive model implemented as a UMAT (Malek 2014; Zobeiry et al. 2016) is considered. Using this material model, the influence of ply anisotropy on the bending behaviour is investigated.

Table 2.1: List of experimental studies on deformation of uncured composites and calibrated material properties for the corresponding FE simulations.

Fibre modulus (E_1) in MPa	Material	Test	Temperature	Loading rate	Reference
1000	Cross-plied UD thermoset prepregs	Bias extension		40 mm/min	(Larberg & Åkermo 2014)
	T700/M21		85°C		
	HTS/977-2		70°C		
1000	Carbon UD/PEEK	Torsion bar	390°C	25, 100, 400 mm/min	(Haanappel et al. 2014)
	Glass 8HS/PPS	Bias extension	310°C		
1000 for HT fibres and 1200 for IM fibres	Stacked UD prepreg with the same epoxy matrix and - HT carbon fibres	Bias extension	70°C	0.05 mm/min	(Sjölander, Hallander & Åkermo 2016)
100 [a]	- IM carbon fibres	Bending			
1000	5HS satin weave (6 k	Bias extension	70°C	20 mm/min	

275[b]	carbon fibre tows with Cycom 5320)	Bending			(Alshahrani & Hojjati 2017a)
1200	5HS satin weave (6 k carbon fibre tows with Cycom 5320)	Bias extension	Room temperature	20 mm/min	(Alshahrani 2020)
580[b]		Bending			
125[b]	PA6-CF UD-Tape	Rheometer bending	260ºC		(Dörr et al. 2017)
735 - 40000[c]	IMA-M21	Bending	110ºC - 30ºC		(Belnoue et al. 2018)
14000 - 44000[d]	Dyneema HB80	Tensile	120ºC - 20ºC	102 mm/min	(Dangora et al. 2016)
0.015[e]	Glass/PP commingled plain weave	Bending			(Yu et al. 2005)
150 - 200[f] for weft/warp	5HS satin weave (6 k carbon fibre tows with Cycom 5320)	Buckling	Room temperature	180 mm/min	(Alshahrani & Hojjati 2017c)
600 - 700[g] for weft/warp		Bending	70ºC		

Note: [a] Bending stiffness in the fibre direction used in the orthotropic elastic model for out-of-plane properties.
[b] Isotropic Hooke modulus represents an elastic spring in the viscoelastic material model for the out-of-plane bending elements.
[c] Young's modulus of the prepreg sheet in the fibre direction against temperature.
[d] Tensile modulus of Dyneema HB80 in the fibre direction against temperature.
[e] Asymmetric factor
[f] Compressive modulus of the prepreg samples
[g] Unrelaxed modulus of the prepreg samples under bending at forming conditions

Chapter 3. Research methodology

In the present research, the multi-scale method originally developed by Malek (2014) implemented which is here for determining the wrinkling during consolidation of thermoset composites. The proposed multi-scale approach ensures high efficiency when analysing the behaviour of large composite structures in practice or in applications where time-dependent (viscoelastic) response (i.e. in process modelling) is of interest. Accuracy requirement was also examined for new composites with directional dependent (orthotropic) properties (Malek 2014).

The approach consists of two key resolution scales, known as micro-scale and macro-scale (see Fig. 3.1). Note that the macro-scale is the scale at which the structural response is of interest. At lower scales such as the micro and meso levels, the effective viscoelastic properties of a unidirectional RVE or RUC of the woven fabric reinforced composites are determined using analytical models developed by Malek (2014) and Naik (1994). The obtained effective mechanical characteristics at small-scale contexts are subsequently used as inputs for structural analysis at the macro-scale. The following sections describe the methodology in detail.

In Malek (2014), the author focused on developing analytical micromechanics equations for predicting accurately the effective viscoelastic properties of the solid unidirectional (UD) circular fibre composites. In this thesis, the accuracy of these equations in determining the effective properties of uncured/cured UD composites with given inputs for component properties (i.e. fibre and resin) under a certain loading condition (i.e compression) is examined. The obtained predictions are compared with with data measured available in the literature. A meso-scale considering the weaving pattern has been included into the multi-scale modelling approach to estimate the effective properties of fabric. Unlike previous studies, the viscoelastic contribution of resin as well as fibre stiffnesses under different loading conditions and fabric architecture (for woven composites) are taken into account. The obtained effective properties have been validated wherever experimental tests are available in the literature. At the macro-scale, the wrinkling analyses (i.e. buckling and bending) during the early stage of cure have been verified and validated with analytical and experimental results using the obtained effective mechanical characteristics at small-scale provided as inputs.
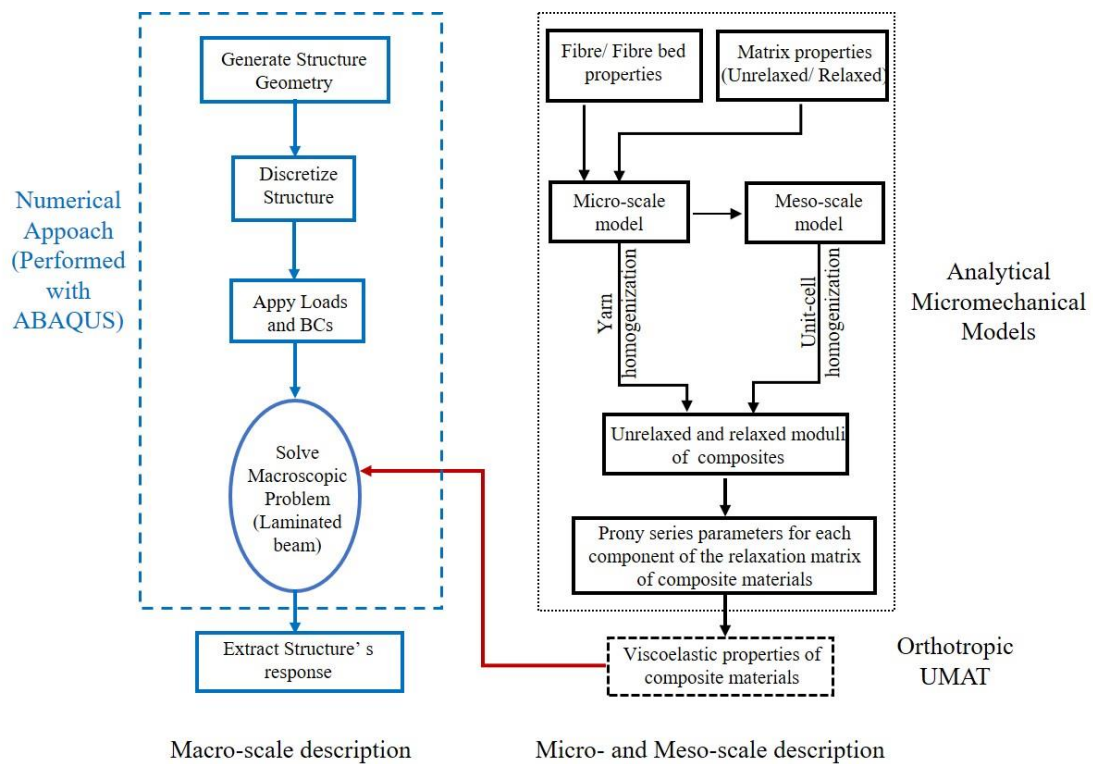
Figure 3.1: Schematic of the multi-scale modelling framework for viscoelastic modelling of orthotropic composites (Adopted from Malek (2014))

3.1. Micro- and meso-scale model

The effective viscoelastic characteristics of orthotropic composites are first modelled in the multi-scale analysis of viscoelastic composites. At the micro-scale, the analytical micromechanics equations described in Malek (2014) serve to to predict the effective elastic and viscoelastic properties of the solid unidirectional (UD) composites with a specific fibre volume fraction (V_f) (see Fig. 2.1). The effective properties obtained from the micromechanics model are then used to estimate the effective properties of the fabric at the meso-scale. The fabric is composed of two sets of interlacing, mutually orthogonal (warp and weft) yarns. The chosen weave type in this study is a 5-harness satin (5HS) (see Fig. 1.4c), which has advantages over plain and twill weaves in terms of drapability and conformity over complex shapes (Alshahrani & Hojjati 2017b). Based on the pattern in the woven fabric, a small RUC which is adequate to represent the fabric architecture is isolated. Details of geometric modelling of 2-D 5-harness satin weave composite along with discretisation technique of yarns within RUC and calculation of 3D effective stiffnesses are presented here, which is based on the work reported in Naik (1994). The analytical procedure was implemented in MATLAB. The obtained effective

40

mechanical characteristics at small-scale contexts are subsequently used as inputs for structural analysis at the macro-scale.

3.1.1. Micro-mechanical modelling of UD composites

As reviewed in Chapter 2, CCA (Hashin & Rosen 1964) and GSC (Christensen & Lo 1979) models are employed at the micro-scale to calculate the longitudinal and transverse elastic properties respectively of the UD composites. Note that the method has already been evaluated and compared with the numerical approach in Malek (2014). In this thesis, the accuracy of these equations in determining the effective properties of UD composites with given parameter inputs for component properties (i.e. fibre and resin) is examined by comparing the obtained predictions with data measured available in the literature. Moreover, such micromechanics models are used as a tool to obtain the mechanical properties of UD composites that would be input parameters for the structural analysis at the macro-scale.

Micromechanical models are used to combine the elastic mechanical properties of the fibre and the unrelaxed and relaxed properties of the polymer. Due to the viscoelastic characteristic of the resin, the combined composite also exhibits viscoelastic behaviour. The viscoelastic properties would be obtained by simply assuming the viscoelastic behaviour of the resulting composite as similar to the viscoelastic behaviour of the resin constituent. It means that the relaxation time and weight factors describing the viscoelastic response of the resin and the corresponding composite are assumed to be the same.

3.1.2. Analytical procedure for predicting elastic engineering constants of woven composites at the meso-scale

At the meso-scale, an easy but accurate geometric modelling and analysis procedure for 5HS satin weave composite developed by Naik (1994) is employed. Firstly, a three dimensional preform architecture of such a fabric reinforcement composite has to be described properly. Based on the pattern of the woven composite, a RUC is represented for the preform architecture. Detail of the geometric modelling technique of 5HS satin weave is demonstrated in section 3.1.2.1. Later, the 3D effective stiffnesses for the woven composite are determined in section 3.1.2.2. This is done by dividing each yarn in the

RUC into discrete yarn slices with specific material characteristics, spatial direction and volume fraction of each yarn slice obtained from the previous step.

3.1.2.1. Geometric modelling of 5HS satin weave

In the first step, the effective properties obtained from the micromechanics model for UD prepregs or yarns at the micro-scale are used to estimate the effective properties of the fabric at the meso-scale. The RUC for the 2-D, 5-harness satin (5HS) weave is presented in Fig. 3.2a. The sectional view (section A-A) illustrates the undulations of a warp yarn over one and under four weft yarns.

The 5HS satin weave composite is commonly described by quantities including yarn spacing, a, yarn filament count, n, yarn packing density, p_d, filament diameter, d_f and overall fibre volume fraction, V_f. The projected length, L_p was a equation of the yarn spacing, a, and defined by $L_p = 5 \times a$ (see Fig. 3.2a). The volume filled with the ten yarns within the RUC was calculated by $10 \times A \times L_p$ in which A was the yarn cross-sectional area. By assuming that A was constant along the yarn length and same for both the warp and the weft yarns, the volume of the RUC was $L_p \times L_p \times H$, where H stood for the RUC thickness. Provided with such known quantities, unknown quantities such as yarn thickness, t, yarn cross-sectional area, A, can be calculated using equations written as follows:

$$V_f = \frac{2p_d A}{Ha},$$
(3.1)

$$A = \frac{\pi d_f^2 n}{4p_d},$$
(3.2)

The yarn thickness, t, was determined from the RUC thickness, H, by $t = H/2$. By assuming there was no gap between adjacent, the yarn width, w, was then computed by $w = a$.

The undulations were centred at cross-over points (COP) where a yarn crosses over or under another yarn (see Fig. 3.2a). For the 5-harness satin weave, by looking at Fig. 3.2a from the bottom, the warp yarns in the first and fourth rows had three COPs while the warp yarns in the second, third and fifth rows had two COPs. In every undulating part, it was assumed that the yarn centreline path followed a sinusoidal

expression. The sine function had its origin at the COP and was formulated using the vertical shift, V_s, and the undulating length, L_u. For instance, the undulation, Z_c, at each COP was given by:

$$Z_c = \pm \frac{V_s}{2} \sin\left(\frac{\pi X_c}{L_u}\right), \qquad (3.3)$$

where X_c was a distance from the corresponding COP in the warp yarn direction (see Fig. 3.2a). The vertical shift, V_s in Eq. (3.3) was equal to the thickness, t, of the yarns. A negative sign in Eq. (3.3) was used to define the undulation at the central COP for the warp yarn shown in section A-A (see Fig. 3.2a). Conversely, at the COPs located on the RUC edges for the same warp yarn, a positive sign was used in Eq. (3.3). Similarly, the undulation path for the other warp yarn in the RUC was defined with the relevant sign and sine wave portion at each COP. The undulations in the weft yarns were also depicted using Eq. (3.3) in which X_c was measured along the weft yarn direction. The parameter, L_u, was calculated by assuming that the cross-sectional shape of the yarns (see in Fig. 3.2b) was composed of a central flat portion of thickness, t, and two sinusoidal lenticular end portions. It was considered that the curved portions of the yarn cross-section followed the sine form of Eq. (3.3). Hence, the width of the curved portion of the yarn cross-section was equal to $L_u/2$. The cross-sectional area, A, was consequently given by:

$$A = wt - L_u V_s \left(1 - \frac{2}{\pi}\right), \qquad (3.4)$$

By combining Eqs. (3.2) and (3.4), the unknown parameter, L_u, was withdrawn. The total length of the straight portions, L_{st}, of each yarn was as follows:

$$L_{st} = 5a - 2L_u, \qquad (3.5)$$

In short, using Eqs. 3.3 – 3.5, geometry parameters necessary for the description of 5HS satin weave such as the yarn cross-sectional area, yarn thickness and yarn paths could be determined with a given knowledge of the yarn filament counts, yarn packing density, yarn spacing, filament diameter and overall fibre volume fraction. Furthermore, the undulation in the yarns is commonly represented by its crimp angle (see Fig. 3.2b). The crimp angle, θ_c, was given by:

$$\tan(\theta_c) = \left| \left(\frac{dZ_c}{dX_c} \right)_{X_c=0} \right|, \qquad (3.6)$$

where θ_c is commonly in a range of θ_{min} and $\pi/2$ with θ_{min} calculated by the constraint $w \geq L_u$.
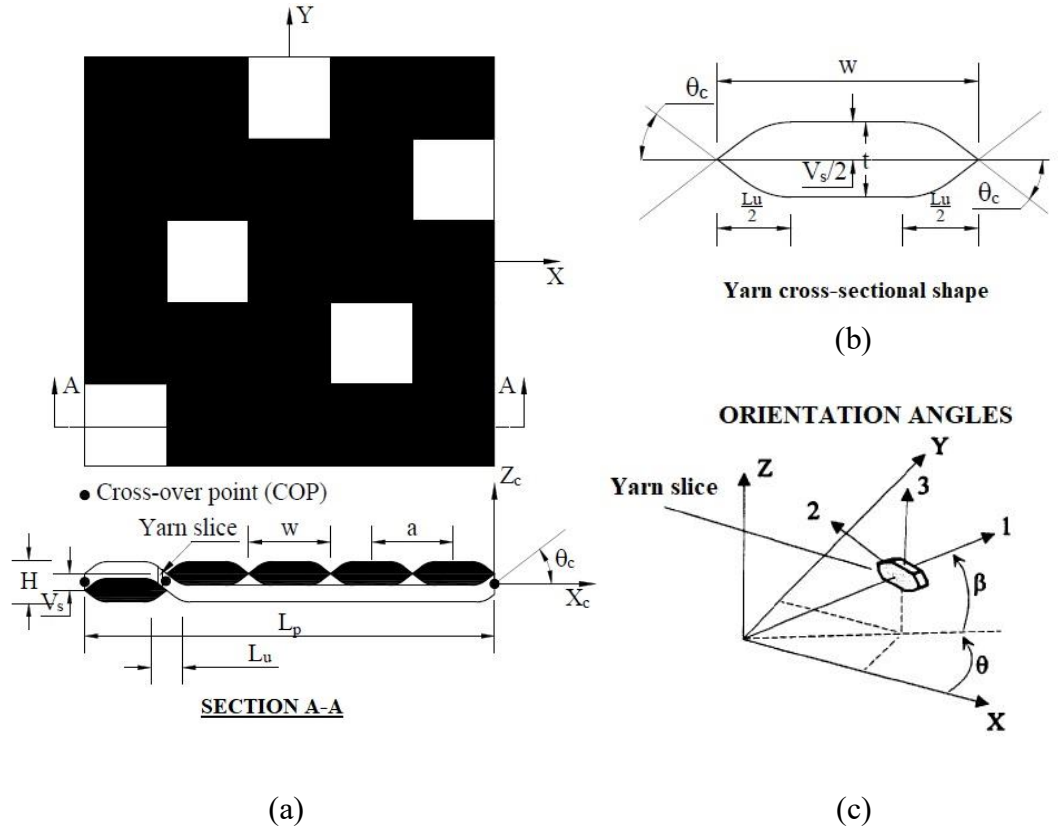
Figure 3.2: (a) The RUC geometry and notation for a 5-harness satin weave composite; (b)Yarn cross-sectional shape (c) Orientation angles

3.1.2.2. Discretisation technique of yarns and determination of three-dimensional effective stiffnesses

Having described the woven architecture, overall composite properties would be calculated by dividing yarns within the RUC into discrete slices. The straight parts of each yarn path, L_{st} were considered as a sole slice. Meanwhile the undulating parts, L_u were discretised into equal straight slices, n, perpendicular to its in-plane and the XY-plane as seen in Fig. 3.2c. The reason for this was to approximate the undulating, sinusoidal yarn path to n straight yarn slices with equal volume of $A \times L_u/n$.

The spatial coordinate of each yarn slice was specified by the in-plane angle, θ and the out-of-plane, β as shown in Fig. 3.2c. It can be seen that θ is made with the X-

axis while β is made with the X-Y plane. As the woven architecture is composed of interlacing, mutually orthogonal (warp and weft) yarns, the angle θ was either 0 for warp yarns or 90 degrees for weft yarns. The angle β was determined for each yarn slice by differentiating the sine function mentioned above for the undulating yarn centerline path. Therefore, the straight portions of the yarn path had $\beta = 0$.

In summary, every yarn within the RUC was approximated by straight yarn slices with known quantities such as volumes and orientation angles (i.e. θ and β). The volume filled with the resin in the RUC was subsequently calculated by subtracting the total volume filled with all the yarn slices from the volume of the RUC. It should be noted that the interstitial resin had orientation angles equal to zero as it was modelled as an isotropic material slice.

As a result, the effective stiffness matrix $[C_{\text{eff}}]$ of the RUC was expressed as a function of the yarn slice stiffness matrices (including resin), transformation matrices and volume fractions as (Naik 1994):

$$[C_{eff}] = \sum_{m=1}^{N} \left(V_m [T]_m^T [C']_m [T]_m \right), \tag{3.7}$$

The transformation matrix $[T_m]$ is defined in Appendix A.3. The 6×6 stiffness matrix $[C']_m$ describes the 3D relationship between stress and strain of the mth yarn slice. Each yarn slice is considered to be a transversely isotropic material which requires five independent material constants (E_{11}, E_{22}, G_{12}, v_{12}, and v_{23}, subscript 1 refers to the longitudinal fibre orientation) to describe the $[C']_m$ matrix. Such engineering material constants had been estimated using micromechanics equations (Malek 2014) from known constituent properties such an fibre properties, matrix properties and the yarn packing density p_d (or yarn fibre volume fraction). Additionally, a mesh convergence study was conducted to decide the relevant number of yarn slices, n, in the undulating parts of the yarns, necessary for the convergence of the overall stiffness values $[C_{\text{eff}}]$. It was found that the minimum value of n equal to 12 could result in an unchanged overall stiffness matrix (Naik 1994). The overall stiffness matrix $[C_{\text{eff}}]$ would be inverted to acquire the overall compliance matrix $[S_{\text{eff}}]$ for a later determination of overall moduli and Poisson'ratios.

3.2. Macro-scale (structural) modelling of viscoelastic composites

While the woven fabrics are discrete on the micro-scale, woven composites are assumed to be uniform and continuous at the macro-scale to simplify the computations and improve the efficiency of the analysis. The macro-scale analysis of woven fabrics is mainly conducted to simulate the overall structural behaviour of the prepreg/fabric with the input parameters obtained from micro-scale and meso-scale analyses. Both analytical and numerical methods are considered to be part of the macro-scale analysis. The analytical approach involves simple mathematical equations for predicting specific structural behaviour of an isotropic elastic beam under a small displacement. In the numerical approach, the finite element method is used to predict the bending moment-curvature relationship of both elastic and viscoelastic composite plates at various loading rates.

The composite plate is first assumed to behave as a viscoelastic isotropic solid and modelled using the Abaqus built-in viscoelastic constitutive model which is based on the integral form (IF) of viscoelasticity. As applying Abaqus viscoelastic model is limited to isotropic materials, a more versatile orthotropic viscoelastic constitutive model (based on a differential form of viscoelasticity – DF) developed and implemented as a UMAT by researchers (Malek 2014; Zobeiry et al. 2016) is then employed to elucidate the effect of ply anisotropy on the structural responses of uncured prepregs/5-harness satin weave plates.

3.2.1. Numerical approach using Abaqus built-in viscoelastic model (IF)

To define the viscoelastic behaviour of an isotropic material in Abaqus, an instantaneous elastic modulus is needed to represent the rate-independent elasticity of the material behaviour. The effective relaxation moduli are obtained by multiplying the instantaneous moduli with the dimensionless effective relaxation functions as given below (Section 22.7.1 in Abaqus Analysis User's Guide) (Abaqus 2013a):

$$G(t) = G_o \left[1 - \sum_{i=1}^{N} g_i \left(1 - exp\left(-\frac{t}{\tau_i}\right) \right) \right], \tag{3.8}$$

$$K(t) = K_o \left[1 - \sum_{i=1}^{N} k_i \left(1 - exp\left(-\frac{t}{\tau_i}\right) \right) \right], \qquad (3.9)$$

where t is time, and G_o and K_o are the instantaneous glassy (unrelaxed) shear and bulk moduli determined from the instantaneous elastic moduli, E_o, and Poisson's ratio, v_o:

$$G_o = \frac{E_o}{2(1 + v_o)}, \qquad (3.10)$$

$$K_o = \frac{E_o}{3(1 - 2v_o)}, \qquad (3.11)$$

The characteristic parameters of the Prony laws, g_i and k_i are the weight factors given by:

$$g_i = \frac{G_i}{G_o}, \qquad (3.12)$$

$$k_i = \frac{K_i}{K_o}, \qquad (3.13)$$

where G_i and K_i are the shear and bulk moduli corresponding to the specific relaxation time (τ_i) and N is the number of Maxwell units.

3.2.2. Numerical approach using orthotropic viscoelastic user material model (UMAT)

A recently developed user material subroutine (UMAT) based on the differential form (DF) of viscoelasticity is employed to simulate the time-dependent behaviour of orthotropic laminates. The DF approach and its implementation in Abaqus are briefly described in Appendices A.2 and A.3 respectively. The DF subroutine has been coded in FORTRAN and then implemented through UMAT subroutine. The DF code is capable of modelling the viscoelastic behaviour of isotropic, transversely isotropic (Zobeiry et al. 2016) and orthotropic (Malek 2014) composite material in 3D. Therefore, the effect of ply anisotropy on the buckling behaviour of the viscoelastic composite material can be studied rigorously.

Based on the DF of viscoelasticity, the relaxation functions $G(t)$ and $K(t)$ of an isotropic viscoelastic solid are defined individually in terms of a series of exponentials known as the Prony series:

$$G(t) = G_\infty + \sum_{i=1}^{N} G_i e^{\frac{-t}{\tau_i}}, \tag{3.14}$$

$$K(t) = K_\infty + \sum_{i=1}^{N} K_i e^{\frac{-t}{\tau_i}}, \tag{3.15}$$

in which G_∞ and K_∞ define the long-term shear and bulk moduli (relaxed), respectively. Comparing Eqs. 3.8 - 3.9 to Eqs. 3.14 – 3.15 respectively, the relaxed moduli can be described as:

$$G_\infty = G_o \left(1 - \sum_{i=1}^{N} g_i \right), \tag{3.16}$$

$$K_\infty = K_o \left(1 - \sum_{i=1}^{N} k_i \right), \tag{3.17}$$

For orthotropic viscoelastic solids, the above equations can be generalised as described in Malek (2014) and Zobeiry et al. (2016) for each component of the stiffness matrix. The generalised formulations were reported in the PhD thesis by Malek (2014). Using the generalised form of DF of viscoelasticity, the orthotropic behaviour of composite laminates is investigated numerically in this study and the results are compared with experimental data reported in the literature.

Chapter 4. Buckling analysis of multilayered elastic beams with soft and rigid interfaces

4.1. Introduction

As a first step in providing a better understanding of wrinkle formation, the buckling behaviour of solid laminated beams under compressive loads are examined using various analytical and numerical approaches. Two types of models are created by either using composite layup option available in Abaqus or physically modelling layers before assigning material properties as shown in Fig. 4.1. The purpose is to examine the capability of commercial numerical tools available to design engineers, i.e. composite editor in Abaqus, in simulating the buckling behaviour of layered systems separated by relatively soft viscoelastic layers occurring in manufacturing of a range of laminated composite products.
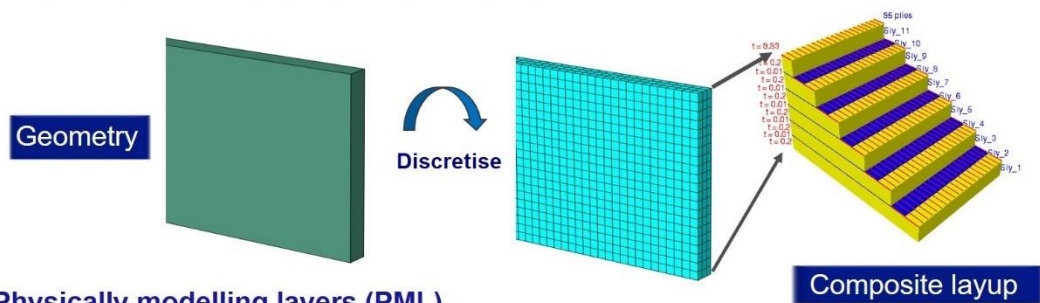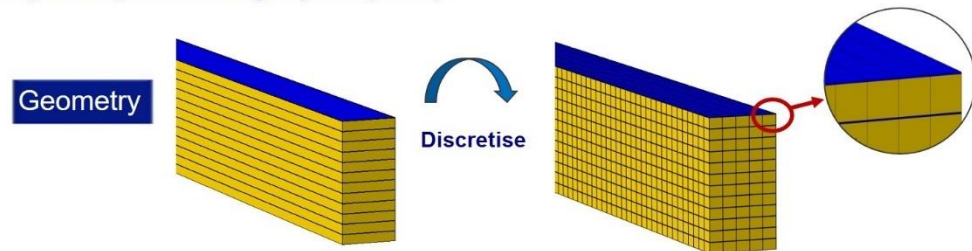
Figure 4.1: Two types of analysis model employed for this study.

In this chapter, predictions of these models are compared with analytical models to verify the proposed modelling approach. Two analytical approaches such as eigenvalue and large deformation analyses are conducted. A new model based on the hypothesis that the resin stiffness dominates the longitudinal compressive strength is also created and shown in Chapter 5. Later, the viscoelastic properties of the resin are included in a macro-scale model by replacing previously assumed elastic inputs for the resin. The effective

properties of the composite would be obtained by using the viscoelastic micromechanical model proposed by Malek, Vaziri & Poursartip (2018). The estimated composite properties are used in the macro-scale FE simulations.

4.2. Method

Three-dimensional multilayered beams are modelled using two approaches; (i) layup composite editor for 3D solid composite elements and (ii) physical modelling of individual layers (with 3D solid elements) and interfaces within Abaqus environment. Each model is composed of $N = 48$ identical stiff layers which are separated by N - 1 soft interfaces similar to reference (Dodwell 2015). The thicknesses of a single layer (ply), t_p, and an interface, t_i, are 0.2 mm and 0.01 mm, respectively, thereby the total thickness of the multilayered beam is $T = Nt_p + (N - 1) t_i$. The generated multilayered beam is 50 mm of length and 1 mm width (h). For verification purposes, both materials are initially assumed to be homogeneous and isotropic. While E_p and v_p, the material properties of the layers, are kept unchanged and equal to 100 GPa and 0.2, respectively, E_i takes a range of values which define the material properties of the interfaces. Identical Poison's ratio is used for plies and interfaces (i.e. $v_p = v_i$).

Using the first approach, the composite characteristic is defined by a composite layup tool in the property module of Abaqus CAE as demonstrated in Fig. 4.2. In the second approach, the beam geometry is partitioned into physical layers (thickness of 0.2 mm) separated by distinct interfaces (thickness of 0.01 mm) before they are meshed and the material properties are assigned.
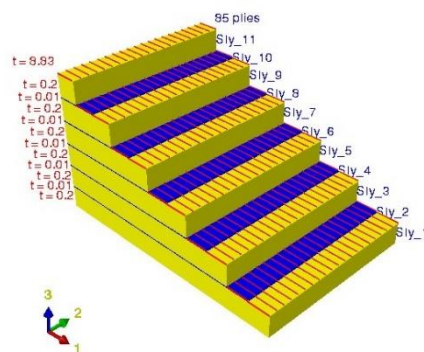
Figure 4.2: Composite layup

To verify the model, the deformation behaviour of multilayered cantilever beams with a range of interface stiffness under a vertical displacement is examined (Case I). Results are compared with a simple beam bending equation to highlight the need for more

sophisticated elements or approaches in this area. Then, the critical buckling loads and the first mode shapes of flat laminates with soft interfaces are compared with those with stiff ones (Case II). The critical buckling loads are presented and compared with Euler buckling estimates. In both cases, the effect of ply anisotropy on the buckling behaviour of laminates with soft and stiff interfaces is investigated.

4.3. Multilayered cantilever beam under bending (Case I)

A $1 \times 10.07 \times 50$ mm multilayered cantilever beam is modelled using a 20-node quadratic brick element with reduced integration element (C3D20R) and mesh size of 0.2 mm. The elastic behaviour of this beam is first examined using the PML approach. While one end of the beam is fixed, a vertical displacement equal to $\varDelta = 0.2$ mm is applied to the other end. Both the layers and interfaces are assumed to be isotropic in Case I. The force, $P,$ at the free edge corresponding to the vertical displacement of 0.2 mm is obtained from finite element analysis and compared with the one calculated from the Euler – Bernoulli beam bending theory (i.e. ignoring shear deflection) (Bauchau & Craig 2009):

$$\Delta = \frac{PL^3}{3EI},$$ (4.1)

where EI is the flexural rigidity of the cantilever beam section. EI is obtained by assuming the layers fully bonded or no interaction between layers which provides a lower bound as demonstrated in Table 4.1. Four cases corresponding to four different values of E_i (interface modulus) are considered; starting at the same stiffness of ply modulus E_p (100 GPa) and reducing by a factor of 10 for the other three subsequent cases.

51

Table 4.1: Comparisons between current FE predictions, Dodwell (2015)'s FE results, and the analytical model based on Euler-Bernoulli kinematics (Eq. 4.1) for a multilayered cantilever beam (Case I).

E_i (GPa)	P (kN)			
	PML$_{FE}$ (Present)	FE (Dodwell)	Lower bound	Upper bound
$1 \times 10^{+2}$	4.485×10^{-2}	4.500×10^{-2}		4.617×10^{-2}
$1 \times 10^{+0}$	3.769×10^{-2}	3.800×10^{-2}		4.412×10^{-2}
1×10^{-2}	3.085×10^{-3}	3.000×10^{-3}	1.6×10^{-5}	4.410×10^{-2}
1×10^{-4}	3.745×10^{-5}	3.700×10^{-5}		4.410×10^{-2}

Table 4.1 highlights a good agreement between results from the present finite element analysis with Dodwell's FE model for all four cases and analytical upper bound when E_i equals E_p, 100 GPa; lower bound when E_i is very soft (1 kPa). It should be noted that only the bending deformation is considered in Eq. (4.1). When $E_i = E_p = 100$ GPa, the contribution of shear deformation is negligible and the multilayered cantilever deforms as a solid isotropic beam based on the assumptions of Eq. (4.1). In the subsequent circumstances with soft interfaces, however, due to severe shear deformations at the interfaces, the layers are more likely to bend more independently, decreasing the apparent flexural stiffness of the entire beam.

To better understand the role of ply anisotropy on the overall beam rigidity, three more cases with transversely isotropic layers are considered. The elastic constants of such layers are listed in Table 4.2.

Table 4.2: Input properties of the transversely isotropic plies.

Properties	Value	Unit
E_{1p}	100	GPa
E_{2p}	8	GPa
G_{12p}	3.98	GPa
G_{23p}	2.86	GPa
v_{12p}	0.26	-*
v_{23p}	0.4	-*

Note: * indicates non-dimensional

52
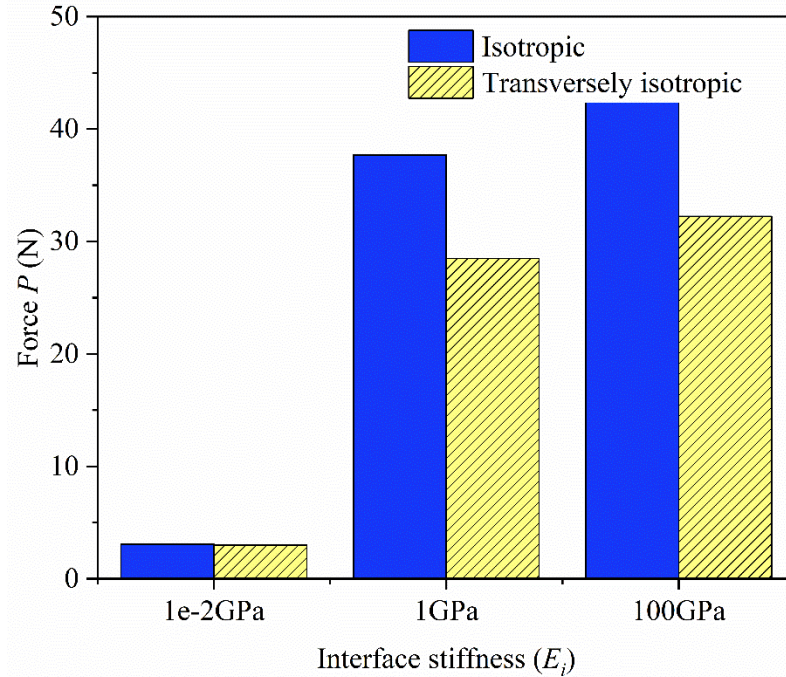
Figure 4.3: The role of interface stiffness and ply anisotropy on the multilayered cantilever beam rigidity.

Fig. 4.3 highlights the role of interface stiffness for isotropic and transversely isotropic laminates. As the interface becomes soft (E_i = 0.01 GPa), the beam flexural rigidity is significantly reduced irrespective of the ply orthotropic nature. In other words, the soft interface dominates the bending response (e.g. uncured prepregs and laminates during cure). However, the beam bending behaviour is dominated by the engineering constants of the plies when the interface is stiff (1 GPa < E_i < 100 GPa). In other words, we could assume that plies are almost perfectly bonded when the interface is relatively stiff (cured laminates).

4.4. Flat laminate under compressive load (Case II)

The buckling behaviour of a flat laminate (10.07 × 1 × 50 mm) is considered here using two different approaches; Abaqus built-in composite editor (CE) and physically modelling layers (PML). Similar cases are also considered with transversely isotropic material properties to understand the role of ply anisotropy on the laminate buckling response.

4.4.1. Two pinned ends

First, the laminate is pin supported and a uniform axial pressure on the free end face is applied. Such a simple buckling scenario is considered because there is an existing analytical solution for verification purposes. The FE results using eigenvalue analyses for both approaches mentioned above along with Euler predictions are summarized in Fig. 4.4. Five interface properties, E_i, ranging from 100 kPa to 100 GPa, equal to constant E_p, are also introduced to investigate the influence of interface stiffness on the overall buckling behaviours.

As seen in Fig. 4.4, results from CE analyses increase slightly as the interface becomes more rigid. With PML models, critical buckling loads reduce significantly in comparison especially when the interfaces are much softer than the plies ($E_i \leq 1$ MPa). PML results are between Euler predictions and when the interfaces are very soft, the results approach the lower bound.

The shapes of buckled beams with stiff interfaces ($E_i = 100$ GPa) are plotted in Fig. 4.5 and 4.6 for CE and PML models respectively. Both mode shapes are identical and buckle in y-plane. However, only PML analysis can capture buckling deformation when the interfaces are very soft (Fig. 4.7). The laminate bends in x-plane, meaning that the layers buckle as N independent beams. The critical buckling stress is therefore dropped significantly, as shown in Fig. 4.4.
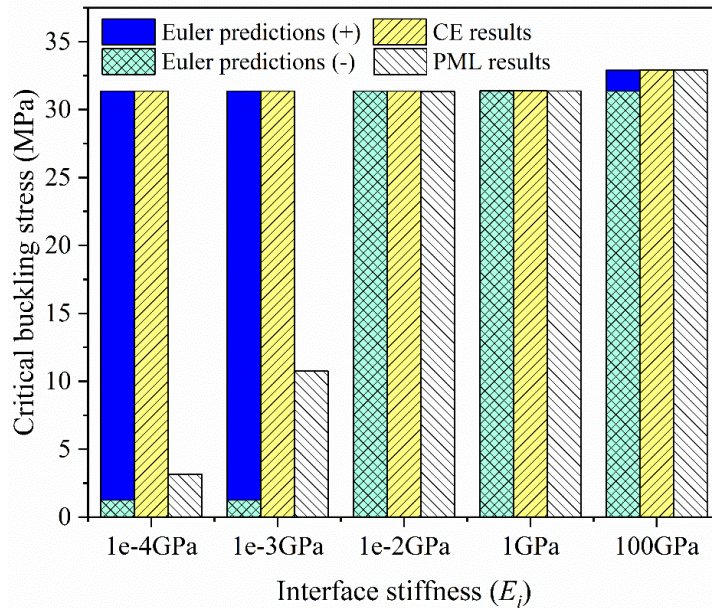
Figure 4.4: Comparisons of FE results with Euler predictions for isotropic plies (E_p= 100 GPa) bonded with a range of interfaces.
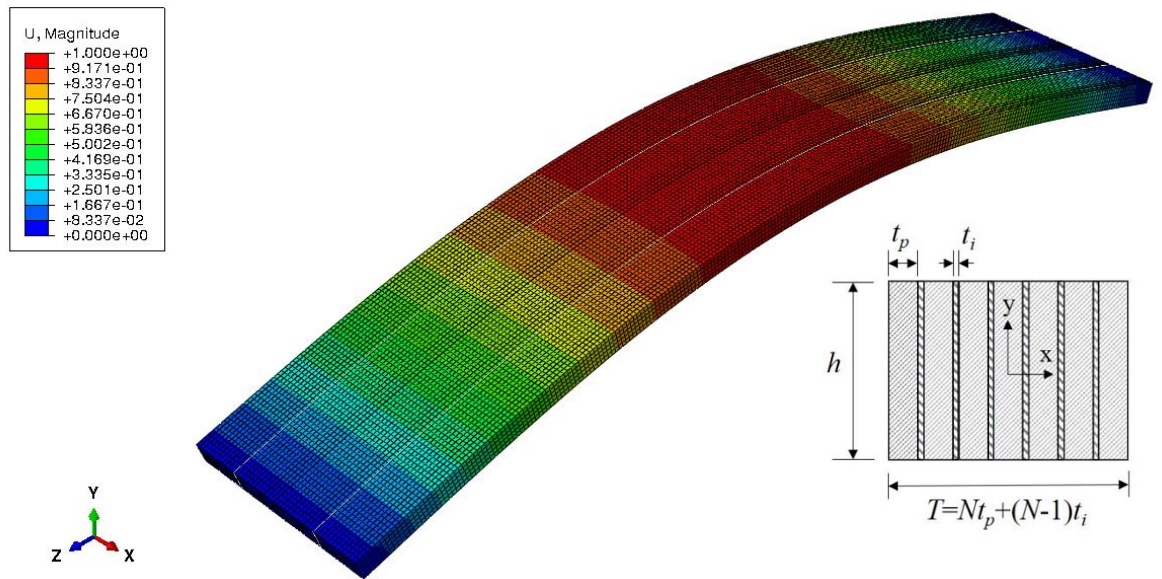
Figure 4.5: Buckling mode shape for flat laminates with stiff interfaces (E_i = 100 GPa) using PML approach. The beam cross section is depicted on the right side.
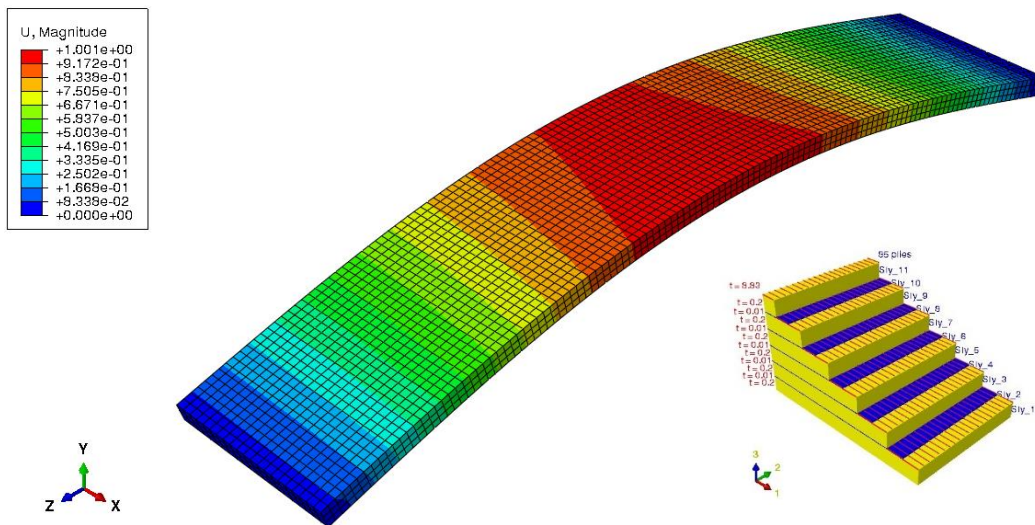
Figure 4.6: Buckling mode shape for flat laminates with stiff interfaces (E_i = 100 GPa) using Abaqus CE. The laminate layup is depicted on the right side for clarity.
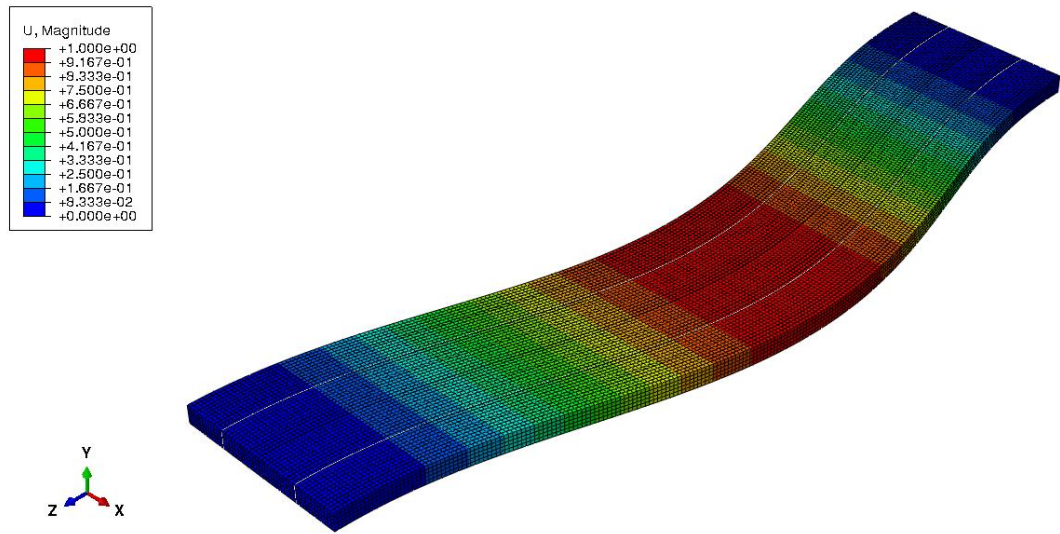
Figure 4.7: Buckling mode shape for flat laminates with soft interfaces (E_i = 100 kPa) using PML approach.

Similar to Case I, the effect of ply anisotropy on the buckling behaviour of laminates is investigated by using PML models and results are presented in Fig. 4.8. Two different transversely isotropic properties listed in Table 4.2 and 4.3 are used for comparison. When the transverse Young's modulus and shear moduli are still high (Table 4.2) their effects on the buckling response are negligible (Fig. 4.8). Results also demonstrate the less significant effect of ply anisotropy compared to the interface stiffness. The interface stiffness (or the presence of resin rich areas between the plies) dominates the buckling response of flat laminates similar to their bending response presented in Case I. During composite processing, the resin modulus may decrease quite significantly. This could lead to formation of wrinkles (buckled plies) under much lower compressive loads which needs to be captured accurately.

Table 4.3: Input properties of the transversely isotropic plies.

Properties	Value	Unit
E_{1p}	100	GPa
E_{2p}	0.8	GPa
G_{12p}	0.398	GPa
G_{23p}	0.286	GPa
v_{12p}	0.26	-*
v_{23p}	0.4	-*

Note: * indicates non-dimensional

56
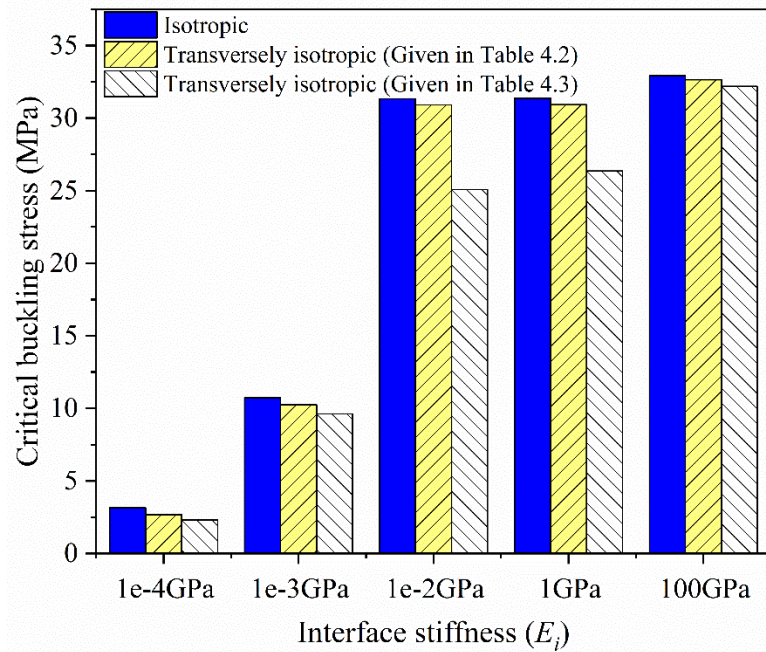
Figure 4.8: The influence of ply elastic constants on the buckling response of flat laminates using PML approach.

4.4.2. Four fixed edges

To look at the role of manufacturing constraints, an additional boundary condition is applied for the two remaining edges of the laminate beam. It is to prevent plies from moving in the plane perpendicular to the compressive load direction, so that plies can buckle internally. Table 4.4 lists preliminary finite element results for beams with a range of interface properties. The four cases correspond to four values of starting with the same stiffness of ply modulus $E_p = 100$ GPa and reducing by a factor of 10 for subsequent cases.

Table 4.4: Comparisons of FE results between composite element models and models layered physically – $E_p = 100$ GPa for all cases

	Laminate 1	Laminate 2	Laminate 3	Laminate 4	Unit
E_i	0.1	1	10	100	GPa
$(P_{cr})_{CE}$	46420	46441	46650	48739	N
$(P_{cr})_{PML}$	6975.8	19152	39494	48698	N

For the beams modelled using Abaqus composite editor (CE), results show that as the interface becomes more rigid, the critical buckling load increases only slightly (see Table 4.4). In contrast, the critical buckling load reduces more than 6 times as the elastic

57

modulus of the interfaces are reduced by a factor 1000 (compare Laminate 1 and Laminate 4) for PML analyses. When the interface and ply modulus are identical (100 GPa), the minimum critical loads obtained using both approaches (CE and PML) are almost the same. As shown in Fig. 4.9, the composite laminate is buckled into seven half waves in the longitudinal direction for the stiff interface (E_i = 100 GPa). Similar mode shape is observed using PML approach for stiff interface as depicted in Fig. 4.10 (red line). However, the predicted critical buckling load (Table 4.4) and first mode shape of laminates with PML become quite different from those modelled using Abaqus CE as the interfaces become soft. It is more likely that the soft interfaces dominate the overall buckling of the multilayered beams which cannot be captured with CE models. When the stiffness of the interfaces decreases, the internal buckling wavelength rises as seen in Fig. 4.10.
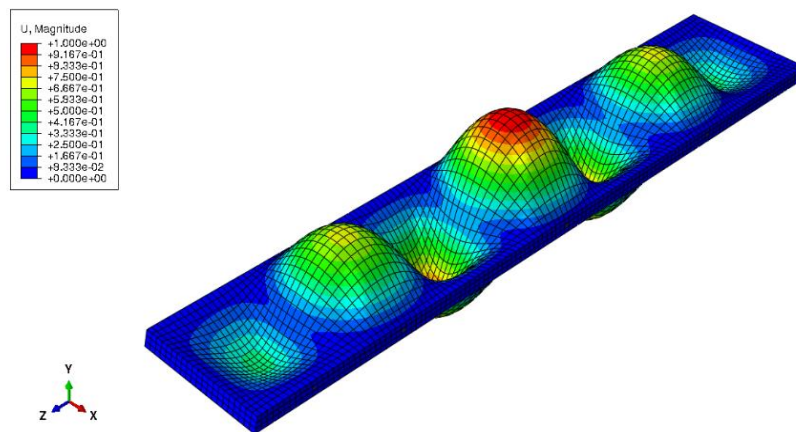
Figure 4.9: Magnitude displacement (in mm) at critical buckling load – Composite element model – E_i = 100 GPa.
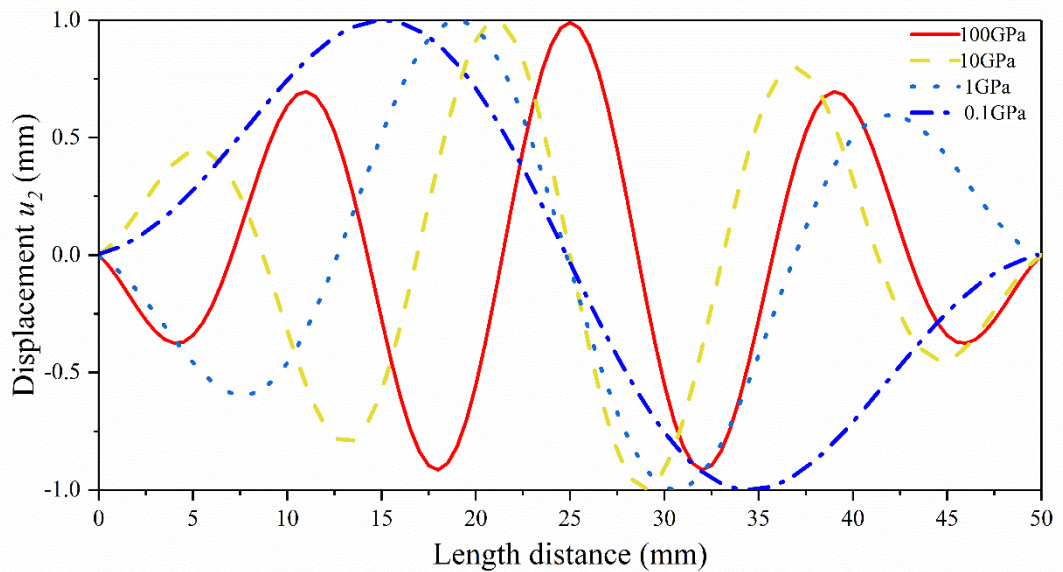
Figure 4.10: Internal buckling wavelength along the beam length – Physically modelling layers.

4.5. Summary and conclusions

The buckling analysis of multilayered composite beams using two different approaches was conducted. The performance of Abaqus built-in composite editor was compared with physically modelling the individual plies and interfaces using solid elements. Results show that Abaqus built-in composite element (CE) is only capable of estimating the composite critical buckling load when the mismatch between layers (plies) and the interface elastic modulus is relatively low. When the interfaces are soft (e.g. at the early stage of cure), a significant difference was demonstrated between finite element results obtained from the composite editor and the physically layered model. Therefore, alternative approaches or elements are required for simulating the deformation of laminates during composite processing accurately. It was demonstrated that by physically modelling the thin interfaces between plies, the significant reduction of critical buckling loads could be captured for laminates bonded with soft interfaces.

The proposed approach is an initial step towards implementing an orthotropic viscoelastic model for multi-scale process modelling of laminated composites with complex microstructures in subsequent chapters.

Chapter 5. Buckling behaviour of laminated viscoelastic composites under axial loads

5.1. Introduction

This chapter considers the viscoelastic nature of the resin during the manufacturing process in the multi-scale modelling approach. The effective properties of the composites obtained from viscoelastic micromechanical models instead of assumed elastic inputs for the resin properties as in Chapter 4 are used in the macro-scale FE model. The orthotropic viscoelastic properties of the laminate are considered by incorporating the fibre-bed elastic properties into the micromechanics equations to estimate the effective viscoelastic properties of the uncured prepreg.

At macro-scale, a more versatile orthotropic viscoelastic constitutive model based on differential form (DF) of viscoelasticity implemented as a user material subroutine (UMAT) compared to using Abaqus built-in viscoelastic model (IF) is employed. This helps to elucidate the effect of ply anisotropy on the buckling response of uncured/partially cured unidirectional (UD) laminates. The numerically viscoelastic modelling approach described in Chapter 3 was used to determine the critical buckling load of both cured elastic and uncured viscoelastic laminated composite under various loading rates. The analytical approach involving simple mathematical equations for estimating the buckling loads in thin elastic plates is provided in the following section for verification purpose. The details of the FE buckling model and its validation by comparing to experimental data available in the literature are also presented in this chapter. Using the numerical model, the influence of various parameters including loading rates, the instantaneous elastic modulus, and in particular the effects of the ply anisotropy on the buckling behaviour of composite laminates are analysed. It has been found that unlike cured composites, the compressive stiffness of uncured prepregs is mainly dominated by the resin modulus rather than the fibre modulus. Additionally, it is shown that the waviness of fibres (fibre-bed effect) which stiffens the prepreg's transverse and shear properties increases its compressive stiffness slightly while the waviness effect on the post buckling stiffness is relatively significant.

5.2. Method

To simulate the buckling response of viscoelastic composites and to study rigorously the role of various parameters on the onset of wrinkle formation, the behaviour of flat unidirectional laminates under axial loads are modelled both analytically and numerically. The analytical approach involves simple mathematical equations for predicting the buckling loads in thin plates. For the numerical approach, finite element method is used to estimate the critical buckling load of uncured viscoelastic laminated composite under various loading rates.

For viscoelastic modelling, the composite laminate could be assumed to behave as a viscoelastic solid with perfect bonding between the layers using the Abaqus built-in viscoelastic constitutive model which is based on the integral form (IF) of viscoelasticity. As the application of Abaqus viscoelastic model is limited to isotropic materials, a more versatile orthotropic viscoelastic constitutive model (based on differential form of viscoelasticity – DF) that has been developed and implemented as a UMAT by researchers at the University of British Columbia (Malek 2014; Zobeiry et al. 2016) is also employed to elucidate the effect of ply anisotropy on the buckling response of uncured unidirectional laminates. The detail of these two viscoelastic approaches was demonstrated in Chapter 3.

The axial compression behaviour of thin laminates with end supports and unsupported sides may be treated similar to the columns under axial loads. Using this very basic approach, the critical buckling load (P_{cr}) of a linear isotropic laminate can be approximately estimated using the Euler buckling theory (Timoshenko & Gere 1961):

$$P_{cr} = \frac{\pi^2 EI}{(KL)^2},$$ (5.1)

where E is the elastic modulus of the isotropic material, I is the minimum area moment of inertia of the rectangular cross section, L is unsupported length of column and K is the effective length factor depending on the end constraints. As the slenderness ratio of the laminates in this study is high (i.e. 192.5), Euler buckling may be considered here.

To obtain more accurate prediction, the critical buckling stress can be determined with the plate buckling theory (Rees 2009) as follows:

$$\sigma_{cr} = \frac{\pi^2 E}{(L_e/k)^2},$$
(5.2)

in which $k^2 = t^2/12$ and t is the thickness of the laminate. The equivalent length, L_e, for fixed ends is defined as:

$$L_e = (a/2)(1 - v^2)^{1/2},$$
(5.3)

where a and v are the total length of the plate and the material Poisson's ratio, respectively.

5.3. Model verification

Although the compaction and the bending behaviour of thin laminates which may lead to wrinkling during viscous composite forming have been investigated in the literature, the buckling behaviour of uncured laminates has not been investigated comprehensively with validated numerical tools. To illustrate the importance of buckling response of laminates at the early stage of cure, the behaviour of linearly isotropic and then transversely isotropic flat laminates with a range of stiffness values representing the uncured and cured composites are considered first. A buckling model, which has shown some advantages over other methods such as 3-point bending test (Wang, Long & Clifford 2009), is employed. For verification purposes, the numerical results for isotropic laminates are compared to the analytical model predictions.

5.3.1. Geometry and input parameters

For verification and validation purposes, a rectangular geometry with the dimensions similar to the experiments of Wang, Long & Clifford (2009) is selected. Three rectangular unidirectional (UD) prepreg plies (0°/0°/0°) are considered as a simple case to minimize the number of variables. According to Wang, Long & Clifford (2009), such a three thin ply model can allow elimination of the deformation under self-weight. The geometry is partitioned in Abaqus environment before the material properties are assigned, as illustrated in Fig. 5.1 (right side). The total length of two clamped ends is 25 mm and the tested region is 50 × 50 mm as in the test set-up of Wang, Long & Clifford (2009). According to Wang, Long & Clifford (2009), the purpose of the long clamps

mounted carefully on the specimen was to protect the fibre from any misalignment which can lead to defects at the early stage of forming process. The thickness of each UD prepreg is 0.3 mm and the fibre orientation is parallel to the compressive load as shown in Fig. 5.1 (left side). All translations were restricted on one of the transverse edges, while the other transverse side was considered to be free of in-plane displacement in the loaded direction. A uniform axial displacement along this transverse edge was applied in the load increment scheme. Since the specimen was mounted in the aluminium clamps, an additional restraint against vertical displacement at the clamped regions was included in the present FE model, as shown in Fig. 5.1 (left side).

Prior to investigating the effect of loading rates on the time-dependent behaviour of prepregs, the material is assumed to behave as an isotropic elastic solid first. Then, the material is changed to a transversely isotropic one to represent the behaviour of UD composite laminates. The material input parameters for the cured laminate are taken from Wang et al. (2009) and summarized in Table 5.1. The elastic modulus along the Y-axis, is the laminate's stiffness in its longitudinal direction E_1, as depicted in Fig. 5.1. The proposed input values were based on the information provided by Hexcel Company for the cured composite laminate. It should be noted that the uncured properties have not been reported and some assumptions need to be made for uncured prepregs as described in Section 5.3.
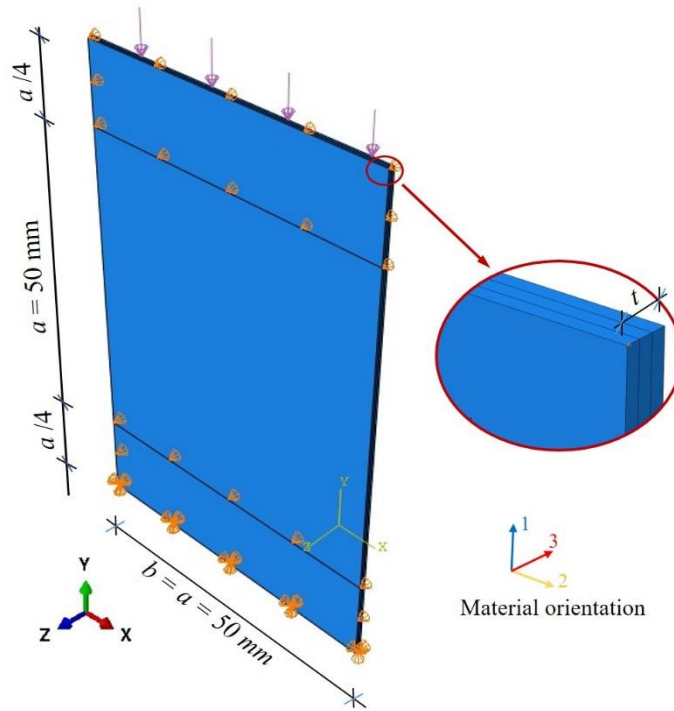
Figure 5.1: Detail of the 3D model under axial displacement
(According to Wang, Long & Clifford (2009))

Table 5.1: Input properties according to Wang, Long & Clifford (2009) for the cured sample

Properties	Value	Unit
E_1	160	GPa
E_2	8	GPa
G_{12}	3.98	GPa
G_{23}	2.86	GPa
v_{12}	0.26	-*
v_{23}	0.4	-*

Note: * indicates non-dimensional

5.3.2. FE analysis

The laminate was modelled using 20-noded solid C3D20R elements in Abaqus environment. A $1.25 \times 1.25 \times 0.3$ mm mesh, as shown in Fig. 5.2, is maintained evenly for the whole laminate. Both eigenvalue buckling and large deformation analysis (Riks method) were used in predicting the critical buckling loads. The former corresponds to an ideal elastic buckling analysis and the latter is a more accurate approach since it involves a static structural analysis with large deflection formulations. Displacement is

gradually applied in this analysis to search for the ultimate strength at which the structure becomes unstable. Therefore, the eigenvalue buckling analysis often yields quick results which would be a good indication for the latter sensitive large deformation analysis. In addition, the post-buckled performance of the structure, which is of the primary interest to us as matrix resin dominates the deformation of uncured prepreg, can be captured using deflection controlled loading analysis.

For the FE analysis, initial time step equal 1×10^{-4} was selected with automatic time increment option turned on in the Step module of Abaqus. The initial time increment is small enough to track the correct buckling behaviour and the selected automatic time increment ensures that Abaqus can get a converged solution. Prior to performing the FE analysis for transversely isotropic behaviour, linearly isotropic material is assumed first to verify the buckling response under uniaxial compression as mentioned in previous section.

A detailed mesh sensitivity analysis is also conducted in this study (see Fig. 5.3). A mesh refinement is performed through the thickness of the ply ($1.25 \times 1.25 \times 0.15$ mm, see Fig. 5.3b) as well as along the laminate longitudinal direction (see Fig. 5.3c & 5.3d). The meshes give similar results in terms of deformed shape and Mises stress distribution. The results are provided in Table 5.2. Based on the mesh convergence study, the $1.25 \times 1.25 \times 0.3$ mm mesh was selected for the case studies considered in this study.

Table 5.3 highlights a good agreement between results from the present finite element analyses with the theoretical predictions for the assumed linearly isotropic case ($E = E_1 = 160$ GPa, $v = 0.26$) for cured laminates. The agreement between eigenvalue analysis and Riks method results in terms of buckled mode shape (Fig. 5.4) and critical loads (Table 5.3) verifies the accuracy of the geometry, applied loads and boundary conditions. The FE procedure for capturing the buckling behaviour of the flat elastic laminate has already been described in details elsewhere (Le et al. 2019). Although in Le et al. (2019), the focus has been on understanding the behaviour of multilayered elastic beams with soft interfaces under compressive loads, the same FE model is employed to compare the results of the two approaches for wrinkle formation.

To consider the effect of the anisotropic ply on the buckling response, the transversely isotropic behaviour is assumed as shown in Table 5.1. It is noted that the

strength of the laminate under compressive loads reduces significantly as the transverse and shear modulus are included in the analysis model (Table 5.3).

Table 5.3 highlights relatively good agreement between results from the present finite element analyses with the theoretical prediction for an assumed linearly isotropic case ($E = E_1 = 160$ GPa, $v = 0.26$). However, significant discrepancies are noted between the two for the transversely isotropic case. In addition, the similarity between eigenvalue analysis and Riks method in terms of buckled mode shape (Fig. 5.2) and FE solutions (Table 5.3) is also presented. These two good correlations verify the nonlinear buckling analysis in terms of mesh size, time increment input and boundary conditions.
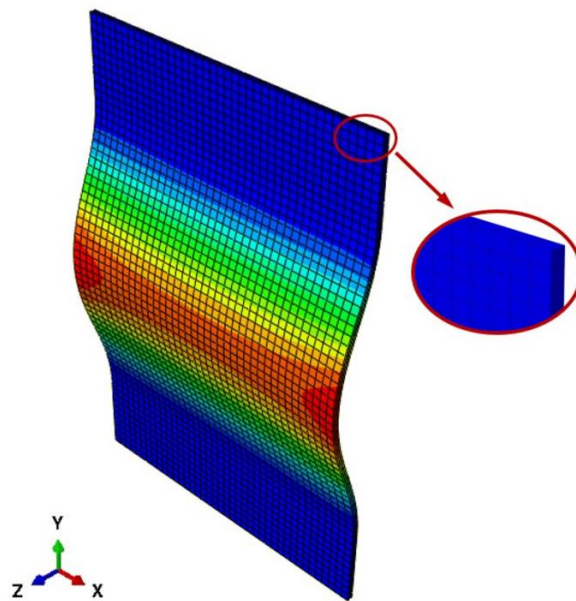
Figure 5.2: FE mesh of the buckled laminated composite under axial loading

Table 5.2: Mesh convergence study results

	Mesh 1	Mesh 2	Mesh 3	Mesh 4
Number of Elements	7,200	14,400	2,592	16,200
Number of Nodes	37,107	66,813	13,627	82,657
Critical buckling load (N)	8,480	8,467	8,481	8,476
User Time (hour)	4	11	1.5	13

Mesh: Num in Y × num in X × num in Z (see XYZ coordinate in Fig. 5.2)
Mesh 1: 60 × 40 × 3   Mesh 3: 36 × 24 × 3
Mesh 2: 60 × 40 × 6   Mesh 4: 90 × 60 × 3
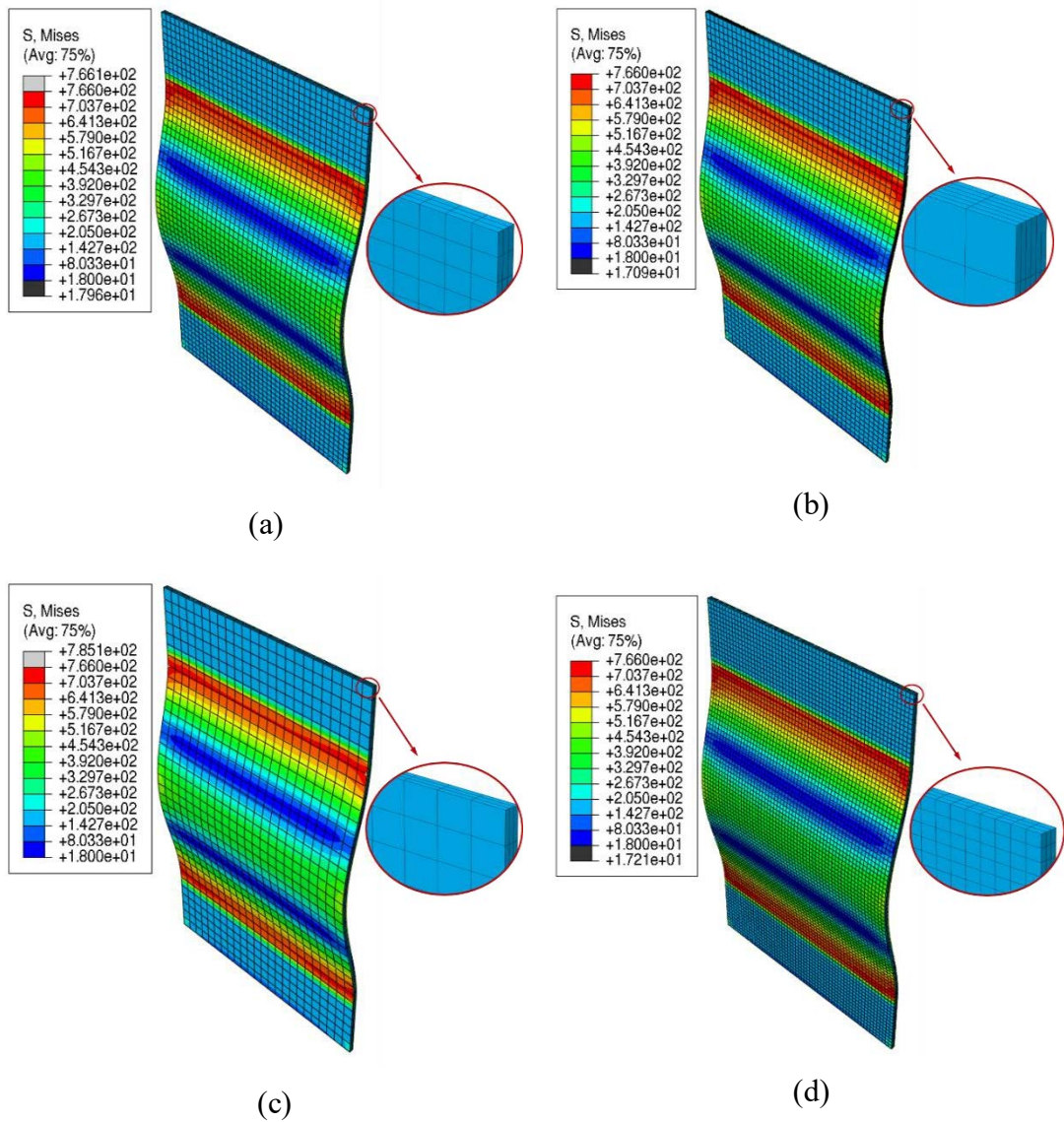
Figure 5.3: Comparison of deformed shape and Mises effective stress (in MPa) at ultimate state for cured isotropic laminates with different mesh sizes: (a) Mesh 1 (b) Mesh 2 (c) Mesh 3 (d) Mesh 4 under uniform axial displacement.

<p align="center">(a)   (b)</p>
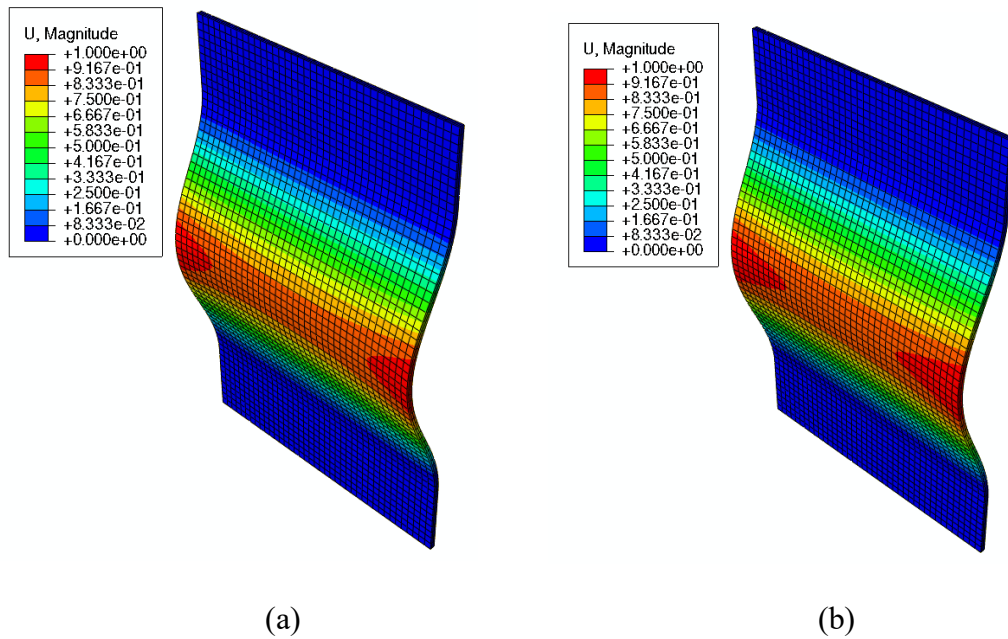
Figure 5.4: Comparison of the deformed shape (mode shape 1) obtained from the eigenvalue for the cured composite assuming: (a) isotropic (b) transversely isotropic material behaviour under uniform axial displacement.

Table 5.3: Comparisons of critical buckling loads between theoretical result and eigenvalue and large deformation analyses for the cured composite assuming isotropic and transversely isotropic input parameters.

Material property	Critical buckling load P_{cr} (N)			
	Theory[1]	Theory[2]	Eigenvalue analysis	Large deformation analysis
Isotropic ($E = E_1 = 160$ GPa)	7675	8231	8357	8480
Transversely isotropic ($E_2 = 8$ GPa)			6152	6164

<p align="center">Note: [1] Equation (5.1); [2] Equation (5.2)</p>

5.4. Model validation and comparison with experiments

To capture the buckling responses of viscoelastic composites, two different forms of viscoelasticity may be employed; the integral form (IF) available in Abaqus built-in and the differential form (DF) as described in Chapter 3. It should be noted that since the unidirectional (UD) plies are transversely isotropic, the general orthotropic viscoelastic constitutive model can be employed to investigate the effect of ply anisotropy on the buckling behaviours during composite forming. Table 5.5 provides a list summary of simulations that are conducted using IF and DF approaches in this section.

5.4.1. Isotropic viscoelastic material

Using Abaqus built-in viscoelastic material model, the material input parameters can be defined in two steps. The selected initial properties for a partially cured resin are the instantaneous Young moduli, E_o, and Poisson's ratio, v_o with 80 MPa and 0.495, respectively. Then, viscoelastic properties are described using Prony series constants. Two different viscoelastic materials are considered; Case 2a is modelled using IF of viscoelasticity with a single-term Prony series (provided in Section 3.1.1 in Abaqus Benchmarks Guide) (Abaqus 2013b), where in Eq. (3.14), $N = 1$; $g_i = 0.901001$ and $\tau_i = 0.9899$, and Case 3a, with twelve different relaxations (12 terms in the Prony's series) that are listed in Table 5.4 is considered to depict the role of viscoelastic parameters. The Prony series constants including the relaxation times (τ_i) and weight factors (w_i) corresponding to MTM45-1 epoxy measured by Thorpe (2012) are selected for Case 3a as such properties are missing in literature for Hexcel M21 epoxy resin. It should be noted that the Hexcel T800S/M21 UD prepreg has been used in the experiments of Wang, Long & Clifford (2009) which have been employed here for validation purposes. The bulk modulus, K, is assumed to be independent of time ($k_i = 0$) and equal to 2.667 GPa, in an acceptable range measured by Nawab et al. (2012). It should be noted that the isotropic elastic case (Case 1) result with the same properties as the resin unrelaxed modulus is provided in the figures for the comparison purpose.

Viscoelastic analysis with four loading rates at 4.4, 10, 100 and 300 mm/min (as in the experiments of in Wang, Long & Clifford (2009) are considered to demonstrate the role of loading rate. To maintain a uniform displacement of 1 mm over all cases, the time increment is calculated and assigned accordingly corresponding to the desired speed. The Nlgeom is turned on to allow the large deformation and displacements. The increment size starts at 1×10^{-3} se for the lowest speed (4.4 mm/min) and is adjusted for the faster rates. Lower time increments were found to lead to much longer computational times at the cost of negligible change of the end results.

69

Table 5.4: Prony series parameters for MTM45-1 epoxy as reported in Thorpe (2012)

Maxwell Element (i)	w_i	τ_i (s)
1	3.44181×10^{-1}	1.00×10^{-2}
2	1.14728×10^{-1}	1.00×10^{-1}
3	1.33849×10^{-1}	1.00×10^{0}
4	1.52970×10^{-1}	1.00×10^{1}
5	1.33849×10^{-1}	1.00×10^{2}
6	0.95606×10^{-1}	1.00×10^{3}
7	0.19121×10^{-1}	1.00×10^{4}
8	0.3824×10^{-2}	1.00×10^{5}
9	0.1338×10^{-2}	1.00×10^{6}
10	0.382×10^{-3}	1.00×10^{7}
11	0.96×10^{-4}	1.00×10^{8}
12	0.38×10^{-4}	1.00×10^{9}

Table 5.5: Summary of case studies considered in Section 5.3.

Case	Material	Number of Prony series	Resin properties (MPa)						Viscoelastic Material model	
			E_∞	E_o	G_∞	G_o	K	v	IF	DF
1	Isotropic elastic resin	N/A	8.00×10^{1}	8.00×10^{1}				0.495	✔	
2a	Isotropic viscoelastic resin	1	7.92×10^{0}	8.00×10^{1}	2.65×10^{0}	2.68×10^{1}	2.67×10^{3}	0.495	✔	
2b										✔
3a		12	1.46×10^{-3}	8.00×10^{1}	4.87×10^{-4}	2.68×10^{1}		0.495	✔	
3b										✔
4	Orthotropic viscoelastic composite	12	1.46×10^{-3}	8.00×10^{1}	4.87×10^{-4}	2.68×10^{1}		0.495		✔

Fig. 5.5 shows the effect of loading rates on the buckling behaviour of a simple isotropic viscoelastic (resin) material using Abaqus built-in (IF, Case 2a). The axial compressive stiffness of the laminated composites increases as the loading rate increases. The initial slope of the load-displacement curve for viscoelastic laminates tends to approach the slope of isotropic elastic laminate (Case 1) by increasing the loading rate as expected from viscoelastic theory. In other words, when a fixed displacement is applied

faster to the viscoelastic material (300 mm/min), its buckling response is almost similar to the elastic material.

Using the DF of viscoelasticity (Zobeiry et al. 2016), the relaxation shear modulus of the simple isotropic material, G(t), is defined by G(t) = 2.649+ 24.107exp$^{(-t/0.9899)}$ MPa while K is constant and equal to 2.667 GPa. Fig. 5.6 presents a comparison of FE results, Case 2a vs Case 2b, conducted using IF and DF approaches, respectively for two representative cases.

Discrepancies between the two models especially at the slowest rate (4.4 mm/min) are apparent. However, similar trend of the initial slope of load-displacement curve approaching the slope of the isotropic elastic laminate is still captured. Small discrepancies between the two modelling approaches have also been reported in Zobeiry et al. (2016) for a single element. These two approaches exhibit different convergence rates under different loading rates based on the assumptions considered in their formulations.

To investigate the effect of various relaxation times on the buckling behaviours of the viscoelastic composite using IF and DF, one more case is considered and referred to as Case 3b in the chapter. Twelve Prony series constants listed in Table 5.4 are used to describe the viscoelastic resin material. The relaxation shear modulus of twelve terms Prony series material is expressed using Eq. (3.14) as $G(t) = 0.0005 + \sum_{i=1}^{12} G_i e^{\frac{-t}{\tau_i}}$, where values of G_i are summarized in Table 5.6. Fig. 5.7 compares IF with DF in terms of the influence of different Prony series constants on the buckling response. The IF of viscoelasticity shows a significant drop in buckling load and different relaxation trend after reaching peak load as the twelve terms of Prony series parameters (Thorpe 2012) are considered (Case 3a vs Case 2a) (see Fig. 5.7).

In addition to buckling behaviour of laminates under compression, their stress relaxation behaviour under tension are examined to assess the discrepancy between the IF and DF approaches. For this purpose, a displacement of 1mm is applied and the stress values are monitored as the laminate is relaxed. Simulations are conducted with and without large deformation feature of Abaqus and results are provided in Fig. 5.8. It is interesting to note that both approaches provide exactly the same initial stiffness and relaxation curves under small deformations regardless of the number of Prony series that are being used. However, under the large deformation assumption the results are quite

71

different. The discrepancy between two approaches becomes larger in the case study with twelve-term Prony series assumed (see Fig. 5.8b). As it is noted in Abaqus documentation, the Abaqus built-in model (IF) is not suggested for problems involving large deformations. According to the case studies conducted in Zobeiry et al (2016), it is believed that the DF of viscoelasticity is more robust under complex 3D loadings scenarios due to less assumptions that are made in the DF formulation. Therefore, experiments are suggested to validate the accuracy of DF approach in analysing large-deformation problems.
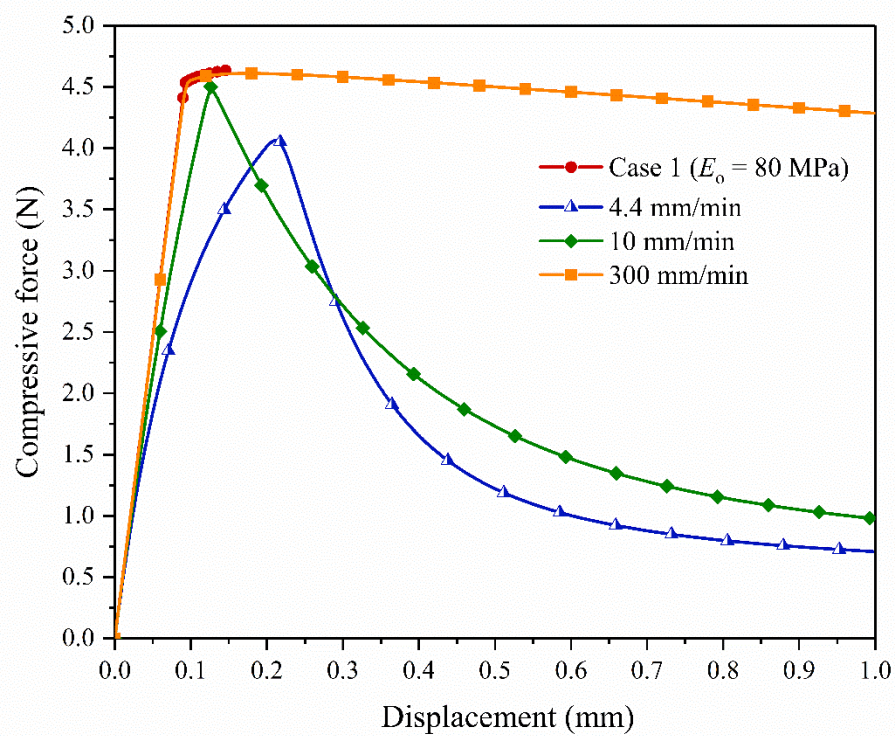
Figure 5.5: Effect of loading rate on force vs displacement relationship using IF (Case 2a). The resin viscoelastic properties are taken from Section 3.1.1 in Abaqus Benchmarks Guide. The material properties are listed in Table 5.5.
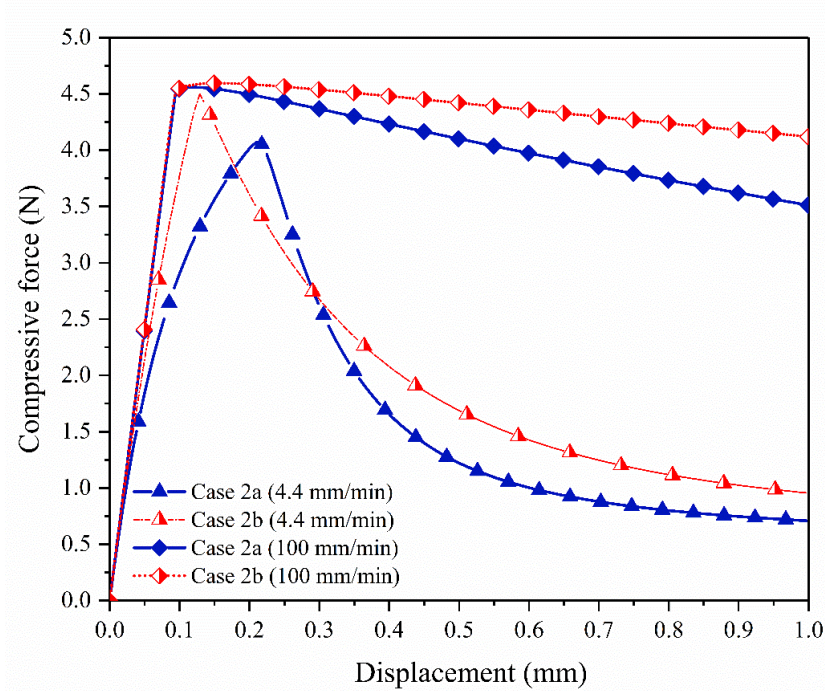
Figure 5.6: Comparison between IF (Case 2a) and DF (Case 2b) approaches for two presentative cases. The viscoelastic properties of the resin are provided in Section 3.1.1 in Abaqus Benchmarks Guide.

Table 5.6: The shear moduli G_i associated with the specific relaxation time, τ_i used for Case 3b.

Maxwell Element (i)	G_i (MPa)	τ_i (s)
1	9.20886	1.00×10^{-2}
2	3.06965	1.00×10^{-1}
3	3.58124	1.00×10^{0}
4	4.09284	1.00×10^{1}
5	3.58124	1.00×10^{2}
6	2.55802	1.00×10^{3}
7	0.51160	1.00×10^{4}
8	0.10231	1.00×10^{5}
9	0.03580	1.00×10^{6}
10	0.01022	1.00×10^{7}
11	0.00256	1.00×10^{8}
12	0.00102	1.00×10^{9}
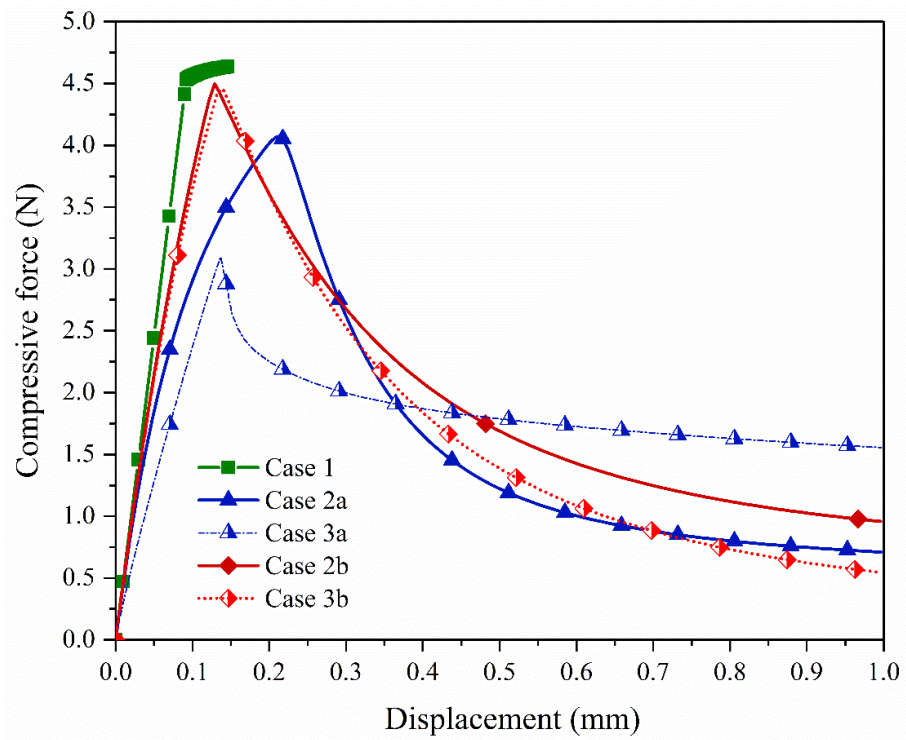
Figure 5.7: Effect of Prony series constants on force vs displacement relationship using IF (Case 2a and 3a) and DF (Case 2b and 3b) viscoelastic model compare to isotropic model (Case 1). The same loading rate of 4.4 mm/min has been used in all cases.
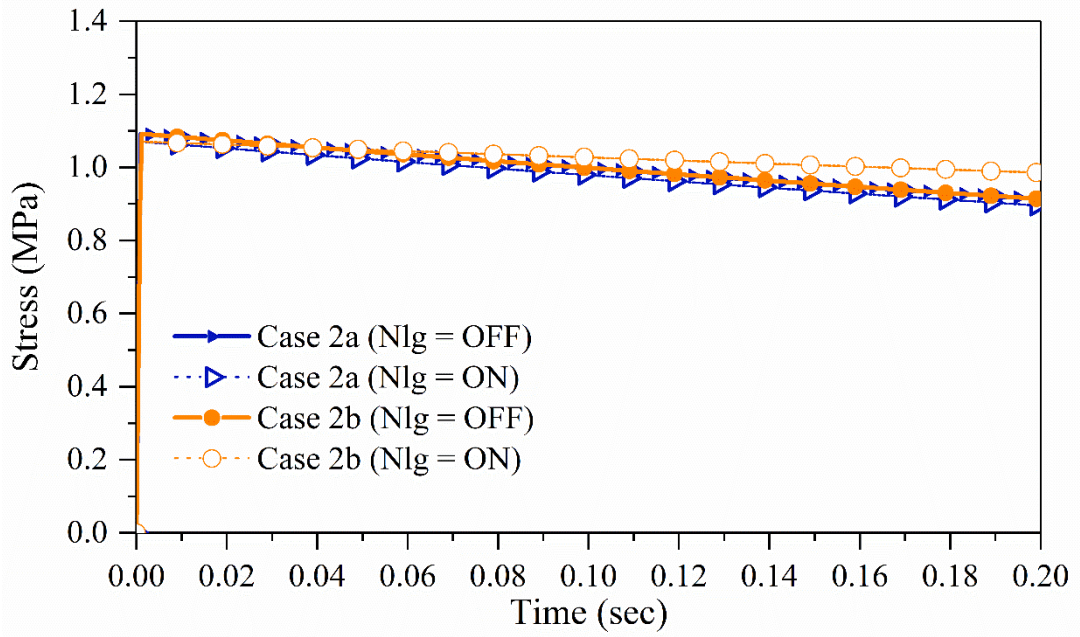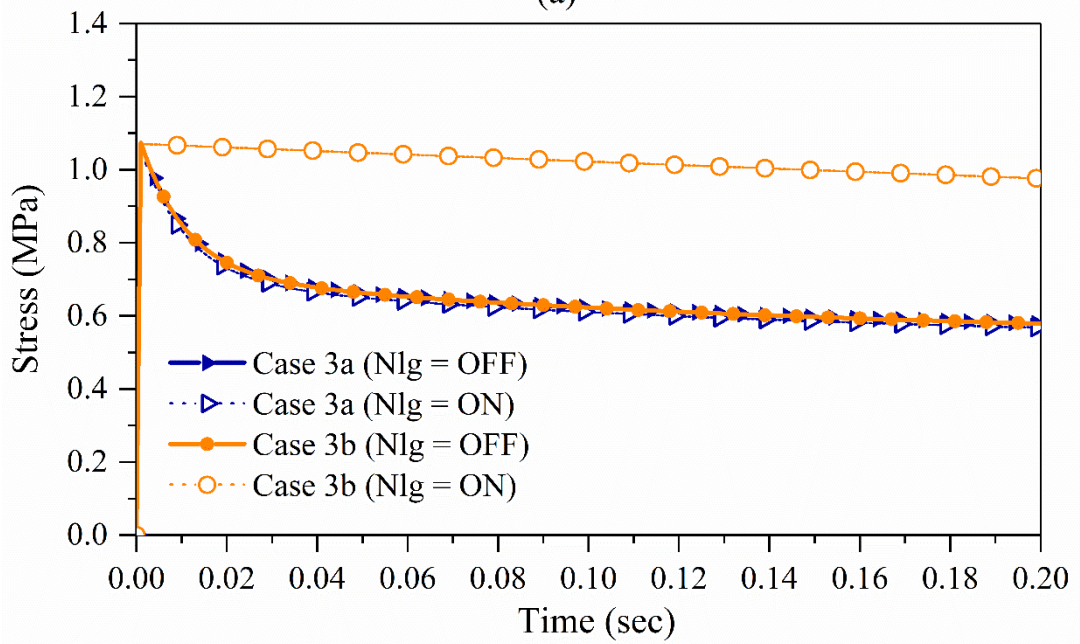
Figure 5.8: Stress relaxation response under tensile load calculated using: (a) a single-term Prony series (b) twelve-term Prony series.
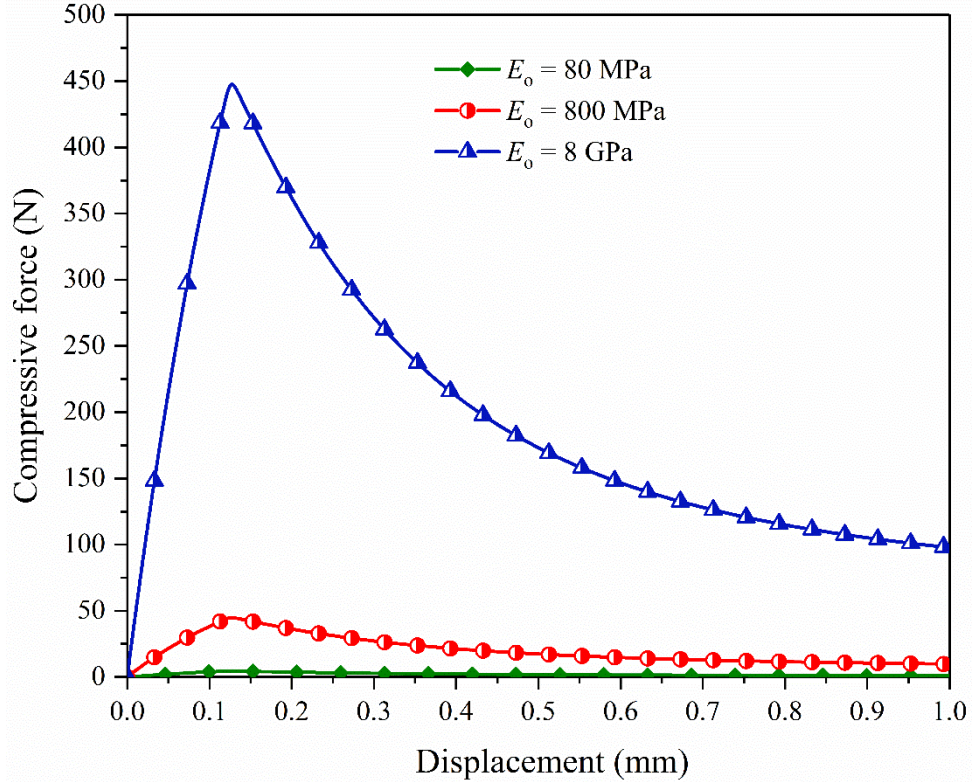
Figure 5.9: Effect of E_o on the buckling behaviour of the isotropic viscoelastic laminates using IF. The resin viscoelastic properties are taken from Section 3.1.1 in Abaqus Benchmarks Guide (Case 2a) at rate of 10 mm/min.

In addition to the loading rate and Prony series parameters effects, the effect of instantaneous elastic modulus, E_o, on the buckling behaviour is also considered using Abaqus built-in material model. Such effect is shown in Fig. 5.9. While keeping the loading rate unchanged (10 mm/min), two additional cases with ten times higher E_o are shown. The higher the value of E_o, the higher the buckling load is as can be noted in Fig. 5.9. It is interesting to highlight that the three buckling loads are reached at nearly the same displacement.

5.4.2. Orthotropic viscoelastic material

As shown previously in Section 5.2, the anisotropic nature of composites may affect the buckling load of the composite laminates. Therefore, in this section, the laminate orthotropic viscoelastic properties are considered by incorporating the fibre-bed elastic properties into the micromechanics equations to estimate the effective viscoelastic properties of the uncured prepreg. The mechanical properties of the resin, fibre and fibre-bed that have been used for validation purpose are listed in Table 5.7. The fibre-bed properties are taken from the effective elastic properties of a dry prepreg estimated in

Malek et al. (2018) The resin viscoelastic properties are kept unchanged to better understand the effect of fibre-bed on the buckling response of composite laminates and comparison purposes. Prony series constants for MTM45-1 (Thorpe 2012) are assumed for validating the model against the experimental data reported in Wang et al. (2009) The fibre properties assumed by Johnston et al. (2001) are used here. As noted in the previous section, the resin modulus dominates the buckling behaviour. Hence, the longitudinal elastic modulus of the fibre and fibre-bed in compression are assumed to be equal to the unrelaxed modulus of the resin (80 MPa). As it will be discussed later, such assumption for compression seems to be realistic due to the very low buckling load of a single fibre.

Table 5.7: Material properties of fibre, resin and fibre bed used in the buckling simulation of composite laminates.

Property	Fibre	Resin	Fibre bed	Unit
E_1	8.00×10^1	8.00×10^1	8.00×10^1	MPa
E_2	1.72×10^2		1.12×10^{-1}	MPa
E_3	1.72×10^2		1.12×10^{-1}	MPa
G_{12}	2.76×10^4		1.13×10^{-1}	MPa
G_{13}	2.76×10^4		1.13×10^{-1}	MPa
G_{23}	6.88×10^1		0.43×10^{-1}	MPa
v_{12}	2.00×10^{-1}	4.95×10^{-1}	7.12×10^{-2}	-*
v_{13}	2.00×10^{-1}		7.12×10^{-2}	-*
v_{23}	2.50×10^{-1}		3.00×10^{-1}	-*

Note: * indicates non-dimensional

Summary of simulation results for the elastic and viscoelastic composite laminate and the experimental data is provided in Fig. 5.10. Case 4 represents the orthotropic viscoelastic laminate. The composite effective viscoelastic properties are determined by using analytical micromechanics equations following the approach presented in Malek (2014) and Malek et al. (2018). It is noted that the fibre-bed elastic constants will be added to the resin relaxed modulus to obtain the modified resin properties which are later combined with fibre properties in the micromechanics equations.

The DF approach for modelling the response of orthotropic viscoelastic composites developed by Malek et al. (2018) requires the components of the relaxation matrix. These values could be defined by the Prony series expansions as given below:

$$E(t) = E^r + (E^u - E^r) \sum_{i=1}^{12} w_i \, e^{\left(-\frac{t}{\tau_i}\right)}, \qquad (5.4)$$

where E^r and E^u are the relaxed and unrelaxed Young's modulus, respectively. Parameters w_i and τ_i are presented in Table 5.4. Table 5.8 and 5.9 provides the relaxed and unrelaxed values and the Prony series parameters corresponding to each component respectively.

Table 5.8: Relaxed and unrelaxed values of components of the composite relaxation matrix.

Component	C_{ij}^r(MPa)	C_{ij}^u(MPa)
C_{11}	64.10	196.10
C_{22}	0.30	297.40
C_{33}	0.30	297.40
C_{44}	0.30	214.00
C_{55}	0.30	214.00
C_{66}	0.30	92.00
C_{12}	0.10	165.60
C_{13}	0.10	165.60
C_{23}	0.10	205.70

Table 5.9: Prony series parameters for each component of the relaxation matrix of the composite material obtained from micromechanics equations following the approach presented in Malek (2014).

i	w_{11}	w_{22}	w_{33}	w_{44}	w_{55}	w_{66}	w_{12}	w_{13}	w_{23}
1	45.432	102.256	102.256	73.551	73.551	31.561	56.962	56.962	70.764
2	15.144	34.086	34.086	24.517	24.517	10.521	18.987	18.987	23.588
3	17.668	39.767	39.767	28.604	28.604	12.274	22.152	22.152	27.519
4	20.192	45.447	45.447	32.690	32.690	14.027	25.317	25.317	31.451
5	17.668	39.767	39.767	28.604	28.604	12.274	22.152	22.152	27.519
6	12.620	28.405	28.405	20.431	20.431	8.767	15.823	15.823	19.657
7	2.524	5.681	5.681	4.086	4.086	1.753	3.165	3.165	3.931
8	0.505	1.136	1.136	0.817	0.817	0.351	0.633	0.633	0.786
9	0.177	0.398	0.398	0.286	0.286	0.123	0.221	0.221	0.275
10	0.050	0.113	0.113	0.082	0.082	0.035	0.063	0.063	0.079
11	0.013	0.028	0.028	0.020	0.020	0.009	0.016	0.016	0.020
12	0.005	0.011	0.011	0.008	0.008	0.004	0.006	0.006	0.008
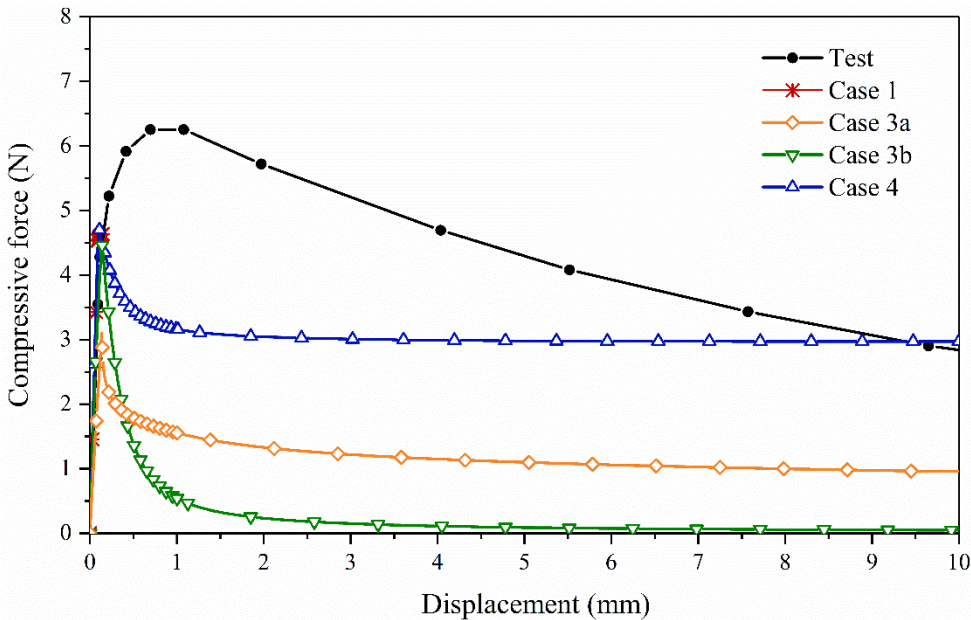
Figure 5.10: Effect of ply anisotropy on the buckling response of viscoelastic composites. Various resin viscoelastic properties are assumed as listed in Table 5.5 and the same loading rate of 4.4 mm/min is considered for all cases.

Fig. 5.10 compares the assumed isotropic viscoelastic behaviours using the IF and DF approaches (Case 3a and Case 3b, respectively) with Case 4 under the same loading

rate (4.4 mm/min). Case 1 along with experimental data for Hexcel T800S/M21 UD prepreg measured by Wang et al. (2009) are also added in the figure for comparison and validation purposes. It should be emphasised that the uncured prepreg properties have not been measured by Wang et al. (2009) and therefore assumptions have been made in this chapter based on available data in the literature for MTM45-1 prepregs to highlight the importance of such missing characterisation data. Reviewing the datasheets for M21 and MTM45-1 epoxy resin reveals that MTM45-1 resin is more viscous than M21 resin at the same temperature. Therefore, the discrepancy between the experimental data and numerical predictions may be attributed to the difference between the rheological characteristics of MTM45-1 and M21 epoxy resins.

A parametric study was conducted to illustrate the effect of resin properties on the post buckling response. Three sets of case studies were considered for this purpose. The viscoelastic parameters of the resin varied in each case study (see Table 5.10) while Prony series remained constant (as listed in Table 5.4). The results of parametric case studies are provied in Fig. 5.11. In each case, the effect of relaxation times and weight factors on the post buckling response of uncured laminates were investigated separately. However, their effects found to be negligible compared to E_o and E_∞.

Table 5.10: Parametric case studies conducted for determining the effect of resin properties on the post buckling response of uncured laminates.

Case	E_o (MPa)	E_∞ (MPa)
Case 5	$(80 \div 200)$	1.46×10^{-3}
Case 6	80	1.46×10^{-3} - 10
Case 7	100 - 165	10 - 30

Fig. 5.11a shows that E_o significantly affects both the peak value and the post buckling response of uncured viscoelastic laminates, while the effect of E_∞ is shown to be quite negligible in Fig. 5.11b. E_∞ only affects the post buckling behaviour at very large displacements. Higher values of E_o and E_∞ may suggest a better match with experimental data at lower displacements as shown in Fig. 5.11c while the discrepancies between model predictions and test data at large displacements may be associated with the fibre-bed effect due to large deformations at higher displacements or simply an experimental error.
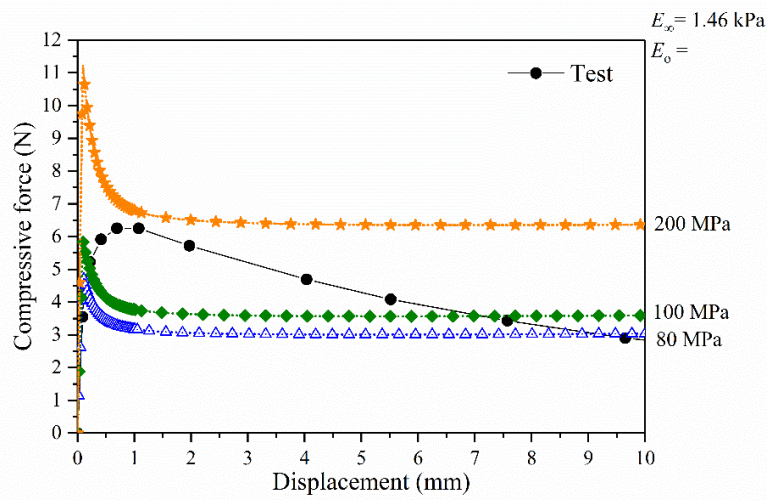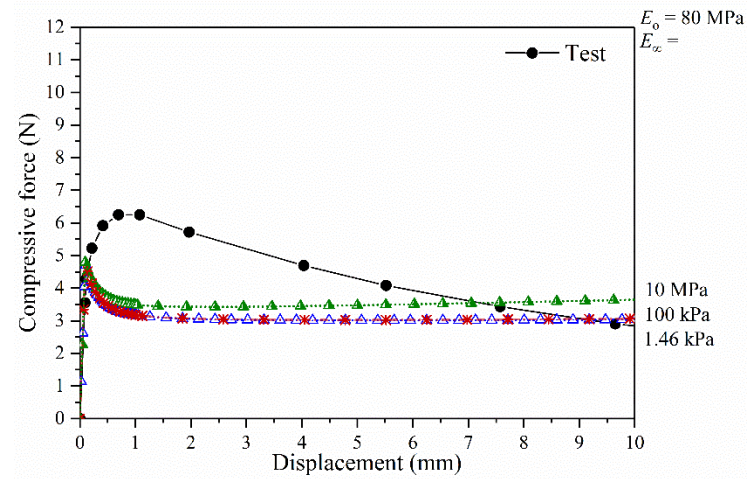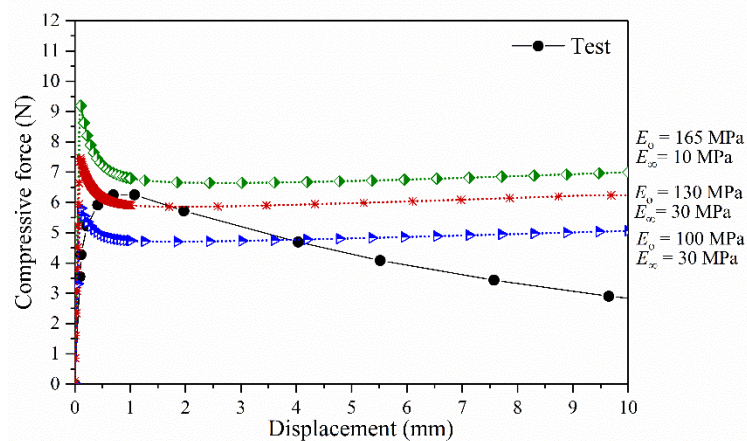
Figure 5.11: Results of parametric studies: Effect of (a) increasing E_o (Case 5), (b) increasing E_∞ (Case 6) and (c) higher E_o and E_∞ (Case 7) on the buckling behaviour of the uncured orthotropic viscoelastic laminates using DF. The resin viscoelastic properties are provided in Table 5.4 (w_i and τ_i) and Table 5.10 (E_o and E_∞). The loading rate is 4.4 mm/min in all cases.

81

By comparing the simulation results with those of the Wang et al. (2009)'s experiment, we may postulate that unlike cured solid composites, the compressive stiffness of uncured prepregs is mainly dominated by the resin modulus even in the presence of the fibres and not the fibre modulus. This could be due to the very small buckling load that each single fibre can carry. Assuming that each fibre has dimensions of d = 4e-6m, L = 100d and E_f= 200 GPa, using the simple Euler buckling equation, the buckling load of each carbon fibre is estimated to be 0.00015 N which is very low. In other words, the fibres easily buckle and the iso-strain assumption for estimating the effective longitudinal modulus of the composite "in compression" is not valid anymore. However, the fibre-bed still improves the shear and transverse modulus of the composite and increases the relaxed composite modulus (E_c^r) compared to the neat resin. The peak load increase in the buckling response of uncured prepreg (Case 4) compared to the uncured resin (Case 3) could be explained due to such stiffening effect of the fibre-bed in the transverse direction. Hence, measuring the degree of cure and characterising the viscoelastic properties of the resin before conducting similar experiments to Wang, Long & Clifford (2009) could improve our understanding of the buckling response of uncured/partially cured prepregs.

5.5. Summary and conclusions

The buckling response of orthotropic viscoelastic composite laminates are analysed numerically using a DF of viscoelasticity proposed for orthotropic composites. It is found that the longitudinal compressive stiffness of the plies affects both the slope and the buckling load while the laminate transverse properties affect the post beak load-displacement behaviour more significantly. Due to the very low buckling load of carbon fibres, the uncured laminate response is found to be more dominated by the resin viscoelastic properties. The fibre-bed is believed to stiffen the transverse and shear properties and therefore increasing the compressive stiffness slightly while increasing the post buckling/wrinkling more significantly.

In terms of the loading rate, the axial compressive stiffness of the laminated composites increased by increasing the loading rate. The initial slope of load-displacement curve for viscoelastic laminates tends to approach the slope of isotropic elastic laminate by increasing the loading rate. In other words, when the displacement is applied faster to viscoelastic laminates (300 mm/min), their buckling response behaviour

is almost similar to the elastic laminates. The observed trend is in accordance with the viscoelastic theory and in contrast to the experimental data in the literature.

Published data on the viscoelastic properties of commercial resin systems and uncured prepregs used in advanced composites are quite limited. Currently, literature is mainly focused on both developing robust experimental methods to measure such properties (in addition to bending stiffness and inter-ply friction) as well as simulation capabilities to account for all such complexities. The focus of this work is on developing a simulation framework using limited experimental data in the literature to demonstrate the importance of such properties. The simulation framework developed here will allow for implementation of proper resin viscoelastic properties. As the viscoelastic properties of uncured prepreg samples were not measured by Wang, Long & Clifford (2009), assumptions are made in this chapter to predict those properties with micromechanics equations (Malek 2014) based on available data on the viscoelastic properties of another commonly used thermoset resin (MTM45-1). Reviewing the datasheets for M21 and MTM45-1 reveals that the MTM45-1 resin is more viscous than M21 resin at the same temperature. Therefore, discrepancies (maximum compressive forces and the shape of the load-displacement curves) between the experimental data and numerical predictions could be attributed to the lower viscosity of the MTM45-1 resin. Conducting further experiments on uncured and partially cured laminates with different thicknesses is suggested to better understand the discrepancy reported between the numerical predictions and the experimental data.

Chapter 6. Bending behviour of viscoelatic woven composite plates

6.1. Introduction

Given that out-of-plane bending is well known as an important deformation mechanism that governs the wrinkle formation during composite manifacturing, this chapter investigates the out-of-plane bending response of cured and uncured viscoelastic composite laminates at different loading rates to gain a better understanding of the fibre waviness and wrinkling evolution during the forming process of advanced composites. This is accomplished by the implementation of a three-dimensional (3D) multi-scale modelling framework that incorporates analyses at different scales (micro-, meso- and macro-scale).

The multi-scale modelling approach that is used in this study was introduced in general in Chapter 3. Combining analytical equations at smaller scales with the DF form of viscoelasticity at macro-scale, a rapid method for estimating the effect of various parameters on wrinkle formation has been developed. The detail of the multi-scale framework for a specific problem (i.e. bending behaviour of uncured woven composites) is described in Section 6.2. The numerical model is validated by comparing the bending behaviour of thin viscoelastic composites with experimental data reported in the literature. The influence of various parameters including fibre stiffness, ply anisotropy, resin properties, and loading rates on the bending behaviour of composites are analysed. The agreement between the numerical predictions and the experimental data highlights the potential of the proposed multi-scale modelling framework to predict the behaviour of viscoelastic composite with a variety of yarn architectures efficiently. Further experimental investigations into the viscoelastic characteristics of woven composites at the micro- and meso-scale are advised to ascertain the limitations and validity range of the predictions.

6.2. Method

The viscoelastic behaviour of cantilever plates subjected to tip displacements can be modelled employing the multi-scale approach introduced in Malek (2014) for orthotropic composites, as described in Fig. 6.1. Although such a method has been introduced in Chapter 3, a more detail of the technique applied for a specific problem (i.e. bending behaviour of cantilever woven plates) is presented here. In addition, for

verification purpose, an analytical method at the macro-scale involving simple mathematical equations for calculating the deflection curve and moment vs curvature relation of an assumed isotropic elastic beam under a small displacement is also demonstrated.

At lower scales (i.e., micro and meso) analytical models including micromechanics equations developed by Malek (2014) and Naik (1994) are used to predict the effective mechanical properties of a RUC of the woven fabric. Such effective properties are consequently used as input parameters for structural analysis at the macro-scale. The following subsections describe the methodology in details.

(a)

(b)
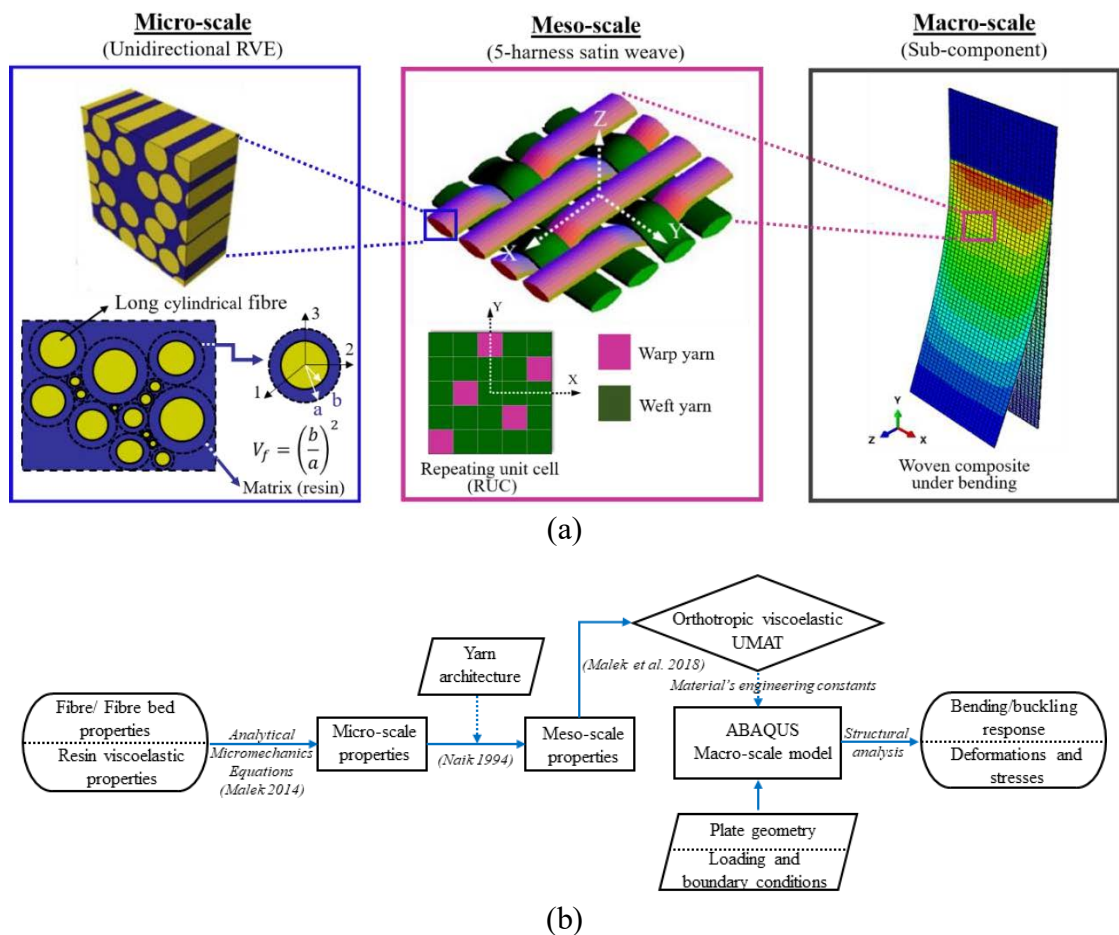
Figure 6.1: (a) Schematic of the multi-scale modelling approach for bending behaviour of 5-harness satin weave composites from micro-scale to macro-scale; (b) Flow chart depicting the analytical and numerical models utilized in the multi-scale analysis.

6.2.1. Micro- and meso-scale properties

At the micro-scale, the analytical micromechanics equations described in Malek (2014) are used to predict the effective viscoelastic properties of the solid unidirectional

circular fibre composites with a specific fibre volume fraction (V_f) (see Fig. 6.1a). The effective properties obtained from the micromechanics model are then used to estimate the effective properties of the fabric at the meso-scale. The fabric is composed of two sets of interlacing, mutually orthogonal (warp and weft) yarns. The selected weave type in this study is a 5-harness satin (see Fig. 6.1a), which has advantages over plain and twill weaves in terms of drapability and conformity over complex shapes (Alshahrani & Hojjati 2017b). The periodicity of the repeating pattern in the woven fabric can be used to separate a small RUC which is adequate to represent the fabric architecture. Details of geometric modelling of 5-harness satin weave composite along with discretisation technique of yarns within RUC and calculation of 3D effective properties were described in Naik (1994). The analytical procedure was implemented in MATLAB for this study. Once the effective meso-scale properties of the composite are determined, they are employed directly in the structural analysis at the macro-scale.

6.2.2. Macro-scale analysis

While the woven fabrics are discrete on the micro-scale, woven composites are assumed to be uniform and continuous at the macro-scale to simplify computations and improve the efficiency of the analysis. The macro-scale analysis of woven fabrics is mainly conducted to simulate the overall bending behaviour of the fabric using the micro- and meso-scale input parameters. To gain a deeper understanding of the deformation mechanisms, an analytical method is employed as an alternative to the numerical method in the macro-scale analysis. The analytical method at the macro-scale involves simple mathematical equations for predicting the deflection curve and moment vs curvature relation of an isotropic "elastic beam" under a small displacement. The numerical (finite element) method is then used to predict the bending moment-curvature relation of both "elastic" and "viscoelastic" composite plates at various loading rates. The elastic results are compared with analytical method predictions for verification purposes.

For the viscoelastic analysis, the composite plate is first assumed to behave as a viscoelastic isotropic solid and modelled using the Abaqus built-in viscoelastic constitutive model which is based on the integral form (IF) of viscoelasticity. As the application of Abaqus viscoelastic model is limited to isotropic materials, a more versatile orthotropic viscoelastic constitutive model (based on a differential form of viscoelasticity – DF) that has been developed and implemented as a UMAT (Malek 2014; Zobeiry et al.

2016) is then employed to elucidate the effect of ply anisotropy on the bending response of uncured 5-harness satin weave plates.

6.2.2.1. Analytical method

To estimate the bending behaviour of isotropic plates, simple mathematical equations for calculating the deflection of isotropic elastic beams are considered first. The beam dimensions and loads are selected based on the bending test conducted in (Alshahrani & Hojjati 2017b). The beam with dimensions of 10 mm in width, 0.55 mm in thickness and 150 mm in length has an overhang and therefore may be treated as a cantilever beam subjected to a load F acting at the free end (see Fig. 6.2a). The y and z-axis are defined as the distance along the axis of the undeformed beam and the vertical deflection of the beam, respectively (see Fig. 6.2b). For linearly elastic materials, moment-curvature relationship may be determined from the condition that the moment resultant of the bending stresses is equal to the bending moment M acting at the cross-section (Gere & Goodno 2009) as given by:

$$\kappa = \frac{1}{\rho} = \frac{M}{EI},$$ (6.1)

in which κ is the curvature, ρ is the radius of curvature of the deformed shape and EI is the flexural rigidity of the beam. It should be noted that an additional deflection term due to the shear deformation in the form of a mutual sliding of adjacent cross-sections along each other may be considered (Timoshenko 1940). However, as a result of the very thin section of the cantilever beam (see Fig. 6.2a), the bending due to shear can be shown to be negligible compared to the bending of plies based on a detailed numerical simulation. For this purpose, a separate FE analysis was conducted on plies bonded with very soft interfaces to capture sliding of adjacent plies. Results suggested that the effect of shear deformation is less than 0.5% for the dimensions of the selected beam. In other words, bending has shown to be the dominating deformation mechanism in this test.

The exact expression for the curvature at any point along the curve is given by:

$$\kappa = \frac{1}{\rho} = \frac{\dfrac{d^2z}{dy^2}}{\left[1+(\dfrac{dz}{dy})^2\right]^{3/2}} , \tag{6.2}$$

Combining Eq. (6.2) with Eq. (6.1), the deflection and the bending moment relation along the beam can be expressed as:

$$\frac{\dfrac{d^2z}{dy^2}}{\left[1+(\dfrac{dz}{dy})^2\right]^{3/2}} = \frac{M}{EI} , \tag{6.3}$$

Since we are limiting to the elastic deformation and assuming that the slope of the elastic beam is small, the $(dz/dy)^2$ term will be small and so can be neglected. This leads to a much simpler differential equation defining the deflection of the beam:

$$\frac{d^2z}{dy^2} = \frac{M}{EI} , \tag{6.4}$$

The bending moment at a cross-section distance y from the fixed support is obtained from the free body diagram as $M = FL - F(y)$ where L is the length of the cantilever beam. By substituting the expression for the bending moment into the differential equation (Eq. 6.4):

$$EI \frac{d^2z}{dy^2} = FL - Fy , \tag{6.5}$$

This equation can be integrated to obtain the slope and deflection of the beam. The constant of integration may be evaluated from the conditions that the deflection of the beam and slope of the deflection curve at the fixed support are equal to zero. Finally, the equation for the deflection curve is:

$$z(y) = \frac{Fy^2}{EI}(\frac{L}{2} - \frac{y}{6}), \tag{6.6}$$

Assuming that the cantilever beam AB subjected to a tip displacement of 10 mm ($\delta_B = 10\ mm$) (see Fig. 6.2), the force required to achieve this displacement can be obtained as:

$$F = \frac{3EI\delta_B}{L^3},$$

(6.7)

Therefore, the resulting bending moment M at any point along the beam can be calculated using Eq. (6.5). Lastly, the obtained moments at each point can be plotted against the corresponding curvature values.
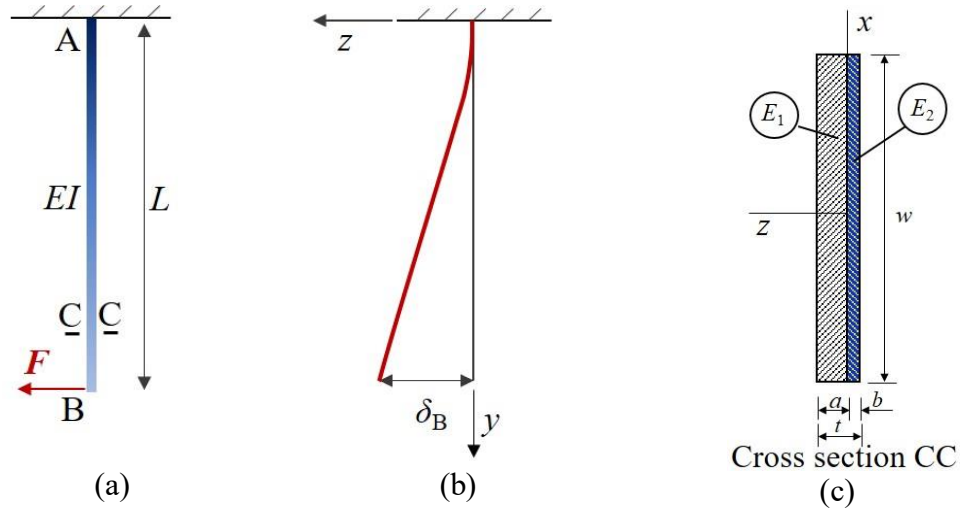
Figure 6.2: Bending of a cantilever beam: (a) beam with load; (b) deflection curve; (c) cross-section of beam showing the x-axis as the neutral axis of the cross-section

6.2.2.2. Numerical method

Based on the review of bending modulus of uncured prepreg samples shown in Table 2.1, the cantilever beam is roughly assumed to be linearly isotropic elastic with Young' modulus and Poisson's ratio equal to 500 MPa and 0.2, respectively. It was restrained from all displacements in a length of 30 mm as it was gripped along this distance (Alshahrani & Hojjati 2017b). The beam was modelled in Abaqus using 20-noded solid quadratic brick element with reduced integration (C3D20R). Number of elements in width, length and thickness directions are 6, 50 and 2 respectively. Based on the convergence study similar to the one conducted in Le et al. (2021), the 1.67 mm × 2 mm × 0.275 mm mesh was selected and maintained uniformly for the whole beam. Because Euler-Bernoulli beam theory is limited to small displacements, the free end of

the cantilever beam is displaced by 10 mm. Indeed, the maximum deflection ($\delta_B = 10$ mm) (see Fig. 6.2b) is less than 10 % of the free span length (120 mm) which meets the requirement of a small deformation problem. It is also noted that the loading point is 4 mm from the free end of the beam as suggested in Alshahrani & Hojjati (2017b). The load value required to achieve a certain tip displacement noted in the experiment is used to calculate the bending moment along the length of the beam. Through capturing the bending curve corresponding to the maximum displacement reached (see Fig. 6.3a), deflection profile $z(y)$ is fitted using a proper polynomial function. The expression for the curvature is subsequently calculated as an equation of the second derivative of z with respect to y according to Euler-Bernoulli's law for small deformation.
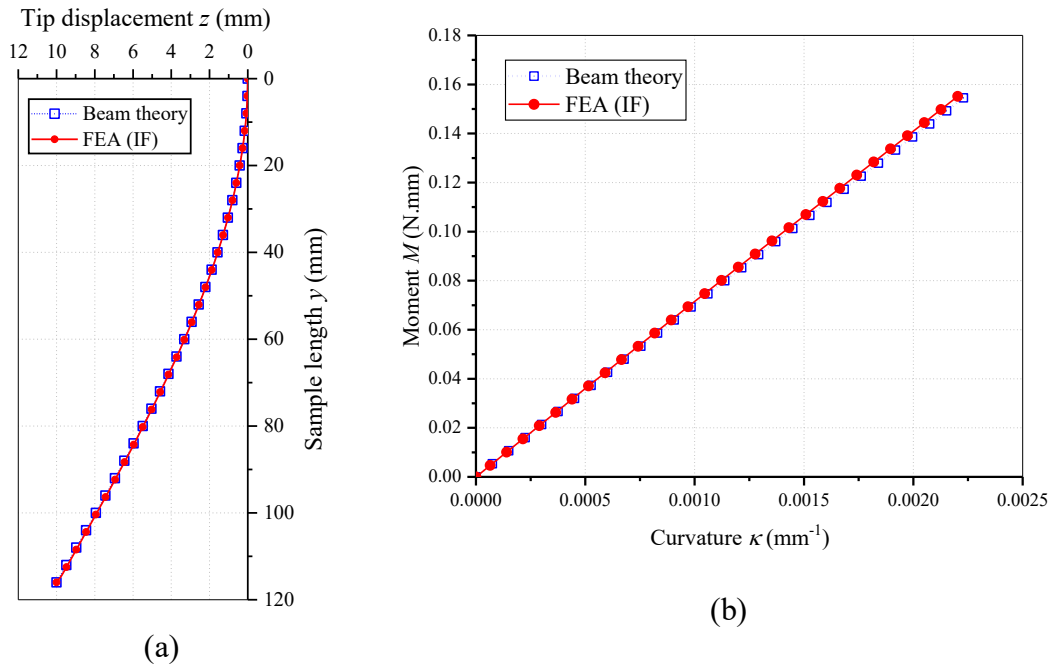
Figure 6.3: (a) Bending profile with tip displacement of 10 mm
(b) Bending moment – curvature relation in the isotropic elastic beam ($E = 500$ MPa, $\upsilon = 0.2$)

The above macro-scale analysis was only conducted to verify the 3D model for bending assuming isotropic elastic properties. For isotropic viscoelastic analysis, viscoelastic input properties are needed. In terms of the viscoelastic analysis of an orthotropic composite, a user material subroutine (UMAT) based on the differential form (DF) of viscoelasticity is employed. The reader is referred to Subsections 3.2.1 and 3.2.2 for a comprehensive review.

6.3. Results and model validation

Due to the lack of experimental data for uncured woven composites at the micro- and meso-scale, it is difficult to determine the accuracy level of the modelling framework at smaller scales. Therefore, two separate analyses on elastic and viscoelastic materials are conducted based on available input parameters. First, the effective elastic characteristics of cured UD and woven composites are estimated and compared with the experimental data available in the literature. For this purpose, analytical micromechanics equations presented in (Malek 2014; Naik 1994) are employed to estimate the mechanical elastic properties of the cured UD (AS4/8552) and 5HS woven (AS4/3501-6) thermoset composites. Results are compared with the experimental data provided in Ersoy et al. (2010) and (Naik 1994) for model validation at the micro- and meso-scale, respectively. For macro-scale model validation, the viscoelastic bending responses of woven prepregs composing 5HS fibres impregnated with an epoxy resin (Cycom 5320) are simulated separately based on limited experimental data for uncured woven composites; bending curves at different loading rates are compared with the experimental data reported in Alshahrani & Hojjati (2017b)

6.3.1. Elastic material

6.3.1.1. Micro-scale results

At the micro-scale, the effective elastic properties of the solid UD composites are predicted using the analytical micromechanics equations described in Malek (2014). The properties of the constituent materials, i.e. the fibres and cured resin (listed in Table 6.1) are selected based on available experimental data for a specific fully cured composite (AS4/8552) in literature (Ersoy et al. 2010). The moduli of AS4/8552 were also predicted by Ersoy et al. (2010) using an analytical approach based on the Self Consistent Field Micromechanics (SCFM) and Finite Element Based Micromechanics (FEBM) and presented in Table 6.2 for further comparisons. Additionally, in order to gain a better understanding of how thermoset resins and their composites develop their properties during cure, the composite properties of the resin in its uncured form are examined using micromechanics equations (Malek 2014). The current predictions are compared to those of two conventional methods described in Ersoy et al. (2010). It should be noted that the elastic modulus of the uncured resin is assumed equal to 30 MPa (Table 6.1) as the authors

(Ersoy et al. 2010) only mentioned that the elastic modulus before vitrification is generally rubber-like modulus of the order of a few MPa.

Table 6.1: Constituent material properties used for cured and uncured UD thermoset composite according to Ersoy et al. (2010).

$V_f =$	0.574			
Property	Fibre	Resin (8552)		Unit
	AS4	Uncured*	Cured	
E_1	228	0.03	4.67	GPa
$E_2 = E_3$	17.20			GPa
$G_{12} = G_{13}$	27.60	0.010	1.70	GPa
G_{23}	5.73			GPa
$v_{12} = v_{13}$	0.2	0.499	0.37	-
v_{23}	0.5			-

Note: * For uncured resin, Young's modulus is assumed to equal to 30 MPa as the authors only mentioned that the elastic modulus before vitrification is generally rubber-like modulus of the order of a few MPa.

Table 6.2 demonstrates a good agreement between the present results for the cured composite and the experimentally measured values reported by Ersoy et al. (2010). Based on the assumption for missing data on uncured resin, the present calculations using the micromechanics equations (Malek 2014) for the uncured composite are very close to the one predicted by FEBM (Ersoy et al. 2010). Additionally, FEBM was found to be a better method than SCFM in predicting the composite elastic properties when the reinforcement and matrix moduli differ significantly. In other words, the micromechanics model described in Malek (2014) has been validated for determining the effective elastic characteristics of cured UD circular fibre composites. Nevertheless, the effective properties of uncured composites have not been determined experimentally by Ersoy et al. (2010). Hence, model validation at the micro-scale cannot be extended to uncured composites.

Table 6.2: Comparison of the UD composite material properties obtained by the present analysis (Malek 2014) and data available in the literature (Ersoy et al. (2010).

| Property | Unit | SCFM | | FEBM | | Measured | Present | |
		Uncured	Cured	Uncured	Cured	Cured	Uncured	Cured
E_{11}	MPa	131,000	133,000	132,200	134,000	135,000	130,890	133,100
$E_{22} = E_{33}$	MPa	122	9,130	165	9,480	9,500	146.2	9,626
$G_{12} = G_{13}$	MPa	41.1	5,210	44.3	5,490	4,900	36.94	5,202
G_{23}	MPa	37.2	3,210	41.6	3,272	4,900	36.71	3,139
$v_{12} = v_{13}$	-	0.327	0.272	0.346	0.271	0.300	0.327	0.267
v_{23}	-	0.639	0.465	0.982	0.448	0.450	0.991	0.534

Notes: The 1-axis is along the fibre direction, the 2-axis is perpendicular to the fibres but in the plane of the lamina and the 3-axis is the out-of-plane direction.
SCFM: Self Consistent Field Micromechanics (Ersoy et al. 2010).
FEBM: Finite Element Based Micromechanics (Ersoy et al. 2010).
Measured: Supplied by AIRBUS UK except for G_{23}; G_{23} is measured by Ersoy et al. 2010 (no data for uncured state).
Present: Based on micromechanical equations (Malek 2014).

6.3.1.2. Meso-scale properties

The effective elastic properties of the UD composites obtained from the micromechanics model can be used to estimate the effective elastic properties of the woven fabrics at the meso-scale considering the yarns' arrangement. As the overall stiffness of the cured woven composites are reported in the literature for certain yarns and resins (see Table 6.3), the meso-scale model can be validated separately from the micro-scale model and for a specific woven composite characterized thoroughly by Naik (1994).

The meso-scale analysis involves discretely modelling the yarn architecture within a RUC (see Fig. 6.1). The woven composite is specified by known quantities such as filament diameter, yarn filament count, yarn packing density p_d, yarn spacing and overall fibre volume fraction. By assuming the same value of yarn architecture as described in Naik (1994), the unknown quantities such as yarn thickness, yarn cross-sectional areas, yarn crimp angle and yarn undulating paths which are required for a discrete yarn can be determined. Then, each yarn is discretised again into yarn slices. Finally, the three-dimensional effective properties are computed using the material properties (see Table 6.3), spatial orientation and volume fraction of each yarn slice in a volume averaging technique. The computed stiffnesses for the woven composites were

found to be unchanged for a minimum number of yarn slices, n, equal to 12 in a convergence study investigated by Naik (1994), a value of $n = 12$ was applied for all the analyses in this study. The analytical procedure for the effective elastic properties of the RUC is implemented in MATLAB and results are compared with experimental data in Table 6.4. Table 6.4 also includes results obtained from 3D finite element analysis and analytical technique using TEXCAD presented in Naik (1994). It can be seen that the predicted elastic constants of 5-harness satin (5HS) weave composite agree well with data provided in Naik (1994).

Table 6.3: Yarn and resin properties used in validation model for woven composite properties according to Naik (1994).

Material	E_{11} GPa	$E_{22} = E_{33}$ GPa	G_{12} GPa	v_{12}	v_{23}
Yarn	144.8	11.73	5.52	0.23	0.3
Resin	3.45	3.45	1.28	0.35	0.35

Table 6.4: Comparison of results for cured woven composites.

Laminate type	Approach	E_{xx}, E_{yy} GPa	E_{zz} GPa	G_{xz}, G_{yz} GPa	G_{xy} GPa	v_{xz}, v_{yz}	v_{xy}
5-harness satin weave	TEXCAD[a]	66.33	11.51	4.93	4.89	0.342	0.034
	FEM[a]	65.99	11.38	5.03	4.96	0.320	0.030
	Test[a]	69.43	-	-	5.24	-	0.060
	Present	65.45	11.77	4.73	4.89	0.337	0.035

Notes: [a]Approaches are presented in Naik (1994)
xy-plane is the plane of woven fabric

6.3.2. Viscoelastic material

As described at the beginning of Subsection 6.3, there exist gaps in the literature regarding the micro- and meso-scale characterisation of uncured woven composites. From an industry perspective, determining nine engineering constants for full characterization of orthotropic woven composites is extremely challenging. Hence, it is almost impossible to validate the accuracy of the modelling framework for estimating the properties of uncured composites at the smaller scales (i.e. micro- and meso-scale).

Considering the importance of bending properties of uncured plies on wrinkle formation, the macro-scale simulation results are presented and the viscoelastic modelling approach is validated separately based on available data on the bending behaviour of a specific woven composite loaded at different rates. A plate geometry with dimensions similar to the experiments of Alshahrani & Hojjati (2017b) is selected for this purpose (Fig. 6.4). The total length of the sample is 150 mm with an un-gripped length of 120 mm. The cross-sectional area of the sheet is 50 mm wide by 0.55 mm thick. Mesh type, mesh size and boundary conditions are similar to the bending verification model described in the previous section.

As the analysis of the bending behaviour during the composite forming process requires high curvature to accurately simulate the process, a tip displacement of 50 mm is applied (Fig. 6.5). It is also noted that the position of applied displacement is located 4 mm from the free end to avoid generating any tensile stresses on the sample during bending (Alshahrani & Hojjati 2017b). This distance is then excluded from the total length of the sample in bending moment calculations. As the deflection curve of the sheet has large slopes, the large deformation cannot be neglected in the expression of the curvature. Hence, the exact expression for curvature (Eq. 6.2) is used.

Prior to investigating the effect of loading rates on the time-dependent behaviour of uncured prepregs, the material is assumed to behave as an isotropic elastic solid. The material is then changed to orthotropic viscoelastic to represent the behaviour of textile composites. Unlike continuous materials such as sheet metal or cured solid composites, uncured textile sheets have a very low bending stiffness due to the possible relative movement of reinforcing fibres. According to (Boisse et al. 2011), the plate theory relation between the tensile and the bending stiffness is no longer valid for uncured samples. In the previous work of the authors, Le et al. (2021), the compressive stiffness of uncured prepregs was found to be mainly dominated by the resin modulus even in the presence of the fibres. The effect of fibres was found negligible on the compressive modulus of uncured composites due to their very small buckling load at the micro-scale. Therefore, for modelling purposes, the uncured composite plate in Fig. 6.2c is assumed to be composed of two different materials with two distinct moduli (E_t and E_c). The left-hand side of the plate is assumed to be under compression with $E_1 = E_c = 200$ MPa while the right-hand side is under tension with $E_2 = E_t = 60$ GPa based on literature data. The

compressive modulus (E_c) has been estimated from the slope of stress-strain curve in the elastic region of the buckling test conducted by Alshahrani & Hojjati (2017c) (see Table 2.1). In the lack of experimental data on tensile properties of uncured composites, E_t is estimated to be 60 GPa based on a micro- and meso-scale analyses considering the fibre modulus of 200 GPa and yarn fibre volume fraction and overall volume fraction for the woven unit cell of 0.6 and 0.5 respectively. Knowing E_t, E_c, and the material cross-section, the position of the neutral axis (the x-axis) (see Fig. 6.2c) has been determined from the assumption that the resultant axial force acting on the cross-section is zero. This simple analysis enables us to estimate the effective bending stiffness of the uncured prepreg ($E_{bend \ or} \ E_e$) by converting the composite plate (E_c, E_t) into an equivalent plate made of only one material with E_e. The approach is known as the transformed-section method given by the following equation (Gere & Goodno 2009):

$$E_1 I_1 + E_2 I_2 = EI \ , \tag{6.8}$$

in which I_c and I_t are the moments of inertia about the neutral axis (the x-axis) of the cross-sectional areas of two distinct materials, E_c and E_t respectively. I is the moment of inertia about the neutral axis of the homogeneous cross-section assumed with an effective bending modulus (E_e). Using Eq. 6.8, E_e becomes 700 MPa for an assumed homogeneous isotropic elastic cross-section. As perfect bonding has been assumed between the plies in this simple analysis, two more cases with E_t and E_c assigned to the entire plate sections are also considered to get the upper and lower bounds; only the lower bound is shown in Fig. 6.6 for clarity. Fig. 6.6 shows the lower bound of bending curve for the isotropic elastic plate with compressive modulus assumed for the entire cross-sections. The case with the effective bending modulus ($E_e = 700$ MPa) gives the same result as the case using biaxial elastic moduli for the cross-section under compression and tension during bending. Experimental data conducted by (Alshahrani & Hojjati 2017b) for 5HS prepregs in warp direction are also presented in Fig. 6.6 for comparison purpose.

A mesh sensitivity analysis is also conducted in this study. The results have been summarized in Table 6.5. Similar results with maximum difference of ~1% in terms of deformed shape as well as the required force (F) to bend the laminate to tip displacement of 50 mm were noted. Based on the conducted convergence study, the 1.92 mm × 2 mm × 0.275 mm mesh (Mesh 2) was selected for subsequent cases.
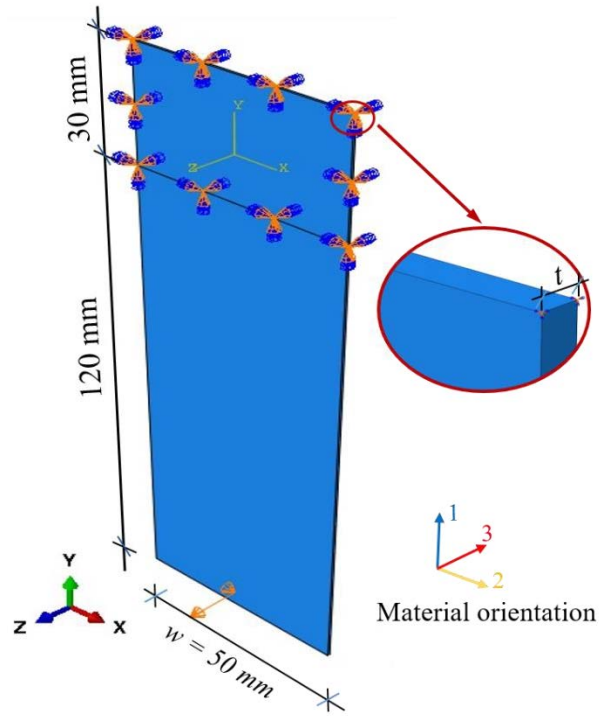
Figure 6.4: Detail of the 3D model under bending
(According to Alshahrani & Hojjati (2017b))
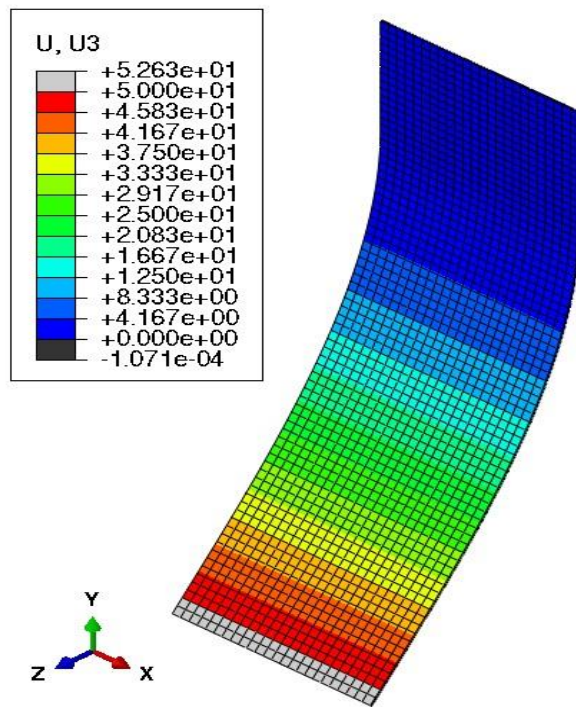
Figure 6.5: Deformed sample at tip displacement of 50 mm (U_3 in mm)
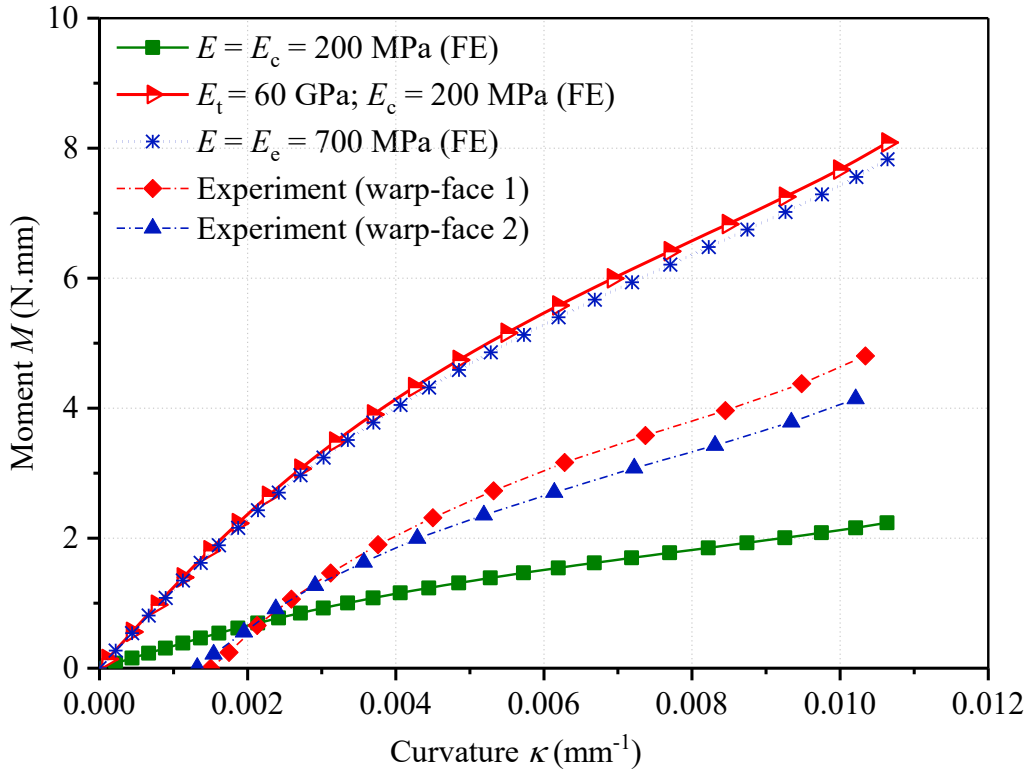
Figure 6.6: Bending moment versus curvature based on isotropic elastic material assumption.

Table 6.5: Mesh convergence study results (isotropic elastic case ($E = 700$ MPa, $v = 0.4$)).

	Mesh 1	Mesh 2	Mesh 3	Mesh 4
Number of Elements	2,401	3,901	8,209	16,417
Number of Nodes	13,846	22,264	46,350	80,086
Force F (N)	6.754×10^{-02}	6.751×10^{-02}	6.746×10^{-02}	6.736×10^{-02}
Simulation time (sec)	167	285	655	1867

Coarse mesh →→→→→→→→→ Fine mesh

Mesh: Num in X × num in Y × num in Z (see XYZ coordinate in Fig. 6.4)

Mesh 1: 20 × 60 × 2   Mesh 3: 36 × 114 × 2
Mesh 2: 26 × 72 × 2   Mesh 4: 36 × 114 × 4

As the anisotropic nature of woven composites may affect the deformation behaviours during forming (Le et al. 2021), the orthotropic viscoelastic properties are considered in the bending behaviour. It should be emphasised, the fibre-bed, i.e. the slight waviness of the fibres in composites, has been considered to play a significant part in carrying the load in the transverse orientation at the early stage of cure (Malek, Vaziri & Poursartip 2018). Therefore, the fibre-bed elastic properties are incorporated into the micromechanics equations (Malek 2014) at micro-scale to estimate the effective viscoelastic properties of the uncured UD prepreg before using such properties as input

parameters for the meso-scale model (Naik 1994). The mechanical properties of the resin, fibre and fibre-bed that have been used for viscoelastic analysis at micro-scale are listed in Table 6.6 for composites assumed under compression (Table 6.6a), tension (Table 6.6b) and bending (Table 6.6c), respectively.

Table 6.6a: Input material properties of fibre, resin and fibre bed used in the bending simulation of textile prepregs. The compressive properties have been assigned to the bending model.

$V_f =$ 0.600

| Property | Unit | Fibre[1] | Resin[2] | | Fibre bed[3] |
			Relaxed	Unrelaxed	
E_1	GPa	8.00×10^{-2}	3.00×10^{-6}	1.65×10^{-1}	8.00×10^{-2}
$E_2 = E_3$	GPa	1.72×10^{-1}	3.00×10^{-6}	1.65×10^{-1}	1.12×10^{-4}
$G_{12} = G_{13}$	GPa	27.60	1.00×10^{-6}	5.52×10^{-2}	1.13×10^{-4}
G_{23}	GPa	0.07	1.00×10^{-6}	5.52×10^{-2}	4.49×10^{-5}
$v_{12} = v_{13}$	-	0.2	0.495	0.495	
v_{23}	-	0.25	0.495	0.495	0.250

Notes: [1] Taken from (Johnston, Vaziri & Poursartip 2001) except E_1, E_2 (compressive moduli); compressive moduli, E_1, E_2 are selected according to Le et al. (2021)
[2] Resin properties are taken from (Niaki et al. 2018)
[3] Taken from (Malek, Vaziri & Poursartip 2018) except E_1 (compressive modulus); compressive modulus, E_1, is selected according to Le et al. (2021)

Table 6.6b: Input material properties of fibre, resin and fibre bed used in the bending simulation of textile prepregs. The tensile properties have been assigned to the bending model.

$V_f =$		0.600			
Property	Unit	Fibre[1]	Resin[2] Relaxed	Resin[2] Unrelaxed	Fibre bed[3]
E_1	GPa	2.10×10^2	3.00×10^{-6}	1.65×10^{-1}	2.10×10^2
$E_2 = E_3$	GPa	1.72×10^1	3.00×10^{-6}	1.65×10^{-1}	1.12×10^{-4}
$G_{12} = G_{13}$	GPa	27.60	1.00×10^{-6}	5.52×10^{-2}	1.13×10^{-4}
G_{23}	GPa	6.88	1.00×10^{-6}	5.52×10^{-2}	4.49×10^{-5}
$v_{12} = v_{13}$	-	0.2	0.495	0.495	
v_{23}	-	0.25	0.495	0.495	0.250

Notes: [1] Taken from Johnston, Vaziri & Poursartip (2001)
[2] Resin properties are taken from Niaki et al. (2018)
[3] Taken from Malek, Vaziri & Poursartip (2018)

Table 6.6c: Input material properties of fibre, resin and fibre bed used in the bending simulation of textile prepregs. The effective bending properties have been assigned to the model.

$V_f =$		0.600			
Property	Unit	Fibre[1]	Resin[2] Relaxed	Resin[2] Unrelaxed	Fibre bed[3]
E_1	GPa	1.50×10^0	3.00×10^{-6}	1.65×10^{-1}	1.50×10^0
$E_2 = E_3$	GPa	1.72×10^{-1}	3.00×10^{-6}	1.65×10^{-1}	1.12×10^{-4}
$G_{12} = G_{13}$	GPa	27.60	1.00×10^{-6}	5.52×10^{-2}	1.13×10^{-4}
G_{23}	GPa	0.07	1.00×10^{-6}	5.52×10^{-2}	4.49×10^{-5}
$v_{12} = v_{13}$	-	0.2	0.495	0.495	
v_{23}	-	0.25	0.495	0.495	0.250

Notes: [1] Taken from (Johnston, Vaziri & Poursartip 2001) except E_1, E_2; E_1, E_2 are selected following the comprehensive review in the literature (see Table 2.1)
[2] Resin properties are taken from (Niaki et al. 2018)
[3] Taken from (Malek, Vaziri & Poursartip 2018) except E_1; E_1 is selected following the comprehensive review in the literature (see Table 2.1)

The fibre-bed properties are derived from the effective elastic properties of a dry prepreg estimated in Malek, Vaziri & Poursartip (2018). Due to the lack of data on the properties of uncured resin (Alshahrani & Hojjati 2017b), assumptions have been made

in this research based on available data in the literature (Niaki et al. 2018; Thorpe 2012). The resin viscoelastic properties are kept unchanged to better understand the effect of fibre-bed on the bending response of composite plates and comparison purposes. Prony series constants for MTM45-1 (Thorpe 2012) listed in Table 6.9 are assumed for validating the model against the experimental data reported in (Alshahrani & Hojjati 2017b). The fibre properties reported in Johnston, Vaziri & Poursartip (2001) are used here, except the stiffness in the fibre direction. The longitudinal elastic modulus of the fibre and fibre-bed in compression (see Table 6.6a) are assumed to be equal to 80 MPa due to the very low buckling load of a single fibre demonstrated in Le et al. (2021). Under tension, the same properties as in Johnston, Vaziri & Poursartip (2001) (i.e. 210 GPa) (see Table 6.6b) are assumed. However, a low value for fibre Young's modulus (1.5 GPa, see Table 6.6c) according to the review conducted in previous section (see Table 2.1) for uncured composites under bending. The effective viscoelastic characteristics of UD composites at micro-scale are determined by using analytical micromechanics equations following the approach presented in (Malek 2014; Malek et al. 2018). It is noted that the fibre-bed elastic constants will be added to the resin relaxed modulus to obtain the modified resin properties which are later combined with fibre properties in the micromechanics equations. Table 6.7a, Table 6.7b and Table 6.7c demonstrate the predictions for UD composites under compression, tension and bending assumptions, respectively.

Table 6.7a: Micro-scale predictions of UD mechanical properties using micromechanics equations with fibre-bed effect (Malek 2014) under compressive load.

Properties of UD	Unit	Present	
		Relaxed	Unrelaxed
E_{11}	MPa	64.03	110.8
$E_{22} = E_{33}$	MPa	1.689	169.1
$G_{12} = G_{13}$	MPa	0.456	219.6
G_{23}	MPa	0.443	63.02
$v_{12} = v_{13}$	-	0.316	0.340
v_{23}	-	0.905	0.341

Table 6.7b: Micro-scale predictions of UD mechanical properties using micromechanics equations with fibre-bed effect (Malek 2014) under tensile load.

Properties of UD	Unit	Present	
		Relaxed	Unrelaxed
E_{11}	GPa	168.0	168.0
$E_{22} = E_{33}$	MPa	1.707	830.5
$G_{12} = G_{13}$	MPa	0.456	219.6
G_{23}	MPa	0.446	213.2
$v_{12} = v_{13}$	-	0.316	0.318
v_{23}	-	0.913	0.947

Table 6.7c: Micro-scale predictions of UD mechanical properties using micromechanics equations with fibre-bed effect (Malek 2014) under bending load.

Properties of UD	Unit	Present	
		Relaxed	Unrelaxed
E_{11}	MPa	1,200	1,246
$E_{22} = E_{33}$	MPa	1.693	193.2
$G_{12} = G_{13}$	MPa	0.456	219.6
G_{23}	MPa	0.443	63.02
$v_{12} = v_{13}$	-	0.316	0.346
v_{23}	-	0.909	0.523

At meso-scale, the mechanical viscoelastic constants for 5-harness satin weave composites are predicted using the analytical model developed by (Naik 1994) and shown in Table 6.8. The analytical technique implemented in MATLAB is similar to the one described in the elastic section. A specific MATLAB script has been created for this purpose. Due to the missing data on the yarn architecture, most of the known quantities for a specified weave composite are taken from Naik (1994). For example, Alshahrani & Hojjati (2017b) only provided information about the used prepreg such as the 6 k yarn size (k – one thousand filaments) and the thickness of the single uncured prepreg (0.55 mm). Inputs for constituents' properties such as resin and yarn properties of a RUC are taken from Table 6.6 and Table 6.7. The estimated mechanical properties of 5-harness

satin weave composites provided in Table 6.8a, Table 6.8b and Table 6.8c correspond to the inputs from Table 6.7a, Table 6.7b and Table 6.7c, respectively.

Table 6.8a: Meso-scale predictions of 5HS prepreg mechanical properties under compression using the analytical technique of Naik (1994).

Laminate type	Material	E_{xx}, E_{yy} MPa	E_{zz} MPa	G_{xz}, G_{yz} MPa	G_{xy} MPa	v_{xz}, v_{yz}	v_{xy}
5HS	Relaxed resin	24.10	5.80	7.08×10^{-1}	3.79×10^{-1}	0.798	0.002
	Unrelaxed resin	190.70	248.90	118.60	187.10	0.360	0.578

Table 6.8b: Meso-scale predictions of 5HS prepreg mechanical properties under tension using the analytical technique of Naik (1994).

Laminate type	Material	E_{xx}, E_{yy} GPa	E_{zz} GPa	G_{xz}, G_{yz} GPa	G_{xy} GPa	v_{xz}, v_{yz}	v_{xy}
5HS	Relaxed resin	57.26	0.02	0.039	3.80×10^{-4}	0.870	1.68×10^{-4}
	Unrelaxed resin	58.94	6.66	1.055	0.192	0.849	0.003

Table 6.8c: Meso-scale predictions of 5HS prepreg mechanical properties under bending using the analytical technique of Naik (1994).

Laminate type	Material	E_{xx}, E_{yy} MPa	E_{zz} MPa	G_{xz}, G_{yz} MPa	G_{xy} MPa	v_{xz}, v_{yz}	v_{xy}
5HS	Relaxed resin	412.60	8.40	5.10	3.80×10^{-1}	0.800	2.94×10^{-4}
	Unrelaxed resin	680.20	394.10	126.20	187.20	0.676	0.212

It is worth mentioning that based on micro- and meso-scale analyses with the assumption of longitudinal fibre modulus (E_1) of 80 MPa (see Table 6.6a) and 210 GPa (see Table 6.6b) for uncured composites under compression and tension respectively, the in-plane properties of unrelaxed prepreg 5HS (E_{xx}) are estimated to be 190 MPa (see

Table 6.8a) and 58 GPa (see Table 6.8b). Such values agree well with the predicted compressive modulus (E_c = 200 MPa) and tensile modulus (E_t = 60 GPa) of the isotropic elastic composite plate described earlier (see Section 6.2.2 and Fig. 6.6). A similar analysis using the transformed-section method (Eq. 6.8) may be applied to estimated the effective bending stiffness of the uncured prepreg. It is interesting that the computed value of 680 MPa matches the unrelaxed modulus of prepreg 5HS (see Table 6.8c) obtained from micro- and meso-scale analyses considering the longitudinal fibre modulus (E_1) of 1.5 GPa.

Table 6.9: Prony series parameters for MTM45-1 epoxy as reported in Thorpe's thesis (Thorpe 2012).

Maxwell Element (i)	w_i	τ_i (s)
1	3.44181×10^{-1}	1×10^{-2}
2	1.14728×10^{-1}	1×10^{-1}
3	1.33849×10^{-1}	1×10^{0}
4	1.52970×10^{-1}	1×10^{1}
5	1.33849×10^{-1}	1×10^{2}
6	0.95606×10^{-1}	1×10^{3}
7	0.19121×10^{-1}	1×10^{4}
8	0.3824×10^{-2}	1×10^{5}
9	0.1338×10^{-2}	1×10^{6}
10	0.382×10^{-3}	1×10^{7}
11	0.96×10^{-4}	1×10^{8}
12	0.38×10^{-4}	1×10^{9}

The DF approach for modelling the response of orthotropic viscoelastic composites developed by Malek et al. (2018) requires the components of the relaxation matrix. These values could be defined by the Prony series expansions as given below.

$$E(t) = E^r + (E^u - E^r) \sum_{i=1}^{12} w_i \, e^{\left(-\frac{t}{\tau_i}\right)}$$
(6.9)

where E^r and E^u are the relaxed and unrelaxed Young's modulus, respectively. Parameters w_i and τ_i are presented in Table 6.9. The relaxed and unrelaxed values and the Prony series

parameters corresponding to each component are then calculated and given in Table 6.10 and Table 6.11 respectively.

Table 6.10: Relaxed and unrelaxed values of components of the composite relaxation matrix. The effective bending properties have been assigned to the model at micro-scale.

Component	C_{ij}^r(MPa)	C_{ij}^u(MPa)
C_{11}	629.6	1757.2
C_{22}	629.6	1757.2
C_{33}	17.6	1212.3
C_{44}	0.8	375.0
C_{55}	19.7	258.2
C_{66}	19.7	258.2
C_{12}	5.0	1039.8
C_{13}	25.1	1041.7
C_{23}	25.1	1041.7

Table 6.11: Prony series parameters for each component of the relaxation matrix of the composite material obtained from micromechanics equations following the approach presented in Malek et al. (2018). The effective bending properties have been assigned to the model at micro-scale.

i	w_{11}	w_{22}	w_{33}	w_{44}	w_{55}	w_{66}	w_{12}	w_{13}	w_{23}
1	388.098	388.098	411.193	128.793	82.087	82.087	356.158	349.894	349.894
2	129.367	129.367	137.066	42.931	27.363	27.363	118.721	116.632	116.632
3	150.928	150.928	159.909	50.086	31.923	31.923	138.507	136.071	136.071
4	172.489	172.489	182.753	57.241	36.483	36.483	158.293	155.509	155.509
5	150.928	150.928	159.909	50.086	31.923	31.923	138.507	136.071	136.071
6	107.805	107.805	114.220	35.776	22.802	22.802	98.933	97.193	97.193
7	21.561	21.561	22.844	7.155	4.560	4.560	19.786	19.438	19.438
8	4.312	4.312	4.569	1.431	0.912	0.912	3.957	3.887	3.887
9	1.509	1.509	1.599	0.501	0.319	0.319	1.385	1.360	1.360
10	0.431	0.431	0.456	0.143	0.091	0.091	0.395	0.388	0.388
11	0.108	0.108	0.114	0.036	0.023	0.023	0.099	0.097	0.097
12	0.043	0.043	0.046	0.014	0.009	0.009	0.040	0.039	0.039

Fig. 6.7 compares the orthotropic viscoelastic behaviours of 5HS prepregs made of different assumed values of fibre stiffness using UMAT with experimental data conducted by Alshahrani & Hojjati (2017b) in warp directions. It is noted that when the longitudinal fibre modulus is assumed to be 1.5 GPa, the obtained bending behaviour of its composites plate agrees very well with the test data reported in Alshahrani & Hojjati (2017b). It is interesting that the predicted uncured in-plane properties of the 5HS prepreg according to the assumed fibre stiffness of 1.5 GPa is 680 MPa (see Table 6.8c). This value is in a good correlation with the predicted parameter extracted from averaged relaxation curves conducted by Alshahrani & Hojjati (2017c) (see Table 2.1). Also, such effective bending stiffness can be computed from the in-plane properties of uncured prepreg under compression and tension using the transformed-method via Eq. 6.8, i.e. 190 MPa (see Table 6.8a) and 58 GPa (see Table 6.8b) for compressive and tensile moduli, respectively. Hence, the low value for the fibre bending stiffness should be attributed to the low compressive modulus of the uncured composites which is dominated by the resin viscoelastic properties for prepregs under bending. Moreover, such a low value of the longitudinal fibre modulus considered here (1.5 GPa) is consistent with previous findings in the literature (see Table 2.1). To better understand the effect of fibre modulus, another bending curve with the assumption of entire section having fibres with $E_1 = 80$ MPa (compression modulus) at micro-scale is added to Fig. 6.7.

To demonstrate the effect of loading rate on the bending behaviours of 5HS prepreg, macro-scale viscoelastic analysis using UMAT with three loading rates at 3 mm/sec, 6 mm/sec and 9 mm/sec as in the experiments conducted by Alshahrani & Hojjati (2017b) are also performed. The results are provided in Fig. 6.8. A similar trend in rate-dependent bending behaviour of both numerical simulations and experimental data can be observed; a higher loading rate results in the higher load required to bend the composite plates to the desired tip displacement of 50 mm.
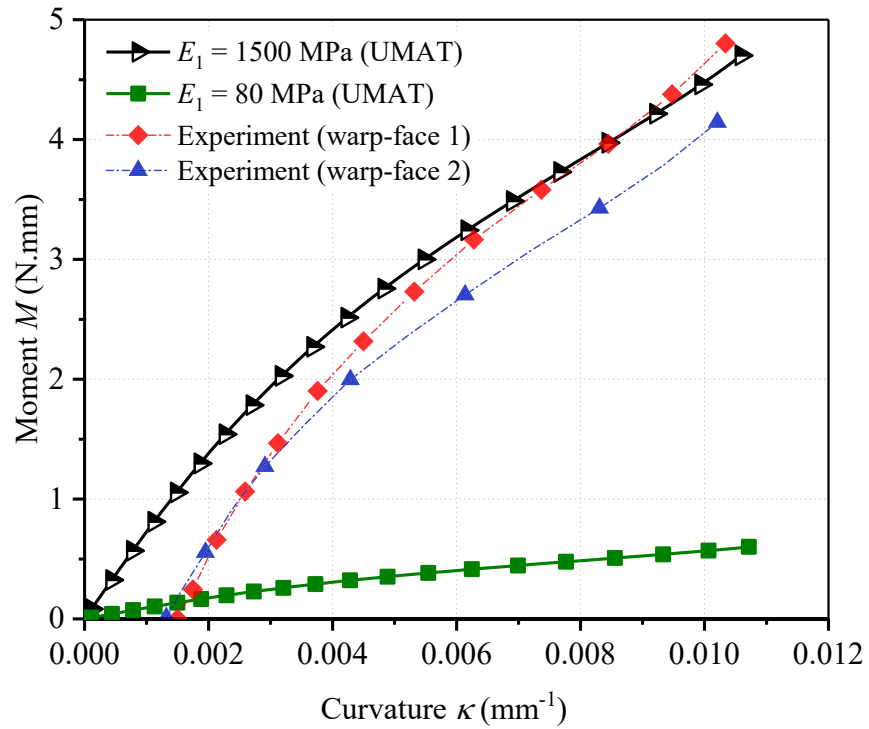
Figure 6.7: Bending moment versus curvature of uncured 5HS prepreg with different values of fibre stiffness (E_1). A loading rate of 3 mm/s is considered for all cases.
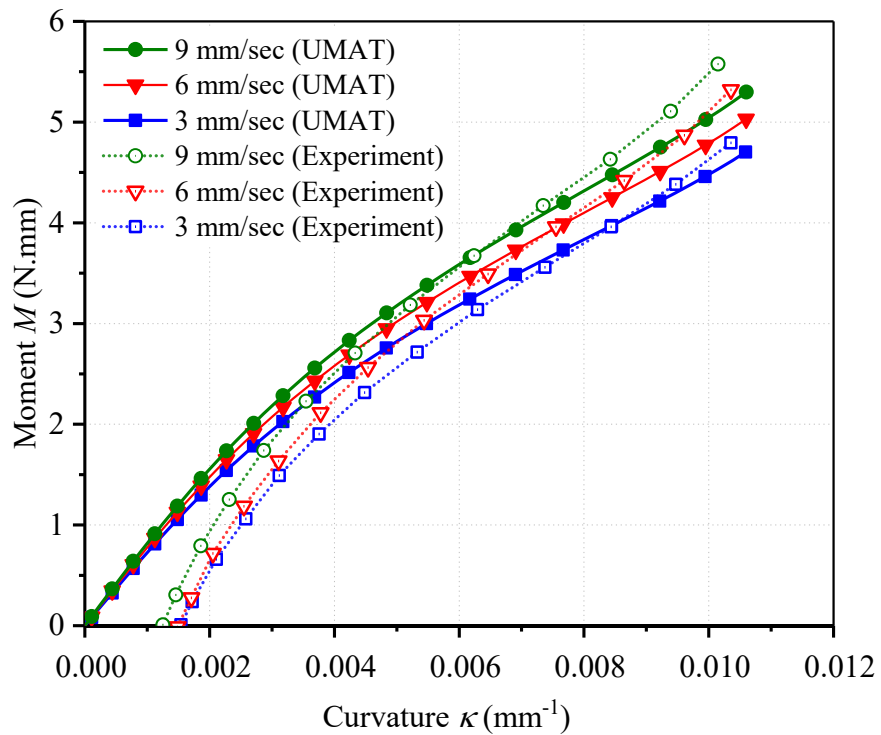
Figure 6.8: Effect of loading rate on bending moment versus curvature of 5HS prepreg. Fibre stiffness is assumed to be $E_1 = 1.5$ GPa in all cases.

6.4. Discussion

To emphasise the effect of ply anisotropy on the bending response of uncured/ partially cured composites during forming, an isotropic viscoelastic case corresponding to the validation case discussed above ($E_1 = 1.5$ GPa, see Table 6.6c) is investigated using Abaqus built-in viscoelastic material model (IF). The initial properties for uncured or partially cured composites are the instantaneous Young's moduli, E_o, and Poisson's ratio, v_o. The instantaneous Young's moduli is assumed as 680 MPa according to the uncured in-plane properties of 5HS composites presented in Table 6.8c. Poisson's ratio is kept unchanged and equal to 0.495. Viscoelastic properties are described using Prony series constants listed in Table 6.8. Experimental data conducted by (Alshahrani & Hojjati 2017b) for 5HS prepregs in warp direction are also shown in Fig. 6.9 for comparison purpose. It can be observed that the higher transverse properties due to the presence of fibre and fibre-bed effect increase the required loads to reach the specific tip displacement.
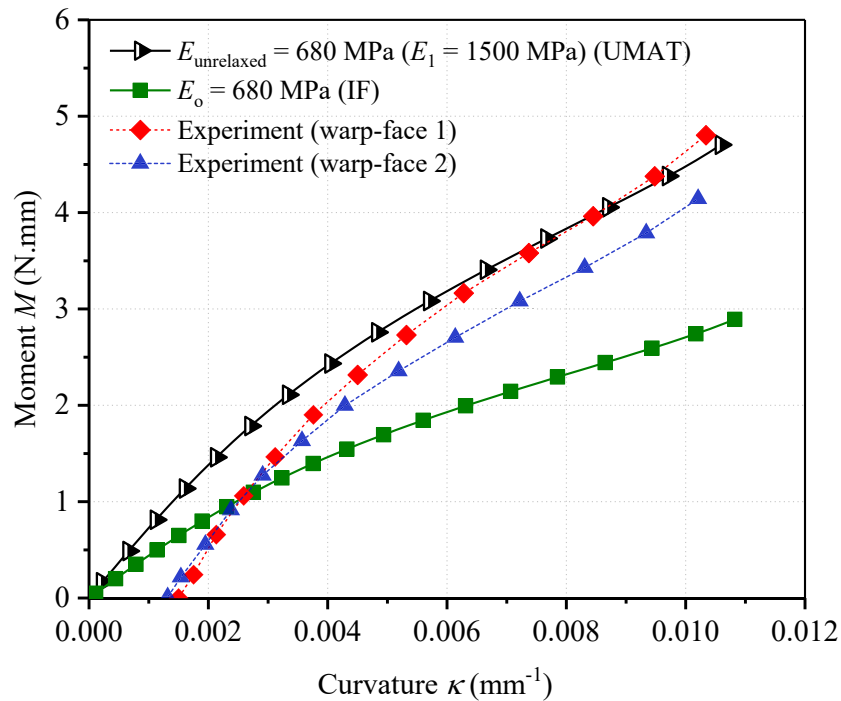
Figure 6.9: Comparison between IF and DF approaches for the validation case (effective fibre modulus $E_1 = 1.5$ GPa). The viscoelastic properties of the resin are provided in Table 6.9.

To investigate the role of resin in viscoelastic bending behaviour, similar cases with the same material inputs for fibre stiffness but ignoring resin contribution in micro- and meso-scale analyses using micromechanics equations (Malek 2014; Naik 1994) are considered. The material properties of UD and 5HS prepreg, as well as dry 5HS according to five selected input parameters of fibre stiffness in between 80 MPa to 2000 MPa are listed in Table 6.12 for consideration purpose. Fig. 6.10 compares bending moments in prepreg and dry 5 HS satin weave sample conducted by Alshahrani & Hojjati (2017b) and numerical analyses. Only two pairs of cases according to assumed fibre modulus of 1.5 GPa and 500 MPa (see Table 6.12) along with the experimental data are plotted in Fig. 6.10 for highlighting the contribution of resin to the bending results. It can be seen that the difference between prepreg and dry samples obtained from the experimental study (Alshahrani & Hojjati 2017b) is higher than the one predicted by numerical analyses. However, it should be emphasised that the uncured resin properties have not been provided by Alshahrani & Hojjati (2017b) and therefore assumptions have been made in this study based on available data in the literature (Niaki et al. 2018; Thorpe 2012). The observed discrepancy in Fig. 6.10 may be attributed to the difference between the real rheological characteristics and the assumed values here. Assuming the fibre bending stiffness of 500 MPa, the bending behaviour of its dry 5HS composite correlates well with the corresponding experimental result.

Table 6.12: Summary of composite properties for UD and 5HS prepregs, as well as dry UD and 5HS according to different values of fibre stiffness, E_1.

E_1 (MPa)	Prepreg				Dry	
	E_{11} (MPa) (UD)		E_{xx}, E_{yy} (MPa) (5HS)		E_{11} (UD) (MPa)	E_{xx}, E_{yy} 5HS (MPa)
	Relaxed	Unrelaxed	Relaxed	Unrelaxed		
2,000	1,600.00	1,645.10	549.10	836.10	1,600.00	549.10
1,500	1,200.00	1,246.00	412.60	680.20	1,200.00	412.60
1,000	800.03	846.30	276.10	519.00	800.03	276.10
500	400.03	446.34	139.50	348.10	400.03	139.50
80	64.03	110.76	24.10	190.70	64.03	24.10
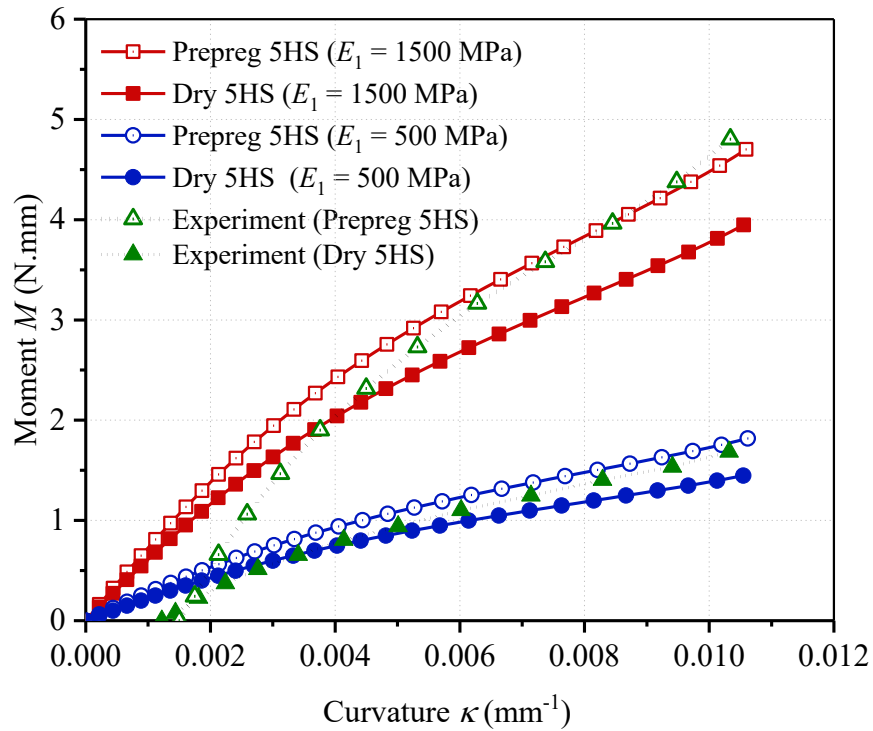
Figure 6.10: Comparision between prepreg and dry 5HS behaviour according to different assumed values for fibre stiffness, E_1.

6.5. Summary and conclusions

An efficient multi-scale modelling approach was presented to predict the bending behaviour of viscoelastic composites under various loading rates. To improve simulation efficiency, analytical models were employed to estimate the effective mechanical properties of uncured/partially cured 5HS composites at micro- and meso-scales. For macro-scale simulations, a 3D orthotropic material model implemented as a UMAT subroutine in Abaqus software was employed to implicitly account for the complex hierarchical nature of woven composites. Consequently, the proposed approach should be emphasised as a rapid method for determining the role of viscoelastic parameters and the yarns architecture on the out-of-plane bending behaviour essential for predicting wrinkle formation in woven composites.

A comprehensive search in the literature was conducted to obtain input properties for the model. While several researchers have explored the in-plane shear characteristics of woven composites, it was discovered that the in-plane Young's moduli of uncured UD and woven composites, as well as the viscoelastic shear properties of resins, have received little attention. Until now, the researchers have concentrated on determining the in-plane

shear properties of uncured composites in order to simulate the forming process. As demonstrated in this study, in addition to in-plane shear properties, the in-plane Young's moduli of composites in both tension and compression can significantly affect the out-of-plane response of thin composites. Hence, these properties should be thoroughly described in order to accurately predict wrinkle formation during composite manufacturing.

In terms of orthotropic properties, it was demonstrated that the transverse moduli associated with the presence of fibre and fibre-bed effect increase the bending stiffness of uncured woven composites. Numerical simulations of dry 5HS as well as their prepregs were performed. There were minor differences between the numerical analyses results and the experimental data presented for dry and uncured samples. Hence, a parametric study was conducted to gain a better understanding of the role of viscoelastic resin on the bending response. The parametric study demonstrated that the discrepancies between the model predictions and test data can be attributed to the assumed viscoelastic characteristics of the resin and the compression modulus of prepreg. Characterising the viscoelastic properties of uncured Cycom 5320 epoxy resin (similar to MTM45-1 resin in the literature) is suggested as a future work that will improve the accuracy of the bending simulations.

Due to the scarcity of published data on the viscoelastic properties of uncured composites, assumptions were made in this chapter for estimating the compression and tension properties of uncured woven composites using data from the literature. For the first time, the numerical results elucidated that the extremely low value for fibre longitudinal modulus commonly used in the majority of other models is in fact an effective value that implicitly captures the combined effect of low compressive modulus and high tensile modulus of uncured composites in bending. Thus, additional experimental research on the viscoelastic characteristics of composites at the micro- and meso-scale is advised to better understand the formation of wrinkles caused by bending during cure.

A large body of research in the past has shown that the inter-ply slippage is one of the most important deformation mechanisms during the process of forming composites, particularly for multilayered textile prepregs. Therefore, the inter-ply slippage and its effect on the bending properties of thicker composites should be explored more rigorously

111

in the future. Finally, it should be noted that the temperature effect was not considered in the chapter. As the temperature is known to be an important parameter during forming, studying the variation of resin viscoelastic properties with temperature as well as inter-ply slippage and their effects on wrinkle formation (using the presented approach) are the subjects of our future work.

Chapter 7: Bending behaviour of multilayered viscoelastic plates with thin and soft interfaces

7.1. Introduction

Wrinkle formation during the forming process of laminated composite components poses obstacles to fully exploiting the potential of advanced composites. In the literature, much attention has been paid to deformation mechanisms behind wrinkle formation during consolidation such as in-plane shear, out-of-plane bending and inter-ply slippage (Alshahrani & Hojjati 2017a; Long 2005). It is now well-understood that bending properties of uncured thin laminates can influence the occurrence of wrinkles including the shape, magnitude and intensity of wrinkles (Belnoue et al. 2018). Analysing bending and buckling deformations of uncured thermoset composites is crucial to understanding contributing mechanisms and underlying physics of the wrinkle formation during hot drape forming process of laminated composites (Le et al. 2022; Le et al. 2021). In previous Chapter, Le et al. (2022) developed an efficient multi-scale approach for viscoelastic analysis of single-ply woven composites under bending. Apart from bending stiffness, inter-ply slippage has been also considered as an important deformation mechanism during the process of forming composites, particularly for multilayered textile composites (Alshahrani & Hojjati 2017a). Therefore, the objective of this chapter is to expand the application of the proposed method in previous chapter for the bending behaviour of multilayered textile composite separated by relatively soft interfaces.

Recently, researchers (Alshahrani & Hojjati 2017a) have employed Aniform Finite Element (FE) software with shell elements to model the viscoelastic bending behaviour of composite plies under conditions relevant to the forming process. Several time-consuming characterisation tests (i.e. bias extension test, bending test) are required to determine the material parameters for a suitable constitutive model. Unlike previous studies, in this study, the influence of various parameters including fibre stiffness, ply anisotropy, resin properties, and loading rates on the viscoelastic bending behaviour of laminated composites are analysed. The weaving pattern and the stacking sequence of plies are considered at the meso-scale while the effect of ply slippage is captured by introducing a thin interface layer between the plies at the macro-scale. Section 7.2 introduces briefly the methodology for simulating the bending behaviour of multilayered woven composites using the analytical homogenisation techniques at micro-and meso-

scale for material properties combined with the DF of viscoelasticity at macro-scale for numerical analysis. The details of the FE model and its verification and validation are provided in Section 7.3. The capabilities, limitations of the developed model and future work as well are summarized and discussed in Section 7.4.

7.2. Method

The viscoelastic behaviour of multilayered cantilever plates subjected to tip displacements has been modelled using the multi-scale approach introduced in Malek (2014) for orthotropic composites, as described with a flow chart in Fig. 7.1. At the micro-scale, the analytical micromechanics equations described in Malek (2014) are used to predict the effective viscoelastic properties of a RVE (see Fig. 7.1) of the solid unidirectional circular fibre composites with a specific fibre volume fraction (V_f). The fibre and resin viscoelastic properties are required for the input parameters of the micro-scale model. The fibre-bed elastic properties are also incorporated into the micromechanics equations (Malek 2014) as the fibre-bed has been known to play an important role in carrying the load in the transverse direction at the early stage of cure.

The effective properties obtained from the micromechanics model along with fabric architecture are then used to estimate the properties of a RUC of such woven fabric at the meso-scale. Details of geometric modelling of 5-harness satin weave composite, discretisation technique of yarns within RUC and calculation of 3D effective properties were described in Naik (1994). Analytical procedure using MATLAB script to determine nine engineering constants for full characterization of orthotropic woven composite has been validated in Le et al. (2022) and was presented in previous chapter. Once the effective meso-scale properties of the composite are obtained, they are employed directly in the structural analysis at the macro-scale. A differential form (DF) of orthotropic viscoelasticity implemented as a UMAT is used for structural level (macro-scale) simulations. For further details, the reader is referred to Chapter 3.

114
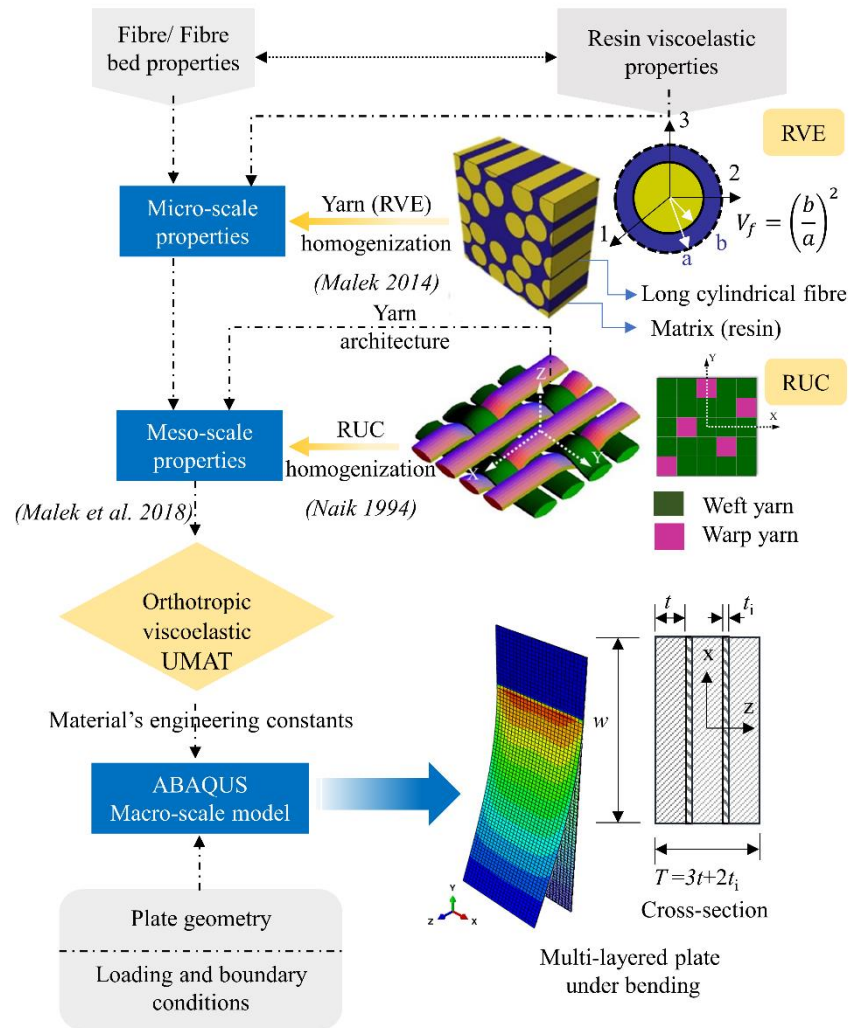
Figure 7.1: Schematic of the multi-scale modelling approach for bending behaviour of 5-harness satin weave multilayered composites from micro-scale to macro-scale.

7.3. Macro-scale model

Dimensions of the bending model are selected based on the bending test of a three-layer textile composite conducted in Alshahrani & Hojjati (2017a). Each ply has dimensions of 50 mm in width (*w*), 0.55 mm in thickness (*t*) and an un-gripped length of 120 mm, out of 150 mm in total length (*L*). Assuming that each ply is separated by a very thin interface, t_i = 0.01 mm (see Fig. 7.2). The three-layer cantilever plate is restrained from all displacements in a length of 30 mm as it was gripped along this distance (Alshahrani & Hojjati 2017a). It is modelled using a 20-node solid quadratic brick element with reduced integration elements (C3D20R). For a detailed mesh sensitivity analysis, the reader is referred to (Le et al. 2021). Based on a convergence study, a mesh size shown in Fig. 7.3 is utilized in this study. As the analysis of the bending behaviour

during the forming process requires high curvature to accurately simulate the process, a tip displacement of 30 mm is applied (Alshahrani & Hojjati 2017a) (see Fig. 7.4). It is noted that such applied displacement is located at a distance of 4 mm from the free end to avoid generating any tensile stresses on the sample during bending (Alshahrani & Hojjati 2017a).
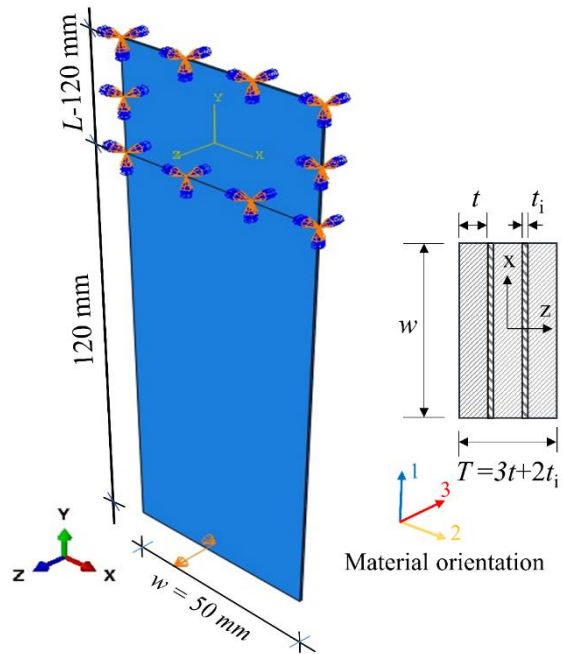
Figure 7.2: Bending model of a three-layer plate. Each layer is separated by a thin interface of 0.01 mm (according to Alshahrani & Hojjati (2017a))

116
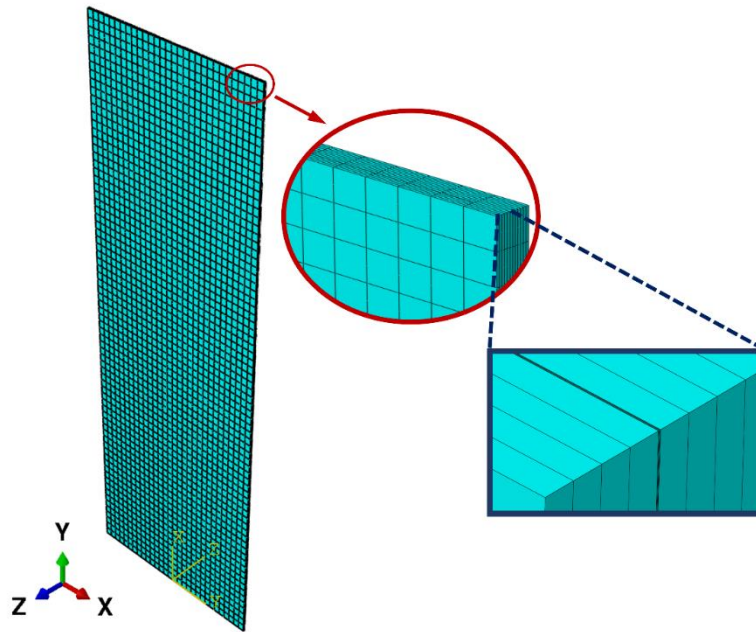
Figure 7.3: FE mesh of the three-layer plate used in this study. Numbers of mesh are 30 × 75 × 24 in X, Y and Z respectively.
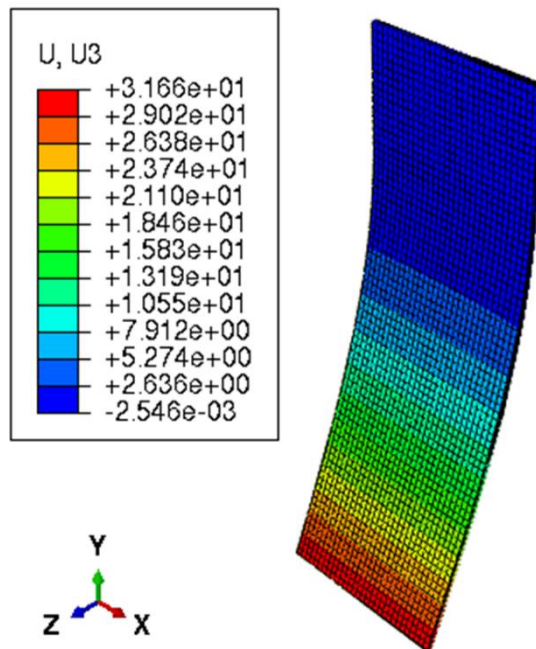
Figure 7.4: Deformed sample at tip displacement of 30 mm (U_3 in mm) under bending. The top end is is restrained from all displacements in a length of 30 mm.

7.4. Results and model validation

7.4.1. Elastic material

Firstly, based on a previous study shown in Chapter 6, the material properties of the layers under bending including E_p and v_p are kept unchanged and equal to 700 MPa

and 0.4 respectively. It is worth noting that such effective bending stiffness could be computed from the in-plane properties of uncured prepreg under bending with known compressive and tensile moduli using the transformed-method (Le et al. 2022). The Young's modulus of the interface, E_i takes a range of values shown in Table 7.1. Identical Poison's ratio is used for plies and the interface (i.e. $v_p = v_i$). The laminated plate has an overhang that may be treated as a cantilever wide beam subjected to a uniform displacement at the free end. Using Roark's formulas (Warren & Richard 2002) for wide beams, the force, F, required to reach the tip displacement of 30 mm is presented in Table 7. 1. Calculations for the upper and lower bound are obtained by assuming the layers to be fully bonded or disconnected. As seen in Table 7.1, the FE result for the homogeneous and isotropic case ($E_i = E_p$) agree very well with the upper bound. This agreement verifies the present FE model in terms of mesh size, applied load and boundary conditions.

Table 7.1: Comparisons between current FE predictions and the analytical model (Warren & Richard 2002)

$E_p = 700$ MPa, $v_p = v_i = 0.4$

E_i (MPa)	F (N)		
	FE (Isotropic)	Upper bound	Lower bound
700	9.372×10^{-1}		
70	9.335×10^{-1}		
7	9.317×10^{-1}	9.324×10^{-1}	9.993×10^{-2}
0.7	9.232×10^{-1}		
0.07	8.757×10^{-1}		

To better understand the role of ply anisotropy on the laminate bending response, ten more cases with transversely isotropic layers are considered. The elastic constants of such layers for two specific sets are listed in Table 7.2. As noted in Fig. 7.5, irrespective of very low interface stiffness (e.g. 70 kPa), the effect of shear deformation on the bending behaviour is less than 6.5% for the dimensions of the selected multilayered plates. In other words, bending is the dominating deformation mechanism in this case study. Also, it seems that the ply anisotropy nature affects the bending behaviours of thin laminated plates with thin and soft interfaces more considerably than the shear properties. The ply anisotropy nature (assumed in Table 7.2) reduces the apparent flexural rigidity of the entire plate up to 14 % (see Fig. 7.5).

Table 7.2: Input properties of the plies

Properties	Set[a]	Set[b]	Unit
$E_{1p} = E_{2p}$	700	700	MPa
E_{3p}	136	13.6	MPa
G_{12p}	40	4.0	MPa
$G_{13p} = G_{23p}$	40	4.0	MPa
v_{12p}	0.2	0.2	-[*]
$v_{13p} = v_{23p}$	0.7	0.7	-[*]

Notes: The 12-plane is the plane of woven fabric
* indicates non-dimensional

7.4.2. Viscoelastic material

Recognizing the role of the ply anisotropy nature as mentioned above along with the variation of resin viscoelastic characteristics (Thorpe 2012) at the early stage of cure that may affect the deformation behaviours, the orthotropic viscoelastic properties are considered in the bending behaviour. The mechanical properties of the resin, fibre and fibre-bed that have been used for viscoelastic analysis at micro-scale are listed in Table 7.3 (Le et al. 2022). It should be noted that the low value for fibre bending stiffness (i.e. 1.5 GPa) could be attributed to the low compressive modulus of the uncured composites which is dominated by the resin viscoelastic properties for prepregs under bending (Le et al. 2022). Such a low value of the longitudinal fibre modulus considered here (1.5 GPa) correlates well with previous findings in the literature (Le et al. 2022). Due to the lack of experimental data for uncured resin (i.e. Cycom 5320), Prony series constants for MTM45-1 (Thorpe 2012) are assumed for validating the model against the experimental data reported in Alshahrani & Hojjati (2017a). Firstly, the fibre-bed elastic properties are incorporated into the micromechanics equations (Malek 2014) at micro-scale to estimate the effective viscoelastic properties of the uncured UD prepreg. The effective properties obtained from the analytical homogenisation at this scale are then used to predict the properties of the fabric at the meso-scale (Naik 1994). The estimated mechanical viscoelastic constants for 5-harness satin weave composite ply are provided in Table 7.4. Similar to previous cases for assumed elastic constants, five interface properties, E_i, ranging from 70 kPa to 700 MPa are introduced to investigate the influence of interface stiffness on the overall bending behaviours. Fig. 7.5 compares the required loads for the multi-layered plates with five different interface properties to reach a tip displacement of

30 mm at room temperature using various material models. As seen in Fig. 7.5, the apparent flexual rigidities of the entire viscoelastic plates reduce by almost 30% in comparison with the corresponding elastic cases while the effect of ply-slippage on the overall bending behaviour is still negligible; a similar trend with the remaining material models.

Table 7.3: Input material properties of fibre, resin and fibre bed used in the bending simulation of textile prepregs (Le et al. 2022).

$V_f = $ 0.600

Property	Unit	Fibre	Resin		Fibre bed
			Relaxed	Unrelaxed	
E_1	GPa	1.50×10^0	3.00×10^{-6}	1.65×10^{-1}	1.50×10^0
$E_2 = E_3$	GPa	1.72×10^{-1}	3.00×10^{-6}	1.65×10^{-1}	1.12×10^{-4}
$G_{12} = G_{13}$	GPa	27.60	1.00×10^{-6}	5.52×10^{-2}	1.13×10^{-4}
G_{23}	GPa	0.07	1.00×10^{-6}	5.52×10^{-2}	4.49×10^{-5}
$v_{12} = v_{13}$	-	0.2	0.495	0.495	
v_{23}	-	0.25	0.495	0.495	0.250

Table 7.4: Meso-scale predictions of 5HS prepreg mechanical properties under bending using the analytical technique of Naik (1994).

Laminate type	Material	E_{xx}, E_{yy}	E_{zz}	G_{xz}, G_{yz}	G_{xy}	v_{xz}, v_{yz}	v_{xy}
		MPa	MPa	MPa	MPa		
5HS	Relaxed resin	412.60	8.40	5.10	3.80×10^{-1}	0.800	2.94×10^{-4}
	Unrelaxed resin	680.20	394.10	126.20	187.20	0.676	0.212
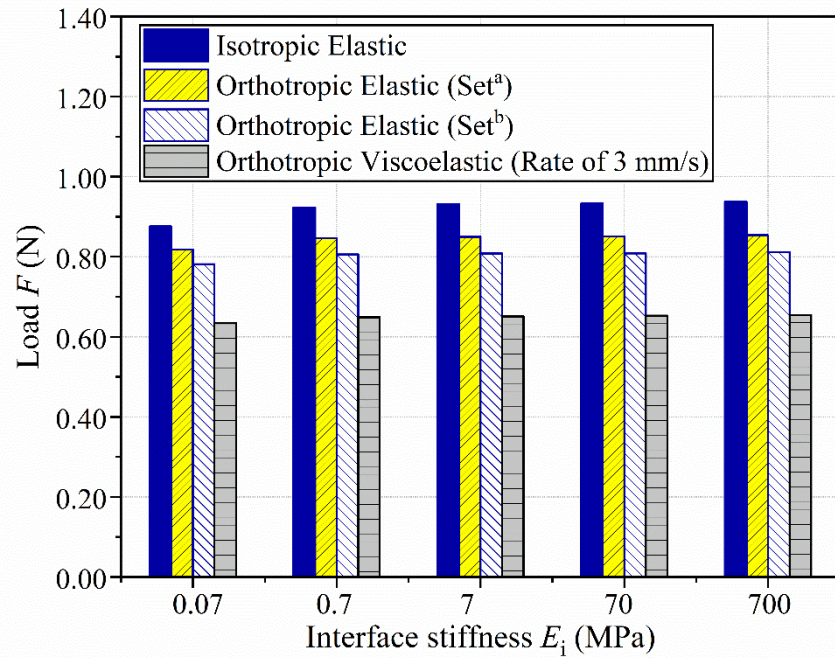
Figure 7.5: The effect of interface properties on the bending loads. Required loads to reach a tip displacement of 30 mm at room temperature are compared using various material models. Resin viscoelastic properties selected for the orthotropic viscoelastic material model are provided in (Thorpe 2012). The model has the length of 150 mm, the width of 50 mm and the thickness of 1.67 mm.

To further consider the capability of capturing the effect of soft interface on the bending response using the multi-layered bending model described above, a similar model with the length of 80 mm and thickness of 7 layers (compared to the previous model of 150 mm in length and 3 layers in thickness) is created. Simultaneously, a variety of cases according to five interface properties (E_i) and effect of ply anisotropy (see Table 7.2) are analyzed. The FE results are shown in Fig. 7.6. It is noted that for such a short and thick plate, shear deformation decreases the bending rigidity significantly, especially for the case ($E_i = 70$ kPa) by more than 50% (see Fig. 7.6).

121
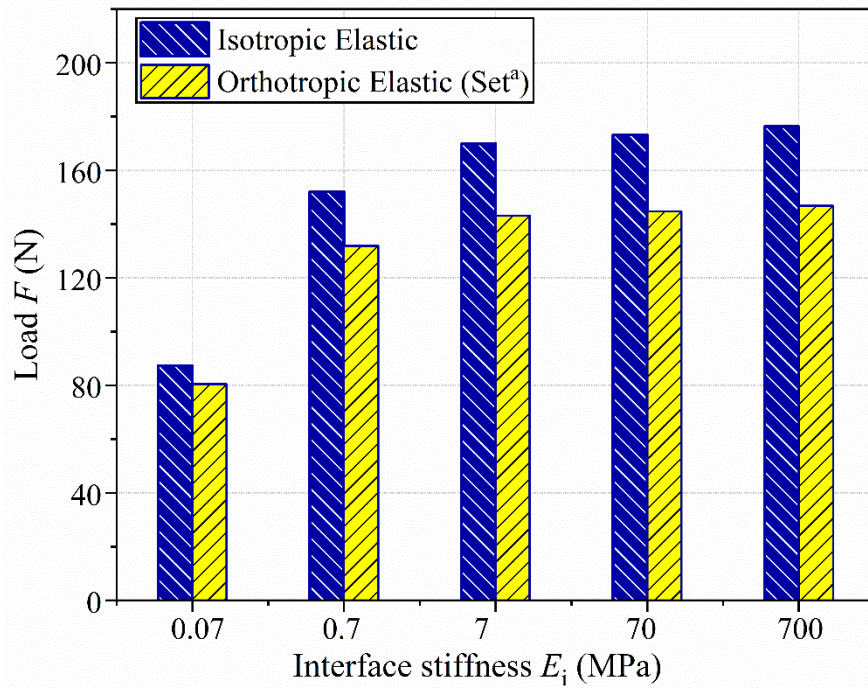
Figure 7.6: The effect of interface properties on the bending loads in a thick laminate. Required loads to reach a tip displacement of 30 mm at room temperature are compared using various material models. The model has the length of 80 mm, the width of 50 mm and the thickness of 3.91 mm.

As a next step towards validating the proposed model with the bending behaviour of different stacking sequences published in the literature, four fabric layups as shown in Fig. 7.7 are considered. Note that by employing the analytical technique (Naik 1994) for the homogenisation technique at the meso-scale, the stiffnesses in warp and weft direction are assumed the same for simplification. Therefore, this study neglects the difference in undulation between weft and warp yarns in woven fabric structure as concerned in Alshahrani & Hojjati (2017a). The load value required to achieve a tip displacement of 30 mm is used to calculate the bending moment along the length of the beam. By capturing the bending curve corresponding to the maximum displacement reached (see Fig. 7.4), deflection profile $z(y)$ is fitted using a proper polynomial function. The expression for the curvature is subsequently calculated as $\kappa = z''(y)/(1 + z(y)'^2)^{3/2}$ (Gere & Goodno 2009). Finally, the moments at each point can be plotted against the corresponding curvature values as shown in Fig. 7.8.

As can be seen in Fig. 7.8, stacking 1 [0°/0°/0°] with respect to fibre direction requires the highest load for the laminated plate to reach the desired displacement. Fig. 7.8 also presents that rotating ply 2 and ply 3 by 45° (stacking 3) decreases the bending stiffness by approximately 15% compared to stacking 1. Stacking 2 and stacking 4 give

slight differences from stacking 1 and stacking 3 respectively. It is noted that FE simulations of multiple plies under bending are considered at room temperature with a speed of 3 mm/s and assumed the interface stiffness of 7 MPa for all cases. Nevertheless, the moment against curvature relation captured by the experiment for selected stacking sequences (Alshahrani & Hojjati 2017a) was conducted at 70°C only, hence, they are not included in Fig. 7.8 for comparison purposes. At room temperature, the maximum bending moment for stacking 1 with a speed of 3 mm/s was measured about 55 N.mm in Alshahrani & Hojjati (2017a), compared to the present FE prediction of 75 N.mm (see Fig. 7.8). This discrepancy can be attributed to the assumed input parameters for the fibre bending stiffness, resin viscoelastic characteristics and yarn architecture due to the lack of experimental data for material properties at micro- and meso-scale. However, the proposed multi-scale approach should be emphasised as a rapid method for estimating the effect of various parameters on wrinkle formation. Moreover, it seems quite difficult to predict accurately the bending behaviour of uncured laminated prepregs using FE analysis as simulation outcome depends strongly on the accurate material inputs at smaller scales that may be missing in the literature. The simulation model using Aniform software in Alshahrani & Hojjati (2017a) underestimated the maximum bending moment for stacking 1 at room temperature with different testing rates measured by the experiment.
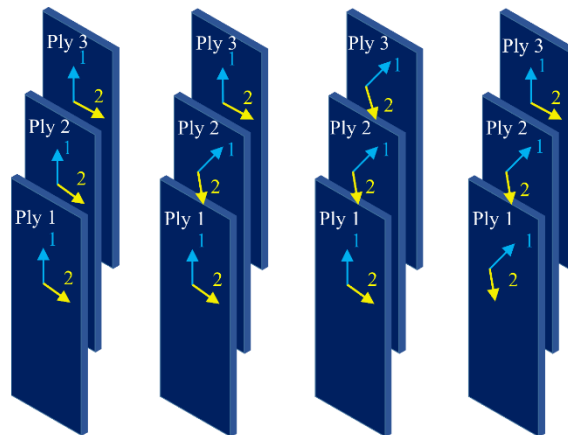
Figure 7.7: Stacking sequences of three-layer plate (a) Stacking 1 [0°/0°/0°]; (b) Stacking 2 [0°/45°/0 °]; (c) Stacking 3 [0°/45°/45°]; (d) Stacking 4 [45°/45°/0 °].
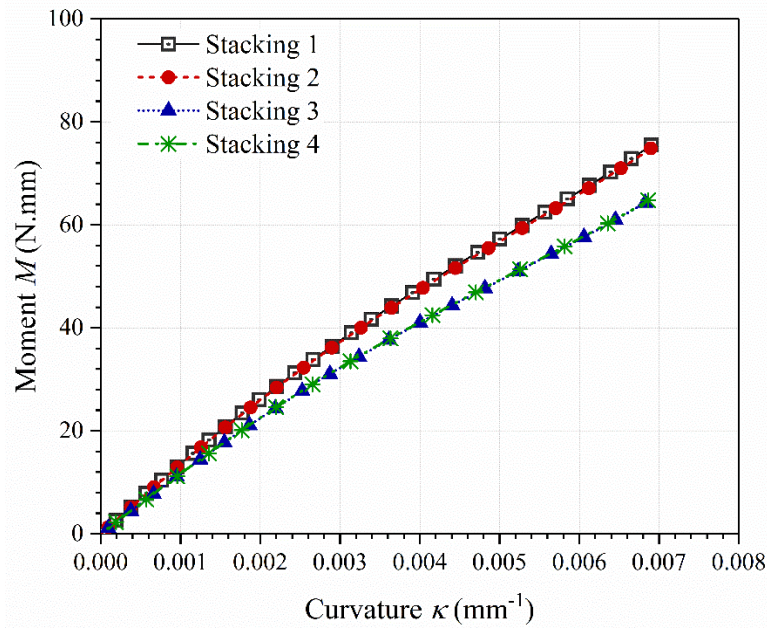
Figure 7.8: Moment vs curvature for all selected stacking sequences at room temperature. A loading rate of 3 mm/s is considered and the interface modulus, E_i, is assumed 7 MPa for all cases. Resin viscoelastic properties selected for the orthotropic viscoelastic material model are provided in (Thorpe 2012).

7.5. Summary and conclusions

The viscoelastic bending behaviour of multilayered composite plates with thin and soft interfaces was analysed using the efficient multi-scale modelling approach. The weaving pattern and the stacking sequence of plies were considered analytically at the meso-scale while the effect of ply slippage was captured by introducing a thin interface layer between the plies at the macro-scale and implemented using UMAT subroutine in Abaqus software. The obtained maximum bending moment for stacking 1 at room temperature with a speed of 3 mm/s was compared to the experimentally measured value. The discrepancy between the numerical result and the experimental data could be attributed to the assumed input parameters for the fibre bending stiffness, resin viscoelastic characteristics and yarn architecture due to the lack of experimental data for material properties at micro- and meso-scale. Therefore, conducting additional experimental research on the viscoelastic characteristics of composites at the small scales and introducing the fibre stiffness in weft and warp yarns separately into the FE model in our future work will improve the accuracy of the proposed method.

In terms of employing various material models in analysing the bending behaviour of multilayered plates, it should be highlighted the effect of resin viscoelastic characteristics on the numerical outcomes. Moreover, the bending response of the

uncured prepregs was found to be dominated by their ply bending stiffness rather than inter-ply friction. Further investigation on the bending mechanism of thicker laminated composites is suggested to ascertain the limitations and validity range of the viscoelastic multi-scale model predictions for wrinkle formation in large composite parts. Finally, it is noted that the temperature effect was not considered in the chapter. As temperature is known to be an important parameter during forming, studying the variation of resin viscoelastic properties with temperature and their effect on wrinkle formation is the subject of our future work.

Chapter 8. Conclusions and recommendations

8.1. Summary

The viscoelastic buckling/bending responses of cured and uncured viscoelastic composite plates were investigated in this thesis in order to obtain a better understanding of the wrinkling behaviour during the forming process. These were accomplished by implementing a three-dimensional (3D) multi-scale modelling framework that incorporates analyses at different scales (micro-, meso and macro-scale). For material level (micro- and meso- scale) simulations, analytical micro- and meso-scale models proposed in the literature were investigated for estimating the material properties. Meanwhile a differential form (DF) of viscoelasticity implemented as a UMAT was employed for structural level (macro-scale) simulations. Combining analytical equations at smaller scales with the DF form of viscoelasticity at macro-scale resulted in a rapid method for estimating the effect of various parameters on wrinkle formation. Within this context, instead of explicitly considering complex mechanisms that may occur concurrently during the formation of woven composites, a modified input value at the micro-scale based on published experiments may be considered for uncured prepregs.

The numerical model was validated by comparing the structural behaviour of thin viscoelastic composites (i.e. buckling and bending responses) with experimental data reported in the literature. As the built-in viscoelastic model of Abaqus is limited to modelling isotropic materials, the DF approach developed for orthotropic composites was employed in this study to elucidate the effect of ply anisotropy on the bending response of uncured/partially cured composites. The influence of various parameters including fibre stiffness, resin properties, yarn's architecture and loading rates on the buckling and bending behaviour of viscoelastic composites were analysed. The good agreement between the numerical predictions and the experimental data indicates the potential of the proposed multi-scale modelling framework to predict the performance of viscoelastic composite with a variety of yarn architectures efficiently.

Inter-ply slippage has now been recognised as a key mechanism affecting the formation of composites with numerous plies, in addition to bending stiffness. To better understand the effect of shear deformation and ply slippage on wrinkle formation, this thesis focused on the bending behaviour of orthotropic elastic and viscoelastic multi-layered plates with thin and soft interfaces exhibiting resin-rich inter-ply zones. Under

bending loads, predicted load-deflection curves of cantilever prepregs were compared to experimental data in the literature.

8.2. Contributions and Key findings

The following contributions were made in this work:

- FE models have been created and validated with experimental data in the literature to efficiently predict wrinkle formation in flat laminates at the early stage of cure.

- The properties of the uncured composites under buckling and bending conditions assumed in the FE model for forming simulations have been well justified.

- A MATLAB script has been created to predict the effective mechanical properties of a RUC of the 5HS woven fabric.

- The effects of ply anisotropy, fibre bed, various fibre architecture and viscoelasticity on the buckling/bending responses of laminated composites have been investigated comprehensively.

- Contribution of different deformation mechanisms such as out-of-plane bending and inter-ply slippage during composite manufacturing has been explored thoroughly.

Some of the notable findings are listed below:

- The interface stiffness (or the presence of resin-rich areas between the plies) dominates the buckling and bending responses of flat laminates compared to the effect of ply anisotropy for the case study in Chapter 4.

- Unlike cured composites, the compressive stiffness of uncured prepregs is mainly dominated by the resin modulus rather than the fibre modulus due to the very low buckling load of carbon fibres. The longitudinal compressive stiffness of the plies affects both the slope and the buckling load.

- The waviness of fibres (fibre-bed effect) which stiffens the prepreg's transverse and shear properties increases its compressive stiffness slightly while the waviness effect on the post-buckling stiffness is relatively significant.

- The axial compressive stiffness of the laminated composites increases by raising the loading rate and the initial slope of the load-displacement curve for viscoelastic laminates moves nearer to the slope of the isotropic elastic laminate for a higher loading rate.

- An efficient multi-scale modelling approach was developed to predict the bending behaviour of viscoelastic composites under various loading rates. The proposed approach should be emphasised as a rapid method for determining the role of fibre stiffness, viscoelastic parameters and the yarn's architecture on the out-of-plane bending behaviour essential for predicting wrinkle formation in woven composites.

- Apart from the viscoelastic shear characteristics of woven composites, the in-plane Young's moduli of uncured UD and woven composites in both tension and compression have been found to affect the out-of-plane response of thin composites significantly. A low value for fibre Young's modulus (1.5 GPa) commonly used in most numerical models in the literature without clear justification has been demonstrated to be the result of low compressive stiffness of uncured prepreg.

- Comparing IF and DF results, it is demonstrated that the transverse moduli associated with the presence of fibre and fibre-bed effect increase the bending stiffness of uncured woven composites.

- The bending response of the uncured multi-layered prepregs was found to be dominated by their ply bending stiffness rather than inter-ply friction. Also, by employing various material models in analysing the bending behaviour of such plates, the effect of resin viscoelastic characteristics on the numerical outcomes should be highlighted.

8.3. Limitations and recommendations for future studies

- There are discrepancies (maximum compressive forces and the shape of the load-displacement curves) between the experimental data and numerical predictions. This could be attributed to the lower viscosity of the MTM45-1 resin. Conducting laboratory experiments on uncured and partially cured laminates of various thicknesses is suggested so that the discrepancy reported between the numerical predictions and experimental data is better understood.

- As demonstrated in this study, in addition to in-plane shear properties, the in-plane Young's moduli of composites in both tension and compression can significantly affect the out-of-plane response of thin composites. Subsequently, in order to accurately predict wrinkle formation during composite manufacture, these properties must be thoroughly described.

- Characterising the viscoelastic properties of uncured Cycom 5320 epoxy resin (similar to MTM45-1 resin in the literature) is suggested as future research that will improve the accuracy of the bending simulations.

- Based on published data, the viscoelastic properties of uncured composite under compression and tension were assumed in this study. The complex deformation mechanisms that may occur simultaneously during bending of uncured composite prepregs were considered implicitly using a low value of fibre stiffness. Thus, additional experimental research on the viscoelastic characteristics of composites at the micro- and meso-scale is advised to better understand the formation of wrinkles caused by bending during cure.

- Many published studies have stated that the inter-ply slippage is one of the most important deformation mechanisms during the process of forming composites, particularly for multilayered textile prepregs. As a result, future research on inter-ply slippage and its impact on the bending properties of thicker composites should be conducted so that this process is better understood.

- During composite processing, the resin modulus may diminish quite significantly under heat. Due to boundary conditions and geometrical constraints, this could result in the formation of wrinkles (buckled plies) under significantly lower compressive loads. The effect of temperature and degree of cure on resin viscoelastic characteristics during forming shall be the focus of our future research.

Appendices

A.1. Transformation matrix used in Eq. (3.7)

The transformation matrix $[T]_m$ in Eq. (3.7) is given by:

$$[T]_m = \tag{A.1}$$

$$\begin{bmatrix} a_{11}^2 & a_{12}^2 & a_{13}^2 & a_{12}a_{13} & a_{11}a_{13} & a_{11}a_{12} \\ a_{21}^2 & a_{22}^2 & a_{23}^2 & a_{22}a_{23} & a_{23}a_{21} & a_{21}a_{22} \\ a_{31}^2 & a_{32}^2 & a_{33}^2 & a_{32}a_{33} & a_{33}a_{31} & a_{31}a_{32} \\ 2a_{21}a_{31} & 2a_{32}a_{22} & 2a_{23}a_{33} & (a_{22}a_{33}+a_{23}a_{32}) & (a_{23}a_{31}+a_{21}a_{33}) & (a_{21}a_{32}+a_{22}a_{31}) \\ 2a_{11}a_{31} & 2a_{12}a_{32} & 2a_{13}a_{33} & (a_{32}a_{13}+a_{33}a_{12}) & (a_{11}a_{33}+a_{13}a_{31}) & (a_{31}a_{12}+a_{32}a_{11}) \\ 2a_{11}a_{21} & 2a_{12}a_{22} & 2a_{13}a_{23} & (a_{12}a_{23}+a_{13}a_{22}) & (a_{13}a_{21}+a_{11}a_{23}) & (a_{11}a_{22}+a_{12}a_{21}) \end{bmatrix},$$

in which the 3×3, $[a_{ij}]$ matrix ($i = 1\text{-}3$, $j = 1\text{-}3$) is expressed as:

$$[a_{ij}] = \begin{bmatrix} cos(\theta)\,cos(\beta) & sin(\theta)\,cos(\beta) & sin(\beta) \\ -sin(\theta) & cos(\theta) & 0 \\ -cos(\theta)\,sin(\beta) & -sin(\theta)\,sin(\beta) & cos(\beta) \end{bmatrix}, \tag{A.2}$$

A.2. Differential approach to modelling generally orthotropic materials

In a general 3-D state of stress, the constitutive equation relating the stress σ_{ij} and the strain ε_{kl} for a linear elastic material can be written as follows (Malek 2014):

$$\sigma_{ij} = C_{ijkl}\varepsilon_{kl}, \tag{A.3}$$

where C_{ijkl} are components of the material stiffness tensor. Using matrix notation, the stiffness tensor can also be written in a 6×6 matrix form, denoted by the symbol $\underline{\underline{C}}$ with the double underscore indicating matrix quantities and single underscore denoting vectors.

For an isotropic material, the stiffness matrix can be expressed in terms of two independent constants (moduli), G and K, representing the shear and bulk behaviour of the material. Therefore, the stress-strain relationship can also be written as follows:

$$\underline{\sigma} = G \begin{Bmatrix} \frac{2}{3}(2\varepsilon_{11} - \varepsilon_{22} - \varepsilon_{33}) \\ \frac{2}{3}(2\varepsilon_{22} - \varepsilon_{11} - \varepsilon_{33}) \\ \frac{2}{3}(2\varepsilon_{33} - \varepsilon_{11} - \varepsilon_{22}) \\ 2\varepsilon_{12} \\ 2\varepsilon_{13} \\ 2\varepsilon_{23} \end{Bmatrix} + K \begin{Bmatrix} \varepsilon_{11} + \varepsilon_{22} + \varepsilon_{33} \\ \varepsilon_{11} + \varepsilon_{22} + \varepsilon_{33} \\ \varepsilon_{11} + \varepsilon_{22} + \varepsilon_{33} \\ 0 \\ 0 \\ 0 \end{Bmatrix}, \tag{A.4}$$

In other words, the total stress vector for an isotropic material can be decomposed into two vectors:

$$\underline{\sigma} = \underline{\sigma}_G + \underline{\sigma}_K, \tag{A.5}$$

where the vectors $\underline{\sigma}_G$ and $\underline{\sigma}_K$ represent the shear and bulk components of the total stress respectively. In order to describe the behaviour of an elastic, orthotropic material, nine constants are needed and the stress-strain relationship can be expressed in terms of these nine constants (stiffness matrix components) as follows:

$$\underline{\sigma} = C_{11}\underline{\varepsilon}_{C_{11}} + C_{22}\underline{\varepsilon}_{C_{22}} + C_{33}\underline{\varepsilon}_{C_{33}} + C_{44}\underline{\varepsilon}_{C_{44}} + C_{55}\underline{\varepsilon}_{C_{55}} + C_{66}\underline{\varepsilon}_{C_{66}} + C_{12}\underline{\varepsilon}_{C_{12}} + C_{13}\underline{\varepsilon}_{C_{13}} + C_{23}\underline{\varepsilon}_{C_{23}}, \tag{A.6}$$

where the stress tensor has been decomposed into nine tensors each corresponding to a stiffness matrix component or a material property, P:

$$\underline{\sigma} = \underline{\sigma}_{C_{11}} + \underline{\sigma}_{C_{22}} + \ldots + \underline{\sigma}_{C_{23}} = \sum_{p=1}^{9} \underline{\sigma}_p, \tag{A.7}$$

For simplicity, the above equation may also be written in vector form as:

$$\underline{\sigma} = \begin{Bmatrix} \sigma_{11} \\ \sigma_{22} \\ \sigma_{33} \\ \sigma_{12} \\ \sigma_{13} \\ \sigma_{23} \end{Bmatrix} = C_{11} \begin{Bmatrix} \varepsilon_{11} \\ 0 \\ 0 \\ 0 \\ 0 \\ 0 \end{Bmatrix} + C_{22} \begin{Bmatrix} 0 \\ \varepsilon_{22} \\ 0 \\ 0 \\ 0 \\ 0 \end{Bmatrix} + C_{33} \begin{Bmatrix} 0 \\ 0 \\ \varepsilon_{33} \\ 0 \\ 0 \\ 0 \end{Bmatrix} \tag{A.8}$$

131

$$
+C_{44}\begin{Bmatrix} 0 \\ 0 \\ 0 \\ 2\varepsilon_{12} \\ 0 \\ 0 \end{Bmatrix} + C_{55}\begin{Bmatrix} 0 \\ 0 \\ 0 \\ 0 \\ 2\varepsilon_{13} \\ 0 \end{Bmatrix} + C_{66}\begin{Bmatrix} 0 \\ 0 \\ 0 \\ 0 \\ 0 \\ 2\varepsilon_{23} \end{Bmatrix}
$$

$$
+C_{12}\begin{Bmatrix} \varepsilon_{22} \\ \varepsilon_{11} \\ 0 \\ 0 \\ 0 \\ 0 \end{Bmatrix} + C_{13}\begin{Bmatrix} \varepsilon_{33} \\ 0 \\ \varepsilon_{11} \\ 0 \\ 0 \\ 0 \end{Bmatrix} + C_{23}\begin{Bmatrix} 0 \\ \varepsilon_{33} \\ \varepsilon_{22} \\ 0 \\ 0 \\ 0 \end{Bmatrix},
$$

For a viscoelastic orthotropic material, similar to the isotropic or transversely isotropic case in Zobeiry et al. (2016), a differential equation is employed to relate the associated stresses and strains as follows:

$$
\dot{\sigma}_P = P^u \dot{\varepsilon}_P - \sum_{i=1}^{N} \frac{1}{(\tau_P)_i}(\sigma_P)_i; \; P = C_{11}, C_{22}, \ldots, C_{23}, \tag{A.9}
$$

In deriving the above equation, for each component of the stiffness matrix (e.g. C_{11}) a generalized Maxwell model has been employed. For each element i of the generalized Maxwell model a governing differential equation can be written as follows:

$$
(\dot{\sigma}_P)_i = P^i \dot{\varepsilon}_P - \frac{1}{(\tau_P)_i}(\sigma_P)_i; \; P = C_{11}, C_{22}, \ldots, C_{23}, \tag{A.10}
$$

In the above equation, the spring stiffness and time constant of Maxwell element i associated with component P of the stiffness matrix are denoted by P^i and $(\tau_P)_i$, respectively. The unrelaxed values of each component of stiffness matrix denoted by superscript u is obtained by summing over all Maxwell elements. Therefore, the unrelaxed value of component P is obtained as:

$$
P^u = \sum_{i=1}^{N} P^i; \; P = C_{11}, C_{22}, \ldots, C_{23}, \tag{A.11}
$$

where N is the number of Maxwell elements.

The overall governing differential equation is obtained by summing over all nine stress vectors, therefore the overall governing differential equation can be written as:

$$\dot{\underline{\sigma}} = \underline{C}^u \dot{\underline{\varepsilon}} - \sum_P \sum_{i=1}^{N} \frac{1}{(\tau_P)_i} (\underline{\sigma}_P)_i, \qquad (A.12)$$

A.3. Implementation

Rewriting Eq. (A.10) at time steps n and $n + 1$ for element i of the generalized Maxwell model, including the free strain ε_{Pf} (e.g. strain generated due to cure shrinkage or thermal expansion) leads to:

$$\begin{cases} (\dot{\underline{\sigma}}_P)_i^n = P^i(\dot{\underline{\varepsilon}}_P^n - \dot{\underline{\varepsilon}}_{Pf}^n) - \frac{1}{(\tau_P)_i^n}(\underline{\sigma}_P)_i^n \\ (\dot{\underline{\sigma}}_P)_i^{n+1} = P^i(\dot{\underline{\varepsilon}}_P^{n+1} - \dot{\underline{\varepsilon}}_{Pf}^{n+1}) - \frac{1}{(\tau_P)_i^{n+1}}(\underline{\sigma}_P)_i^{n+1} \end{cases} \qquad (A.13)$$

As it is described by Zobeiry et al. (2016), using the finite difference method with a central difference scheme and rearranging, the stresses in each Maxwell element "i" can be calculated as:

$$(\underline{\sigma}_P)_i^{n+1} = \left(\frac{1 - \frac{1}{2(\tau_P)_i^n}\Delta t}{1 + \frac{1}{2(\tau_P)_i^{n+1}}\Delta t} \right)(\underline{\sigma}_P)_i^n + \frac{P^i}{\left(1 + \frac{1}{2(\tau_P)_i^{n+1}}\Delta t\right)}\left[(\underline{\varepsilon}_P^{n+1} - \underline{\varepsilon}_P^n) - (\underline{\varepsilon}_{Pf}^{n+1} - \underline{\varepsilon}_{Pf}^n)\right], \qquad (A.14)$$

The total stress vector at time increment ($n + 1$) can be calculated by summing over all Maxwell elements ($i = 1, 2, 3, \ldots, N$) and material properties P, as follows:

$$\underline{\sigma}^{n+1} = \sum_P \sum_{i=1}^{N} (\underline{\sigma}_P)_i^{n+1}; P = C_{11}, C_{22}, \ldots, C_{23}, \qquad (A.15)$$

Details of the finite element formulation and solution convergence conditions could be found in Zobeiry et al. (2016).

References

Abaqus, I. 2013a, *Abaqus Analysis User's Guide*, Dassault Systèmes Simulia Corp., USA, viewed 20th May 2020, <http://130.149.89.49:2080/v6.13/books/usb/default.htm>.

Abaqus, I. 2013b, *Abaqus Benchmarks Guide*, Dassault Systèmes Simulia Corp., USA, viewed 27 May 2020, <http://130.149.89.49:2080/v6.13/books/bmk/default.htm>.

Alshahrani, H. 2017, 'Bending behaviour of textile thermosetting composite prepregs during forming processes', Concordia University, Montreal, Canada.

Alshahrani, H. 2020, 'Characterization and finite element modeling of coupled properties during polymer composites forming processes', *Mechanics of Materials*, vol. 144.

Alshahrani, H. & Hojjati, M. 2017a, 'Bending behavior of multilayered textile composite prepregs: Experiment and finite element modeling', *Materials & Design*, vol. 124, pp. 211-24.

Alshahrani, H. & Hojjati, M. 2017b, 'A new test method for the characterization of the bending behavior of textile prepregs', *Composites Part A: Applied Science and Manufacturing*, vol. 97, pp. 128-40.

Alshahrani, H. & Hojjati, M. 2017c, 'A theoretical model with experimental verification for bending stiffness of thermosetting prepreg during forming process', *Composite Structures*, vol. 166, pp. 136-45.

Amini Niaki, S., Forghani, A., Vaziri, R. & Poursartip, A. 2019, 'An Orthotropic Integrated Flow-Stress Model for Process Simulation of Composite Materials-Part II: Three-Phase Systems', *Journal of Manufacturing Science and Engineering*, vol. 141, no. 3.

Balokas, G., Czichon, S. & Rolfes, R. 2018, 'Neural network assisted multiscale analysis for the elastic properties prediction of 3D braided composites under uncertainty', *Composite Structures*, vol. 183, pp. 550-62.

Bauchau, O.A. & Craig, J.I. 2009, *Solid mechanics and its applications*, vol. 163, Springer, New York, USA.

Belnoue, J.P.H., Nixon-Pearson, O.J., Thompson, A.J., Ivanov, D.S., Potter, K.D. & Hallett, S.R. 2018, 'Consolidation-Driven Defect Generation in Thick Composite Parts', *Journal of Manufacturing Science and Engineering*, vol. 140, no. 7.

Beyle, A.I., Gustafson, C.G., Kulakov, V.L. & Tarnopol's kii, Y.M. 1997, 'Composite risers for deep-water offshore technology: Problems and prospects. ', *Mechanics of Composite Materials*, vol. 33, no. 5, pp. 404-14.

Bilbao, E., Soulat, D., Hivet, G. & Gasser, A. 2009, 'Experimental Study of Bending Behaviour of Reinforcements', *Experimental Mechanics*, vol. 50, no. 3, pp. 333-51.

Bloom, L.D., Wang, J. & Potter, K.D. 2013, 'Damage progression and defect sensitivity: An experimental study of representative wrinkles in tension', *Composites Part B: Engineering*, vol. 45, no. 1, pp. 449-58.

Bocciarelli, M., Colombi, P., Fava, G. & Poggi, C. 2009, 'Fatigue performance of tensile steel members strengthened with CFRP plates', *Composite Structures*, vol. 87, no. 4, pp. 334-43.

Boisse, P., Colmars, J., Hamila, N., Naouar, N. & Steer, Q. 2018, 'Bending and wrinkling of composite fiber preforms and prepregs. A review and new developments in the draping simulations', *Composites Part B: Engineering*, vol. 141, pp. 234-49.

Boisse, P., Hamila, N. & Madeo, A. 2016, 'Modelling the development of defects during composite reinforcements and prepreg forming', *Philos Trans A Math Phys Eng Sci*, vol. 374, no. 2071, p. 20150269.

Boisse, P., Hamila, N., Vidal-Salle, E. & Dumont, F. 2011, 'Simulation of wrinkling during textile composite reinforcement forming. Influence of tensile, in-plane shear and bending stiffnesses', *Composites Science and Technology*, vol. 71, pp. 683-92.

Boisse, P., Huang, J. & Guzman-Maldonado, E. 2021, 'Analysis and Modeling of Wrinkling in Composite Forming', *Journal of Composites Science*, vol. 5, no. 3.

Camanho, P.P. & Hallett, S.R. 2015, *Numerical modelling of failure in advanced composite materials*, vol. 62, Woodhead publishing series in composites science and engineering.

Cao, Y., Cai, Y., Zhao, Z., Liu, P., Han, L. & Zhang, C. 2020, 'Predicting the tensile and compressive failure behavior of angle-ply spread tow woven composites', *Composite Structures*, vol. 234.

Christensen, R.M. & Lo, K.H. 1979, 'Solutions of effective shear properties in three phase sphere and cylinder models', *J.Mech. Phys. Solids*, vol. 27, pp. 315-30.

Dangora, L.M., Mitchell, C., White, K.D., Sherwood, J.A. & Parker, J.C. 2016, 'Characterization of temperature-dependent tensile and flexural rigidities of a cross-ply thermoplastic lamina with implementation into a forming model', *International Journal of Material Forming*, vol. 11, no. 1, pp. 43-52.

Dangora, L.M., Mitchell, C.J. & Sherwood, J.A. 2015, 'Predictive model for the detection of out-of-plane defects formed during textile-composite manufacture', *Composites Part A: Applied Science and Manufacturing*, vol. 78, pp. 102-12.

Danilov, A.I. 2016, 'Some Aspects of CFRP Steel Structures Reinforcement in Civil Engineering', *Procedia Engineering*, vol. 153, pp. 124-30.

Dixit, A., Mali, H.S. & Misra, R.K. 2013, 'Unit Cell Model of Woven Fabric Textile Composite for Multiscale Analysis', *Procedia Engineering*, vol. 68, pp. 352-8.

Dixit, A. & Singh, M.H. 2013, 'Modelling techniques for predicting the mechanical properties of woven-fabric textile composites: A review', *Mechanics of Composite Materials*, vol. 49, no. 1, pp. 3-30.

Dodwell, T.J. 2015, 'Internal wrinkling instabilities in layered media', *Philosophical Magazine*, vol. 95, no. 28-30, pp. 3225-43.

Dodwell, T.J., Butler, R. & Hunt, G.W. 2014, 'Out-of-plane ply wrinkling defects during consolidation over an external radius', *Composites Science and Technology*, vol. 105, pp. 151-9.

Doitrand, A., Fagiano, C., Irisarri, F.X. & Hirsekorn, M. 2015, 'Comparison between voxel and consistent meso-scale models of woven composites', *Composites Part A: Applied Science and Manufacturing*, vol. 73, pp. 143-54.

Dörr, D., Schirmaier, F.J., Henning, F. & Kärger, L. 2017, 'A viscoelastic approach for modeling bending behavior in finite element forming simulation of continuously fiber reinforced composites', *Composites Part A: Applied Science and Manufacturing*, vol. 94, pp. 113-23.

DSM 2014, 'HB80 product specification sheet', 26-02-2014 edn, US, p. 1/.

Ersoy, N., Garstka, T., Potter, K., Wisnom, M.R., Porter, D., Clegg, M. & Stringer, G. 2010, 'Development of the properties of a carbon fibre reinforced thermosetting composite through cure', *Composites Part A: Applied Science and Manufacturing*, vol. 41, no. 3, pp. 401-9.

Farnand, K., Zobeiry, N., Poursartip, A. & Fernlund, G. 2017, 'Micro-level mechanisms of fiber waviness and wrinkling during hot drape forming of unidirectional prepreg composites', *Composites Part A: Applied Science and Manufacturing*, vol. 103, pp. 168-77.

Gere, J., M,. & Goodno, B.J. 2009, *Mechanics of material*, Global Engineering.

Gutowski, T.G., Cai, Z., Bauer, S., Boucher, D., Kingery, J. & Wineman, S. 1987, 'Consolidation experiments for laminate composites', *Composite Materials*, vol. 21, pp. 650-69.

Haanappel, S.P. & Akkerman, R. 2014, 'Shear characterisation of uni-directional fibre reinforced thermoplastic melts by means of torsion', *Composites Part A: Applied Science and Manufacturing*, vol. 56, pp. 8-26.

Haanappel, S.P., ten Thije, R.H.W., Sachs, U., Rietman, B. & Akkerman, R. 2014, 'Formability analyses of uni-directional and textile reinforced thermoplastics', *Composites Part A: Applied Science and Manufacturing*, vol. 56, pp. 80-92.

Hallal, A., Younes, R. & Fardoun, F. 2013, 'Review and comparative study of analytical modeling for the elastic properties of textile composites', *Composites Part B: Engineering*, vol. 50, pp. 22-31.

Hallal, A., Younes, R., Fardoun, F. & Nehme, S. 2012, 'Improved analytical model to predict the effective elastic properties of 2.5D interlock woven fabrics composite', *Composite Structures*, vol. 94, no. 10, pp. 3009-28.

Hallander, P., Akermo, M., Mattei, C., Petersson, M. & Nyman, T. 2013, 'An experimental study of mechanisms behind wrinkle development during forming of composite laminates', *Composites Part A: Applied Science and Manufacturing*, vol. 50, pp. 54-64.

Hallander, P., Sjölander, J. & Åkermo, M. 2015, 'Forming induced wrinkling of composite laminates with mixed ply material properties; an experimental study', *Composites Part A: Applied Science and Manufacturing*, vol. 78, pp. 234-45.

Hashin, Z. 1972, 'Theory of fibre reinforced materials', *NASA, USA*.

Hashin, Z. & Rosen, W. 1964, 'The elastic moduli of fibre reinforced materials', *Journal of Applied Mechanics*, vol. 31, pp. 223-32.

Hilburger, M.W. & Starnes Jr, J.H. 2002, 'Effects of imperfections on the buckling response of compression-loaded composite shells', *International Journal of Non-Linear Mechanics*, vol. 37, pp. 623-43.

Huang, J., Boisse, P., Hamila, N. & Zhu, Y. 2020, 'Simulation of Wrinkling during Bending of Composite Reinforcement Laminates', *Materials (Basel)*, vol. 13, no. 10.

Hubert, P. & Poursartip, A. 2001, 'A method for the direct measurement of the fibre bed compaction curve of composite prepregs', *Composites Part A: Applied Science and Manufacturing*, vol. 32, pp. 179-87.

Ishikawa, T. & Chou, T.-W. 1982, 'Stiffness and strength behaviour of woven fabric composites', *Journal of Materials Science*, vol. 17, pp. 3211-20.

Johnson, K.J., Butler, R., Loukaides, E.G., Scarth, C. & Rhead, A.T. 2019, 'Stacking sequence selection for defect-free forming of uni-directional ply laminates', *Composites Science and Technology*, vol. 171, pp. 34-43.

Johnston, A., Vaziri, R. & Poursartip, A. 2001, 'A plane strain model for process-induced deformation of laminated composite structures', *Journal of Composite Materials*, vol. 35, no. 16, pp. 1435-69.

Larberg, Y. & Åkermo, M. 2014, 'In-plane deformation of multi-layered unidirectional thermoset prepreg – Modelling and experimental verification', *Composites Part A: Applied Science and Manufacturing*, vol. 56, pp. 203-12.

Larberg, Y.R. & Åkermo, M. 2011, 'On the interply friction of different generations of carbon/epoxy prepreg systems', *Composites Part A: Applied Science and Manufacturing*, vol. 42, no. 9, pp. 1067-74.

Le, A., Zobeiry, N., Erkmen, E. & Malek, S. 2019, 'Buckling analysis of multilayered beams with soft and rigid interfaces', *ICCM22*, Engineers Australia, Melbourne, Vic, pp. 204-12.

Le, V.A., Nimbalkar, S., Zobeiry, N. & Malek, S. 2022, 'An efficient multi-scale approach for viscoelastic analysis of woven composites under bending', *Composite Structures*, vol. 292.

Le, V.A., Zobeiry, N., Erkmen, E. & Malek, S. 2021, 'Buckling behaviour of laminated viscoelastic composites under axial loads', *Mechanics of Materials*, vol. 159.

Leissa, A.W. 1987, 'A review of buckling of laminated composite plates', *Applied Mechanics Reviews*, vol. 40, no. 5, pp. 575-91.

Lemanski, S.L. & Sutcliffe, M.P.F. 2012, 'Compressive failure of finite size unidirectional composite laminates with a region of fibre waviness', *Composites Part A: Applied Science and Manufacturing*, vol. 43, no. 3, pp. 435-44.

Li, J.-C., Chen, L., Zhang, Y.-F. & Pan, N. 2012, 'Microstructure and finite element analysis of 3D five-directional braided composites', *Journal of Reinforced Plastics and Composites*, vol. 31, no. 2, pp. 107-15.

Liang, B., Hamila, N., Peillon, M. & Boisse, P. 2014, 'Analysis of thermoplastic prepreg bending stiffness during manufacturing and of its influence on wrinkling simulations', *Composites Part A: Applied Science and Manufacturing*, vol. 67, pp. 111-22.

Lightfoot, J.S., Wisnom, M.R. & Potter, K. 2013, 'A new mechanism for the formation of ply wrinkles due to shear between plies', *Composites Part A: Applied Science and Manufacturing*, vol. 49, pp. 139-47.

Long, A.C. 2005, *Design and manufacture of textile composites*, Woodhead Publishing Limited, Cambridge.

Lukaszewicz, D.H.J.A. & Potter, K.D. 2011, 'The internal structure and conformation of prepreg with respect to reliable automated processing', *Composites Part A: Applied Science and Manufacturing*, vol. 42, no. 3, pp. 283-92.

Malek, S. 2014, 'Efficient multi-scale modelling of viscoelastic composites with different microstructures', PhD Thesis thesis, University of British Colombia, Canada.

Malek, S., Gereke, T., Zobeiry, N. & Vaziri, R. 2018, 'Multi-scale modelling of time-dependent response of composite structures made of orthotropic viscoelastic materials', *13th International Conference on Steel, Space and Composite Structures*, Perth, Australia.

Malek, S., Thorpe, R. & Poursartip, A. 2011, 'Adaptation of solid micromechanics for modelling curing resins in process simulations', *18th International conference on composite materials (ICCM18)*.

Malek, S., Vaziri, R. & Poursartip, A. 2018, 'Application of a generalised cellular solid model for predicting the fibre-bed effective properties in viscoelastic modelling of fibre reinforced composites', *18th European Conference on Composite Materials*, Athens, Greece.

Margossian, A., Bel, S. & Hinterhoelzl, R. 2015, 'Bending characterisation of a molten unidirectional carbon fibre reinforced thermoplastic composite using a Dynamic Mechanical Analysis system', *Composites Part A: Applied Science and Manufacturing*, vol. 77, pp. 154-63.

Martin, T.A., Bhattacharyya, D. & Collins, I.F. 1995, 'Bending of fibre-reinforced thermoplastic sheets', *Composites Manufacturing*, vol. 6, pp. 177-87.

Mukhopadhyay, S., Jones, M.I. & Hallett, S.R. 2015, 'Compressive failure of laminates containing an embedded wrinkle; experimental and numerical study', *Composites Part A: Applied Science and Manufacturing*, vol. 73, pp. 132-42.

Naik, N.K., Azad, S.N.M., Durga prasad, P. & Thuruthimattam, B.J. 2001, 'Stress and failure analysis of 3D orthogonal interlock woven composites', *Journal of Reinforced Plastics and Composites*, vol. 20, no. 17, pp. 1485-523.

Naik, N.K. & Kuchibhotla, R. 2002, 'Analytical study of strength and failure behaviour of plain weave fabric composites made of twisted yarns', *Composites Part A: Applied Science and Manufacturing*, vol. 33, no. 5, pp. 697-708.

Naik, N.K. & Shembekar, P.S. 1992, 'Elastic behavior of woven fabric composites: I - Lamina analysis', *Journal of Composite Materials*, vol. 26, no. 15, pp. 2196-30.

Naik, N.K. & Sridevi, E. 2002, 'An analytical method for thermoelastic analysis of 3D orthogonal interlock woven composites', *Journal of Reinforced Plastics and Composites*, vol. 21, no. 13, pp. 1149-91.

Naik, R.A. 1994, *Analysis of woven and braided fabric reinforced composites*, National Aeronautics and Space Administration, Washington DC, NASA CR-194930.

Nali, P., Carrera, E. & Lecca, S. 2011, 'Assessments of refined theories for buckling analysis of laminated plates', *Composite Structures*, vol. 93, no. 2, pp. 456-64.

Naouar, N., Vidal-Sallé, E., Schneider, J., Maire, E. & Boisse, P. 2014, 'Meso-scale FE analyses of textile composite reinforcement deformation based on X-ray computed tomography', *Composite Structures*, vol. 116, pp. 165-76.

Nawab, Y., Casari, P., Boyard, N. & Jacquemin, F. 2012, 'Characterization of the cure shrinkage, reaction kinetics, bulk modulus and thermal conductivity of thermoset resin from a single experiment', *Journal of Materials Science*, vol. 48, no. 6, pp. 2394-403.

Nguyen, D.H., Wang, H., Ye, F. & Hu, W. 2021, 'Investigation and multi-scale optimization design of woven composite cut-out structures', *Engineering Computations*, vol. 38, no. 3, pp. 1134-56.

Niaki, S.A., Forghani, A., Vaziri, R. & Poursartip, A. 2018, 'A three-phase integrated flow-stress model for processing of composites', *Mechanics of Materials*, vol. 117, pp. 152-64.

Potter, K., Khan, B., Wisnom, M., Bell, T. & Stevens, J. 2008, 'Variability, fibre waviness and misalignment in the determination of the properties of composite materials and structures', *Composites Part A Applied Science and Manufacturing*, vol. 39, pp. 1343-54.

Qi, Z., Liu, Y. & Chen, W. 2019, 'An approach to predict the mechanical properties of CFRP based on cross-scale simulation', *Composite Structures*, vol. 210, pp. 339-47.

Rashidi, A., Belnoue, J.P.H., Thompson, A.J., Hallett, S.R. & Milani, A.S. 2021, 'Consolidation-driven wrinkling in carbon/epoxy woven fabric prepregs: An experimental and numerical study', *Composites Part A: Applied Science and Manufacturing*, vol. 143.

Rees, D.W.A. 2009, *Mechanics of optimal structural design: Minimum weight structures*, Wiley.

Sankar, B.V. & Marrey, R.V. 1997, 'Analytical method for micromechanics of textile composites', *Composites Science and Technology*, vol. 57, pp. 703-13.

Sjölander, J., Hallander, P. & Åkermo, M. 2016, 'Forming induced wrinkling of composite laminates: A numerical study on wrinkling mechanisms', *Composites Part A: Applied Science and Manufacturing*, vol. 81, pp. 41-51.

Skordos, A.A., Monroy Aceves, C. & Sutcliffe, M.P.F. 2007, 'A simplified rate dependent model of forming and wrinkling of pre-impregnated woven composites', *Composites Part A: Applied Science and Manufacturing*, vol. 38, no. 5, pp. 1318-30.

Soutis, C. 2005, 'Carbon fiber reinforced plastics in aircraft construction', *Materials Science and Engineering: A*, vol. 412, no. 1-2, pp. 171-6.

Sun, C.T. & Vaidya, R.S. 1996, 'Prediction of composite properties from a representative volume element', *Composites Science and Technology*, vol. 56, pp. 171-9.

Sun, H., Di, S., Zhang, N., Pan, N. & Wu, C. 2003, 'Micromechanics of braided composites via multivariable FEM', *Computers & Structures*, vol. 81, no. 20, pp. 2021-7.

Täljsten, B., Hansen, C.S. & Schmidt, J.W. 2009, 'Strengthening of old metallic structures in fatigue with prestressed and non-prestressed CFRP laminates', *Construction and Building Materials*, vol. 23, no. 4, pp. 1665-77.

Tan, P., Tong, L. & Steven, G.P. 1997, 'A three-dimensional modelling techniques for predicting the linear elastic property of opened-packing woven fabric unit cells', *Composite Structures*, vol. 38, pp. 261-71.

Tan, P., Tong, L. & Steven, G.P. 1999, 'Micromechanics models for mechanical and thermomechanical properties of 3D through-the-thickness angle interlock woven composites', *Composites Part A Applied Science and Manufacturing*, vol. 30, pp. 637-48.

Tan, P., Tong, L. & Steven, G.P. 2000, 'Behavior of 3D orthogonal woven CFRP composites. Part II. FEA and analytical modeling approaches', *Composites Part A Applied Science and Manufacturing*, vol. 31, pp. 273-81.

Tan, P., Tong, L., Steven, G.P. & Ishikawa, T. 2000, 'Behavior of 3D orthogonal woven CFRP composites. Part I. Experimental investigation', *Composites Part A Applied Science and Manufacturing*, vol. 31, pp. 259-71.

Thorpe, R. 2012, 'Experimental characterization of the viscoelastic behavior of a curing epoxy matrix composite from pre-gelation to full cure', University of British Colombia, Canada.

Timoshenko, S. 1940, *Strength of materials*, vol. I, United States of America.

Timoshenko, S.P. & Gere, J.M. 1961, *Theory of elastic stability*, 2 edn, McGraw-Hill.

Udhayaraman, R. & Mulay, S.S. 2017, 'Multi-scale approach based constitutive modelling of plain woven textile composites', *Mechanics of Materials*, vol. 112, pp. 172-92.

Varkonyi, B., Belnoue, J.P.H., Kratz, J. & Hallett, S.R. 2019, 'Predicting consolidation-induced wrinkles and their effects on composites structural performance', *International Journal of Material Forming*, vol. 13, no. 6, pp. 907-21.

Wang, J., Long, A.C. & Clifford, M.J. 2009, 'Experimental measurement and predictive modelling of bending behaviour for viscous unidirectional composite materials', *International Journal of Material Forming*, vol. 3, no. S2, pp. 1253-66.

Wang, J., Potter, K.D., Hazra, K. & Wisnom, M.R. 2011, 'Experimental fabrication and characterization of out-of-plane fiber waviness in continuous fiber-reinforced composites', *Journal of Composite Materials*, vol. 46, no. 17, pp. 2041-53.

Warren, C.Y. & Richard, G.B. 2002, *Roark's formulas for stress and strain*, Seventh Edition edn, McGraw-Hill, United States of America.

Weber, T.A., Englhard, M., Arent, J.-C. & Hausmann, J. 2019, 'An experimental characterization of wrinkling generated during prepreg autoclave manufacturing using caul plates', *Journal of Composite Materials*, vol. 53, no. 26-27, pp. 3757-73.

Wehrkamp-Richter, T., De Carvalho, N.V. & Pinho, S.T. 2018, 'A meso-scale simulation framework for predicting the mechanical response of triaxial braided composites', *Composites Part A: Applied Science and Manufacturing*, vol. 107, pp. 489-506.

Wu, Z.J. 2009, 'Three-dimensional exact modeling of geometric and mechanical properties of woven composites', *Acta Mechanica Solida Sinica*, vol. 22, no. 5.

Wu, Z.J., Brown, D. & Davies, J.M. 2002, 'An analytical modelling techniques for predicting the stiffness of 3D orthotropic laminated fabric composites', *Composite Structures*, vol. 56, pp. 407-12.

Xie, N., Smith, R.A., Mukhopadhyay, S. & Hallett, S.R. 2018, 'A numerical study on the influence of composite wrinkle defect geometry on compressive strength', *Materials and Design*, vol. 140, pp. 7-20.

Yang, X., Gao, X. & Ma, Y. 2018, 'Numerical Simulation of Tensile Behavior of 3D Orthogonal Woven Composites', *Fibers and Polymers*, vol. 19, no. 3, pp. 641-7.

Yu, W.R., Zampaloni, M., Pourboghrat, F., Chung, K. & Kang, T.J. 2005, 'Analysis of flexible bending behavior of woven preform using non-orthogonal constitutive equation', *Composites Part A: Applied Science and Manufacturing*, vol. 36, no. 6, pp. 839-50.

Zhou, R., Gao, W., Liu, W. & Xu, J. 2022, 'An Analytical Model for the Uniaxial Tensile Modulus of Plain-Woven Fabric Composites and Its Application and Experimental Validation', *Aerospace*, vol. 9, no. 1.

Zobeiry, N., Malek, S., Vaziri, R. & Poursartip, A. 2016, 'A differential approach to finite element modelling of isotropic and transversely isotropic viscoelastic materials', *Mechanics of Materials*, vol. 97, pp. 76-91.